IMPERIAL COLLEGE LONDON

Department of Earth Science and Engineering

Centre for Petroleum Studies

Experimental Investigation of the Recovery of Gas and Oil by Spontaneous Water Imbibition

By

Russell Anderson

A report submitted in partial fulfilment of the requirements for the MSc and/or the DIC.

September 2012

Declaration of own work

I declare that this thesis "**Experimental Investigation of the Recovery of Gas and Oil by Spontaneous Water Imbibition**" is entirely my own work and that where any material could be construed as the work of others, it is fully cited and referenced, and/or with appropriate acknowledgement given.

Signature:.....

Name of student: Russell Anderson

Name of supervisor: Professor Martin Blunt

Acknowledgements

Thanks go to Nayef Al-Ansi, who without which the project would not have gone ahead and whose assistance and knowledge have been vital throughout the project. Further thanks go to Professor Martin Blunt whose guidance and supervision have been invaluable throughout this thesis.

I am indebted to Alex Toth for his technical expertise along with his patience when providing equipment and maintenance for the laboratory equipment. Thanks also go to Yukie Tanino for her advice throughout the time spent in the laboratory.

I would like to thank Imperial College for giving me the opportunity to undertake this research work. The past 3 months has given me the experience and technical knowledge to understand and appreciate laboratory work in the context of Oil and Gas engineering. This material is based on work supported by Qatar Petroleum, Shell and the Qatar Science and Technology Park under the Qatar Carbonates and Carbon Storage Research Centre.

Table of Contents

List of Figures

List of Figures in Appendices

List of Tables

List of Tables in Appendices

Imperial College London

Experimental Investigation of the Recovery of Gas and Oil by Spontaneous Water Imbibition

Russell Anderson

Supervisor: Professor Martin J. Blunt

Abstract

Spontaneous imbibition is of great importance to many hydrogeological applications. In this work, the rate of imbibition into water wet carbonates was investigated experimentally and then further analyzed analytically. Three carbonate rocks ranging in porosity from 16% to 28% and permeability from 1 to 250 $10^{-11}m^2$ were analyzed in this study. In addition to this, three different lengths (7.6, 20, and 28 cm) of the each rock core were used. To ensure reproducibility each experiment was repeated three times using different cores from the same block. The experiments were completed to analyse both co-current and counter current spontaneous imbibition and were conducted at room temperatures and pressures. It was found that the rate of imbibition was highly dependent of the permeability of the core, with a higher permeability producing a much faster rate of imbibition. Furthermore, the length of the core has a large effect on the imbibition time to residual saturations due to the rate of imbibtion slowing as the brine saturation advances. The validity of the scaling models presented by Ma et al. (1995), Li and Horne (2004), and Schmid and Geiger (2012) was tested on the experimental data. Schmid and Geiger's correlation was found to be the most reliable. The correlation could be fitted with the mass transfer function proposed by Aronofky et al. (1958) using the 0.05 constant proposed by Ma et al. (1995), and using the analytical oil recovery solution presented by Tavossoli et al. (2005 a) with a γ=0.01. It has been shown that imbibition oil and gas recovery behavior for large reservoir matrix blocks can be predicted using small reservoir samples without finding the permeability. This along with the ability to find the S_{gr}, S_{wi}, k_w, P_c, Corey Parameters and wettability of the core make imbibition experiments like the one shown vital for any reservoir engineer modeling a fractured reservoir. Furthermore, it has been shown that capillary trapping is higher in water wet media with liquid compared to gas as the non-wetting phase. This has great implications for CO_2 storage.

Introduction

Water spontaneous imbibition (SI) occurs in water wet and mixed wet rocks when a wetting phase is drawn into the porous media, displacing a non-wetting phase. An understanding of this phenomenon is useful due to its high importance in a large variety of hydrogeological applications, primarily oil and gas recovery through water injection and aquifer drive. Further areas of interest lie in displacement of non-aqueous liquids (NAPLs) in aquifers, flow in geothermal systems and of increasing importance, CO_2 sequestration (Tavassoli et al 2005a; Morrow and Mason, 2001).

Imbibition is driven by surface energy, through the action of capillary pressure (Morrow and Mason, 2001). Capillary pressure is dependent on the interfacial tension along with the magnitude of the curvature of the interface, which, depends on the surface forces between the fluid phases and the porous media. If this curvature is concave with respect to the fluid phase, the resulting displacement will be spontaneous (Morrow and Mason, 2001). Spontaneous imbibition is capillary pressure dominated, therefore the imbibition rate is highly dependent on the porous media (permeability, relative permeability, pore structure, boundary conditions, and the wettability of the porous media) and fluids properties (fluid viscosity and interfacial tension). Wettability is an important consideration for the rate of imbibition and is related to the contact angles of the various phases within the media. It has been noted that the SI of liquid and air will not occur for contact angles above 48 degrees for a dry core (Anderson, 1987).

Fractured water wet reservoirs will have a high initial oil production from the fractures. This can be short lived, therefore water injection or aquifer drive will be needed which will be dependent on SI (Morrow and Mason, 2001). A result of SI is the trapping of the non-wetting phase due to the movement of the wetting phase. This is known as capillary trapping and occurs in hydrocarbon reservoirs when the encroaching brine surrounds the hydrocarbon fluid leaving it immobile. The residual hydrocarbon saturations which are trapped are an extremely important factor which needs to be taken into account with any preliminary assessment of the maximum recovery from a reservoir.

The effect of capillary trapping is becoming increasingly important in the area of CO_2 sequestration, where it is seen as useful tool for long term CO_2 storage (Tanino et al., personal comm.). When supercritical CO_2 is injected into an aquifer or a depleted reservoir, spontaneous imbibition occurs with some of the brine surrounding the CO_2 in the pores leaving it immobile by the capillary pressure caused by the brine. By putting values to the potential initial immobilisation of CO_2 along with the rate at which trapping could occur within a carbonate reservoir will give a better notion of whether these rock formations are adequate for long term carbon storage. Analysing the residual saturation established by spontaneous imbibition is also important due to being comparable to that established by waterflooding (Tanino & Blunt, 2012).

Fractured water wet reservoirs with low matrix permeabilities are of special interest within the area of SI due to the need

for aquifer drive and secondary recovery methods for the maximum recovery of hydrocarbons (Morrow and Mason, 2001). In these dual-porosity reservoirs the water will flow rapidly through the high mobility fracture network then will imbibe into the low mobility matrix displacing the oil in place (Tavassoli et al., 2005 a). The rate of mass transfer between the rock matrix and the fractures determines the oil production (Zhang et al., 1996). A large body of work has been undertaken on dual porosity North Sea chalk reservoirs leading to an overall increase in oil recovery (Morrow and Mason, 2001). This report and analysis will look at this effect in carbonate cores.

The main aim of the project is to gain a greater understanding of SI in carbonate reservoirs of varying permeabilities, specifically the rate in which the wetting phase imbibes. The experimental data can then analysed using a model describing the process according to governing equations using sample size, shape, boundary conditions, viscosity and viscosity ratios, interfacial tension, pore structure, wettability, capillary pressure and relative permeabilities (Zhang et al., 1996). Using a general scaling equation with normalised parameters, the model can be then used to scale up laboratory results to reservoir conditions to predict potential oil recovery (Mattax and Kyte, 1962).

Experiment 1 will have a cylindrical core suspended from a scale with one of the open faces of the core touching the surface of a reservoir of brine (Zhang et al., 1996). When SI occurs, the weight increase of the core will be measured against time to acquire the rate of imbibition. Using a scaling equation, the wetting brine and the non-wetting air in this experiment can be compared to the wetting brine and the non-wetting hydrocarbon in a reservoir (Morrow and Mason, 2001). The aim of Experiment 1 is to have one wetting fluid (brine) flowing into the core displacing a second immiscible non-wetting fluid (air) in the direction of flow. This imbibition process is known as co-current imbibition, a representation of which can be seen in **Fig. 1** (Pooladi-Darvish and Firoozabadi, 2000).

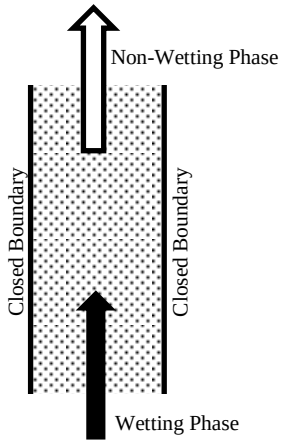

Fig. 1: Co-current imbibition expected from Experiment 1

Experiment 2 will involve an oil saturated core with an initial water saturation immersed in a reservoir of brine (Mattax and Kyte, 1962). The rate of imbibition of the brine into the core will be measured by analysing the volume of oil ejected against time. This is counter current flow (**Fig. 2)**

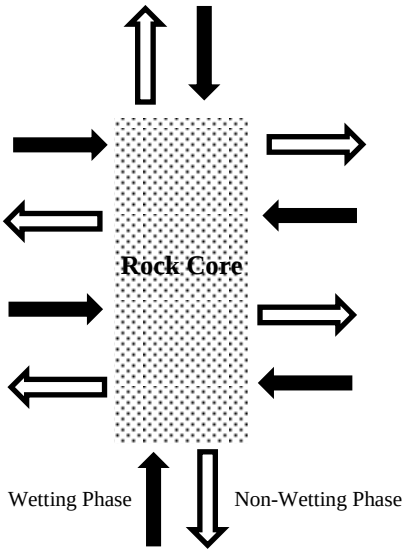

Fig. 2: Counter-current imbibition expected from Experiment 2

This study aims to test the validity of a set of scaling Equations on carbonate cores of varying petrophysical properties. Using these scaling Equations along with an analytical solution it is hoped a that a correlation can then be devised as to predict recovery behaviour for fractured- matrix, water- drive carbonate reservoirs in which imbibition is the dominant oil-producing mechanism (Mattax and Kyte, 1962). Furthermore, by analysing co-current and counter-current imbibition theoretical ideas proposed in the literature can be examined using experimental data. This will give a better idea of the physical processes occurring in imbibition. Additionally results from imbibition experiments may be used to gain further petrophysical properties such as S_{wi}, S_{gr}, k_w, P_c and the corey exponents used in relative permeability plots. These parameters along with the field recovery rates will be of great value to engineers when modelling a reservoir. Twenty Seven cores will be analysed in total to gain the experimental data needed for further analysis.

Literature Review

In practice, reservoir matrix blocks have shapes, sizes and boundary conditions very different from any experimental set up. There is a vast collection of various scaling models to undertake the task of predicting field performance from laboratory measurements. A scaling law taking into account gravitational and capillary forces was first investigated by Rapoport (1955). Handy (1960) analysed piston like imbibition and found $Q_w{}^2 \propto t$. A broader scaling group was devised by Mattax and Kyte (1962) (**Equation 1**).

$$t_{D,MK} = t\sqrt{\frac{k}{\Phi}}\frac{\sigma}{\mu_w}\frac{1}{L^2}, \quad \text{.....(1)}$$

Where $t_{D,MK}$is the dimensionless time, t is the imbibition rate, k is the permeability, Φ is the porosity, σ is the interfacial tension, μ_w is the water viscosity, and L is the length. A vast amount of separate data sets could be analysed using this equation, however, the boundary conditions set to ensure the validity of this equation means that the wettability and pore structure must be very similar between the porous media for this equation to work.

Lefebvre (1978) analysed the numerical models used for fissured reservoirs and found that for small blocks recovery time is proportionate to the square of the size of the block. However for large blocks gravity takes over and recovery time is proportionate to the size of the block. It was shown that generally accepted scaling rules were not reliable for reproducing a recovery curve mainly due to local heterogeneities within the core matrix. This is further analysed by Hamon and Videl (1986) who said that any heterogeneity needs to be taken into account in numerical simulation. They found the two-phase flow Equations adequately described the relevant mechanisms in small cores like the ones to be analysed in this study and the predictive model and can be history matched to a real reservoir, although the recommendation from Hamon and Videl's (1986) paper is to perform the imbibition tests under reservoir pressure and temperature with live fluids.

A shape factor was proposed by Kazemi et al (1992) to be used to compensate for the effect of geometry (**Equation 2**).

$$F_s = \frac{1}{V_b}\sum_{i=1}^{n}\frac{A_i}{s_{Ai}}, \quad \text{.....(2)}$$

Where V_b is the bulk volume, A_i is the Area open to imbibition at the ith point, s_{Ai} is the distance from A_i to the centre of the matrix and n is the total number of surfaces open to imbibition.

A characteristic length can then be defined as **Equation 3.**

$$L_s = \frac{1}{\sqrt{F_s}}, \quad \text{.....(3)}$$

Using the data of Hamon and Vidal (1986), Ma et al. (1995) modified the characteristic length (**Equation 4)**.

$$L_c = \sqrt{V_b \Big/ \sum_{i=1}^{n}\frac{A_i}{l_{Ai}}}, \quad \text{.....(4)}$$

Where l_{Ai} is the distance travelled by the imbibition front from the open surface to the no-flow boundary. This difference can change from the s_{Ai} with different boundary conditions.

To take into account differences in the shape and viscosity ratios Ma et al. (1995) proposed the following scaling group for strongly water wet rocks, where the geometric mean of the water and oil viscosities is used (**Equation 5)**.

$$t_D = t\sqrt{\frac{k}{\Phi}}\frac{\sigma}{\sqrt{\mu_w\mu_o}}\frac{1}{{L_c}^2}, \quad \text{.....(5)}$$

It was found that $\sqrt{\frac{k}{\Phi}}$ provides a satisfactory correlation for the effects of pore structure and transport properties for two-phase counter-current flow (Ma et al., 1995).

Li and Horne (2004) devised a scaling model based on characterising spontaneous water imbibition into gas-saturated porous media while calculating the endpoint relative permeability of the water phase and capillary pressure. The model reveals a linear relationship between the imbibition rate and the reciprocal of the gas recovery (**Equation 6).**

$$Q_w = \frac{dN_{wt}}{dt} = a\frac{1}{R} - b, \quad \text{.....(6)}$$

Where $Q_w$is the volumetric rate of water imbibition, N_{wt} is the accumulative volume of water imbibed into rocks, and R is the recovery in terms of pore volume and is equal to N_{wt}/V_p (V_p is the pore volume).

The constant a is associated with capillary forces (**Equation 7).**

$$a = \frac{Ak_w(S_{wf}-S_{wi})}{\mu_w L}P_c \quad \text{.....(7)}$$

Where A is the cross sectional area, L is the length of the core, μ_w is the viscosity of water, S_{wi} is the initial water saturation $S_{wf}$is the water saturation behind the imbibition front $k_w$is the effective permeability of the

water phase at a water saturation S_{wf} and, $P_c$is the capillary pressure at S_{wf}.

The constant b is associated with gravity forces (**Equation 8)**

$$b = \frac{Ak_w}{\mu_w}\Delta pg\sin\beta \quad \text{.....(8)}$$

Where Δρ is the density difference between water and gas, g is the acceleration due to gravity, and β is the longitudinal angle between the axis of the core sample and the horizontal direction. This gives the dimensionless time seen in **Equation 9.**

$$t_d = \left(\frac{b}{a}\right)^2 \frac{k_w}{\phi}\frac{P_c}{\mu_w}\frac{S_{wf}-S_{wi}}{{L_a}^2}t \quad \text{.....(9)}$$

Schmid and Geiger (2012) took the 2 phase Darcy model from first principles and derived a scaling group from an exact solution to Darcy's Equation for SI. This was done by relating the cumulative water phase imbibed to the normalized pore volume. Their scaling group is seen as "Master Equation", taking into account many of the previously derived scaling cases (**Equation 10 and 11)**.

$$t_d \propto \left(\frac{2A^*}{\emptyset L_c}\right)^2 t \text{ , ...(10)}$$

$$Q_w(t) = 2A^* t^{0.5} \quad \text{.....(11)}$$

Where A* is the constant for each rock which includes all the information about the capillary-hydraulic properties and the initial fluid content (it is still dependent on L_c).

The validity of the scaling group was shown on 42 published imbibition studies, showing that the Darcy model is suitable for describing SI, although the model does break down at early times.

Morrow and Mason (2001) have argued that imbibition in a reservoir occurs by counter-current flow, although other papers have contested this belief (Bourbiaux and Kaladjian, 1990). For fractured reservoirs, it has been shown that co-current imbibition may be the dominant process and that oil recovery when this process is taking place is faster and the displacement efficiency is higher (Bourbiaux and Kaladjian, 1990). For co-current imbibition to take place there has to be gravity segregation of oil and water in the fractures, with only part of the matrix block exposed to water (Pooladi-Darvish and Firoozabadi, 2000). This will exist in a fractured reservoir for a significant period during hydrocarbon recovery. Once a zero-capillary pressure inlet-boundary condition starts to occur, counter current imbibition will take place which will slow the oil recovery rate (Pooladi-Darvish and Firoozabadi, 2000). This has been shown to be the case in North-Sea chalk reservoirs which exhibit small block size and high imbibition capillary pressure, where a large portion of the oil is recovered from the matrix before the block becomes surrounded by water (Pooladi-Darvish and Firoozabadi, 2000).

Chen et al. (2005) investigated SI using DDIF and centric-scan SPRITE techniques and observed that co-current imbibition is a piston-like mechanism with the brine displacing the air through pores and connecting the throats uniformly. Counter-current imbibition is a film thickening mechanism, with the brine flowing along the corners and the surfaces of the pore space. After the penetrating waterfronts meet at the centre of the pore space, the water film thickens which leads to a uniform increase in water saturation. Oil recovery calculations based on scaling studies of counter-current imbibition do not work well for co-current predictions, principally when applying the diffusion equation (Pooladi-Darvish and Firoozabadi, 2000). This is not the case when looking at gas as the non-wetting phase where, due to low gas viscosity, the gas-phase pressure gradient would be small and a diffusion coefficient could be used.

The boundary conditions of the experiment are extremely important as they set out the scaling model that should be used. They should not be so constrictive as to leave the numerical model unpractical. For Experiment 1 the core needs to be curved as to verify co-current imbibition (Ceil et al., 1998). Furthermore the length of the core during Experiment 1 should be below 40 cm so the gravity forces do not affect the capillary force driven experiment (Tavassoli et al., 2005b; Schmid and Geiger, 2012). Experiment 1 will use 3 different core lengths to compare the effect of length on imbibition rate. Bourbiaux and Kalaydjian (1990) recommend carrying out experiments with equal densities as to eliminate gravity forces and ensure stability of the front. However air's negligible viscosity and density compared to brine should lead to the same result (Zimmerman et al., 1990; Schembre and Kovscek, 2003).

Due to its simplicity it is popular to adopt a zero initial water saturation (S_{wi}) in most scaling mechanisms such as will be done for Experiment 1 (Mattax and Kyte., 1962; Zhang et al., 1996). However, this is physically unrealistic due to the presence of an initial water saturation in hydrocarbon bearing reservoirs. Morrow and Mason (2001) discuss this, pointing out that a high S_{wi} results in a reduced capillary pressure, but increased mobility of any invading water. Hamon and Vidal (1986) did further work correlating sandstone S_{wi} with results for zero S_{wi}. They found that that for some strongly water wet systems and a S_{wi} less than 20% the imbibition rate was not very sensitive to initial water content. It has been found for sandstone and chalk that imbibition's rates could be higher or lower than those for S_{wi} =0 (Viksund B.G. et al., 1998).

Experiments

The experiments took place using three carbonate cores of three varying lengths (7.6, 20, 28, ±0.05 cm) and a diameter of 3.8±0.05 cm. These cores were taken from the Ketton, Estaillades and Portland quarries. Ketton is an oolitic limestone of 99.1% calcite (CaCO3) and 0.9% quartz (SiO2) (Tanino and Blunt, personal comm.). Estaillades is an upper cretaceous bioclastic limestone (Watson, 1911), which contains 99% calcite and traces of dolomite and silica (Le Guen et al., 2007). Portland is an ooparite limestone, with a matrix composed of sparitic carbonate and some micritic carbonate (Albion Stone Technical Data, 2010). A representation of the cores can be seen in **Fig. 3** with the measured permeability and porosity values in **Table 1**.

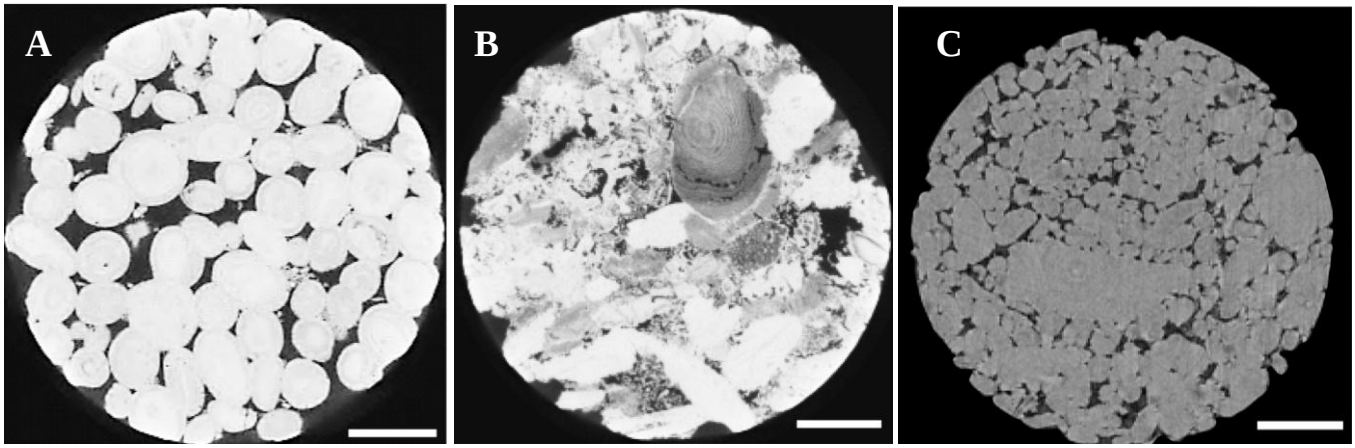

Fig. 3: Slices (two-dimensional sections in the xy-plane) of X-ray micro tomography scans of (A) Ketton (A), (B) Estaillades (B), and (C) Portland (C) X-ray scans. (Blunt et al., 2012). The white bar in each image represents 1 mm.

Table 1: The petrophysical properties of the cores.

	Measured ϕ (%)	Measured K (10^{-11}m2)
Ketton	21-24	200-250
Estaillades	26-28	15-30
Portland	16-20	1-5

The purpose of the primary experiment is to produce spontaneous imbibition curves documenting the rate of weight of brine imbibed. Other petrophysical properties such as porosity, volume and permeability will also be measured experimentally so each core can be analysed using varying scaling correlations. The basic method of acquiring the SI curve is to place the open flat side of a cylindrical core so it is level with a brine reservoir, then record the weight change of the core as it imbibes the brine. To ensure that the imbibition is a co-current process a heat shrink will be applied around the curved edge of the cylindrical core (Ceil et al., 1998).

A secondary experiment will take place to compare how a connate water saturation along with counter current flow effects the SI curve and the scaling model. This experiment will involve fully saturating a core with brine, then injecting oil to mimic drainage. The core will then be placed inside a brine reservoir and the rate of volume of oil displaced will be measured.

Experimental Conditions

Experiments 1 and 2 were both conducted at atmospheric pressure and at a room temperature of 20±1^{o}C. The brine used was made up from 5 wt.% NaCL and 1wt.% KCl along with deionised water at a quality of 0.067μC/cm. The density of the brine was 1.042±0.005g/cm^3 at 20 ^{o}C, and the viscosity was taken as 1.085 mPa s (CRC Handbook, 2007). To keep results consistent, evaporation from the brine mixture was prevented through the use of parafilm and the density was checked for consistency using an Anton PAAR DMA 48 density meter which is calibrated regularly ($\pm 10^{-4} \mathrm{gcm}^{-3}$). To prevent the brine reacting with the core during the experiments, sections of the carbonates are added to separate batches of the brine, stirred for 24 hours, left to settle for 72 hours, then filtered.

Experimental Description

The porosity of the 7.6 cm long cores was found using a helium porosimeter (average of 6 measurements taken). The results were checked using a comparison of the mass of the core after finding the permeability using brine and completely dry. A digital calliper was used to find the diameter and length of the cores (average of 6 measurents for finding the diameter, and 2 for finding the length). The volume was found using these measurements.

The mass balance method was used to find the porosity of the longer 20cm and 28 cm cores. These cores were fully saturated with brine by submerging the core into a brine solution then placing them under a vacuum for 72 hours to remove the air out of the core. The weight of the fully saturated cores were then then compared against the core when dry.

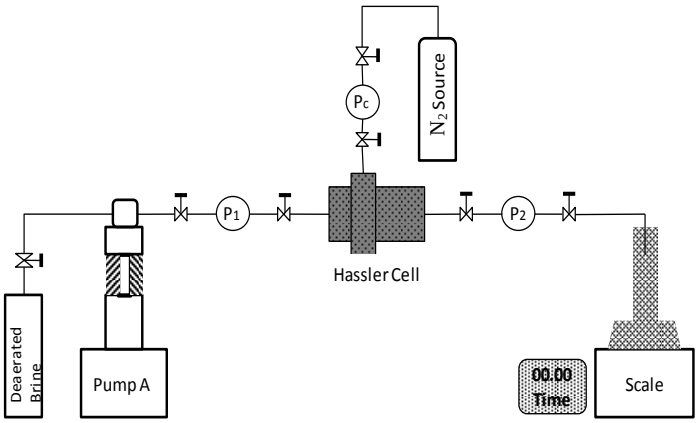

Fig. 4: A schematic of the brine permeability experiment.

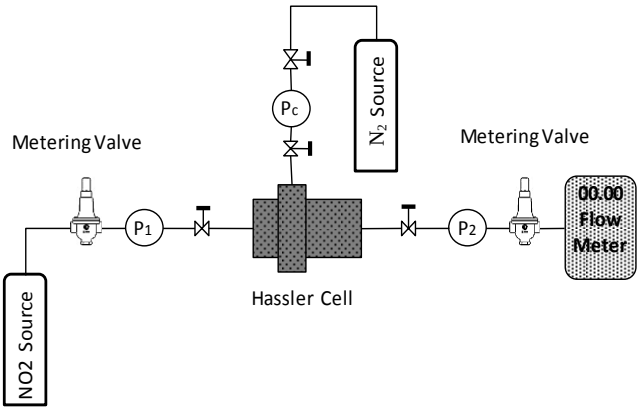

Fig. 5: A schematic of the nitrogen permeability experiment.

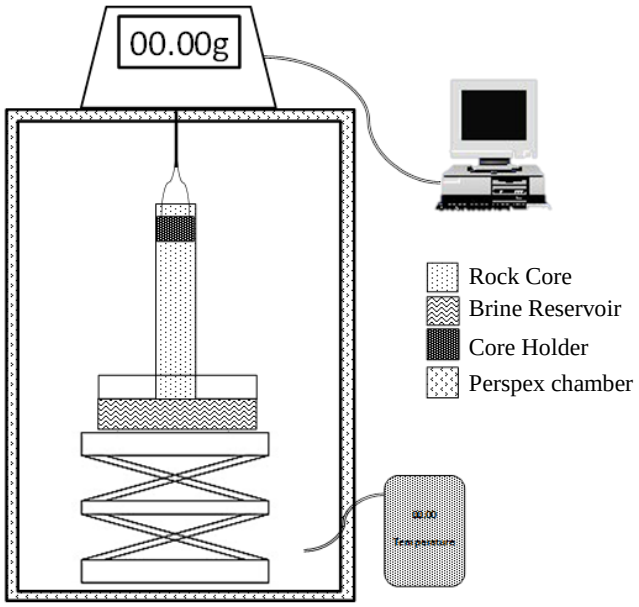

Fig. 6: A schematic of the spontaneous imbibition experiment.

The permeabilities of the 7.6 cm cores were analysed using a standard Hassler cell in the set up shown in **Fig. 4**. The core was inserted into the cell with a confining fluid of nitrogen applied at a pressure 1.5 times higher than the inlet pressure, the purpose of which was to certify that there was no brine leakage. Inlet and outlet tubes were then monitored for 10 minutes to verify that the N_2 confining fluid was not contaminating the core. The outlet valve was sealed so the core could be vacuumed to 0 Pa. After 3 hours CO_2 was injected for 1 hour to displace any additional air or other contaminating particles. The cell was then re-vacuumed for 24 hours. The brine to be used in the experiment was vacuumed for a period of 48 hours in a vacuum oven to de-aerate the fluid to ensure that it was single phase passing through the core. Pump A was used to fully saturate the core with 10 pore volume of brine, then the pump was run at 5 different flow rates checking the transducers at P_1 and P_2 continuously until a stabilisation of pressure occurred. At this point the pressures were taken along with the flow rate for a permeability measurement. The accuracy of the flow rate shown on the pump was doubtful therefore the mass flow rate of brine being discharged was found. The transducers at P_1, P_2 were accurate up to ±0.0005 psi and P_c was accurate up to ±0.05 psi.

For the 20 and 28 cm cores, Weatherfords Hassler Cell was used, with nitrogen as the injection fluid and nitrogen as the confining fluid (**Fig. 5**)(N_2, μ=0.0148 mPa.s). The cores were injected with N_2 for a period of 1 hour as to fully saturate them. Then 10 readings at varying flow rates were taken with changing back pressure. The cores were then injected with air for 1 hour in preparation for the spontaneous imbibition experiment.

Experiment 1 took place with dry cores with the addition of a heat shrink around the curved edge of the cylindrical core. A wire core holder was attached to the heat shrink to suspend the core above a brine reservoir (**Fig. 6**). This brine resevoir was saturated with air for a period of 1 hour before the experiment took place. The flow of fluid to find the permeability was in the

same direction as the direction of flow during the SI experiments. The high precision balance used has 0.001 g accuracy. For the Ketton core it was set to take 10 data points per second, as to gather as much data as possible for the early time imbibition, for Estaillades 5 data points per second were taken, while for Portland due to the slow speed of imbibition 2 data per second were taken. The experiment was contained in a Perspex chamber as to decrease evaporation and turbulence.

Experiment 2 involved just the 7.6 cm cores. The cores were placed into a Hassler cell and injected with 10 pore volumes of vacuumed brine, then 5 pore volumes of n-decane (ρ =0.73 g/cm³ μ= 0.920 mPa s). The core was then recovered from the cell and weighed in a n-decane reservoir to analyse the value of the connate water saturation produced. It was then placed in an Amott cell and fully submerged in vacuumed brine. The volume of oil displaced from the core was then read on a regular basis from the scale on the Amott cell.

Experimental Analysis

The permeability for all the cores was found by flowing a fluid of known viscosity through the core at a set rate and then measuring the pressure drop across the core. When using the brine the measurement was relatively straightforward as the requirement for incompressibility and for laminar flow was met. However, when nitrogen was used for the permeability measurements, the compressibility of the gas meant that it would expand at the outlet end leading to an increase in the velocity. To gain an accurate reading of the permeability of the cores, the Klinkenberg correction was needed (Klinkenberg, 1941). The Klinkenberg correction is needed most at low gas pressures where there will be an overestimation of permeability due to fewer molecules occupying the smaller pores. At higher pressures there are more gas molecules per unit volume so the 'Klinkenberg effect' becomes smaller. The Klinkenberg permeability represents the gas as a near perfect liquid by analysing what the gas's permeability would be when compressed by an infinite pressure. In this work, this is done by taking 10 different flow rates and differential pressures, putting the data on a graph of K vs. $1/P_{mean}$, then finding what the permeability would be at $1/P_{mean}$ =0.

When the permeability was found using vacuumed brine the cores had to be cleaned with methanol before the SI experiments could take place. They were also cleaned and reused if there were errors or incomplete data from the permeability or SI experiments. To clean the cores, they were placed in a Hassler cell and 10 pore volumes of 2-propanol was injected through them. The cores were then dried until the weight of the core was the same as the original dry weight. There were concerns over the consistency of this method so after the core had been cleaned the porosity was checked. A 5-10% decrease in the porosity was found. This is believed to be from deposited salt during experimentation. This difference after core cleaning was the principal reason that the permeability was measured with nitrogen for the larger cores.

During Experiment 1 the cores were not fully submerged into the brine as to mitigate the chance of water pressure affecting the results of the experiment. Furthermore, because the core was suspended above the brine reservoir there may have been an initial negative weight effect from the surface tension of the brine pushing the core upwards.

The cores for Experiment 2 were used after Experiment 1 so there may have been salt deposition affecting these results. There were contamination issues with some of these experiments due to the confining nitrogen fluid leaking into the core during brine and oil flooding. This, along with residual air in the core from a partially saturated brine flood, was noticed during the experiment when gas collected at the top of the cell and also when the weight of the core after removing it from the Hassler Cell was lower than expected. These results were discarded and it is thought a higher back pressure is needed along with a slower injection rate to provide full saturation.

Results

Experiment 1

The imbibition rate is seen to decrease as the brine imbibes through the core until the rate plateaus at the residual saturation. **Fig. 7, Fig. 8** and **Fig. 9** shows graphs of the recovery factor (amount of the pore volume saturated) against time in seconds for the 7.6 cm, 20cm, and 28 cm cores for the Portland, Ketton and Estaillades cores. **Table 2** summarizes the range of petrophysical properties found for each length of core for the Portland, Estaillades and Ketton rock types respectively. There is a strong relationship between the permeability to the time taken for imbibition to reach S_{gr} as would be expected. This can be seen with the highly permeable Ketton rock type in **Fig. 7** having a steep sloped plot, while the Estiellades plot is less steep (**Fig. 8**), and the Portland plot is comparably quite shallow (**Fig. 9**). Statistically, Estaillades is about 10 times as permeable as Portland and imbibition is around 4 times as quick. While Ketton is about 10 times as permeable as Estaillades and imbibition is around twice as quick. For all cores there is a constantly decreasing imbibition rate from the initial saturation. Because of this, it takes about 10-15 times longer for the 28 cm core length to fully imbibe compared to the 7.6 cm of core length for each rock type. These relationships between length, permeability and porosity will be examined along with the total time for imbibition later in the report.

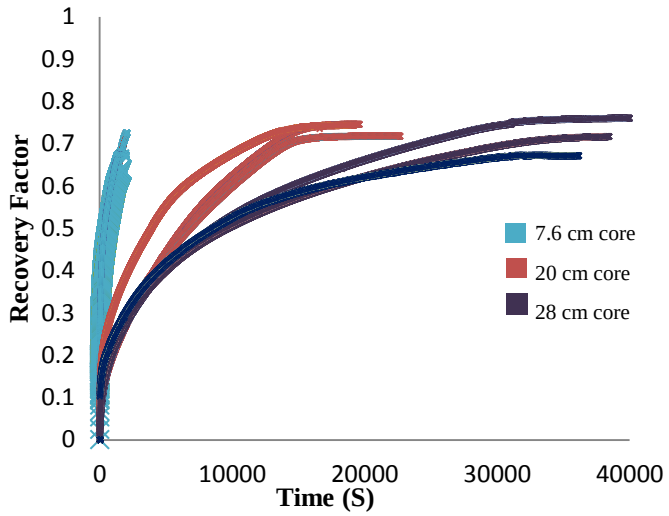

Fig. 7: SI rate (recovery factor vs time) into Ketton cores of varying length.

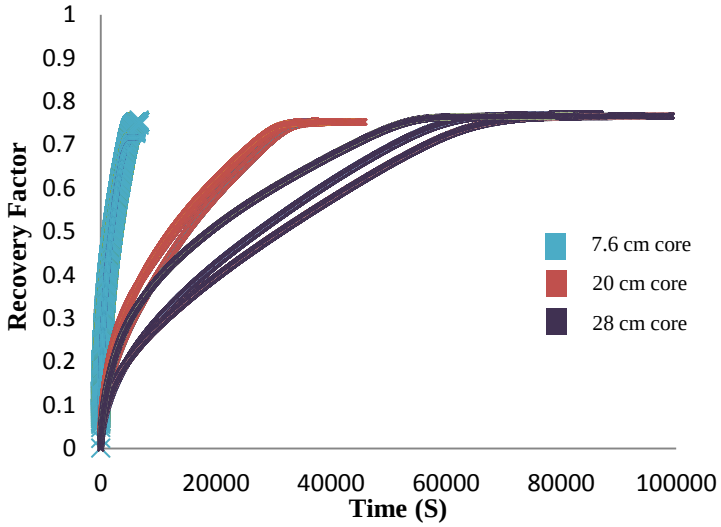

Fig. 8: SI rate (recovery factor vs time) into Estaillades cores of varying length.

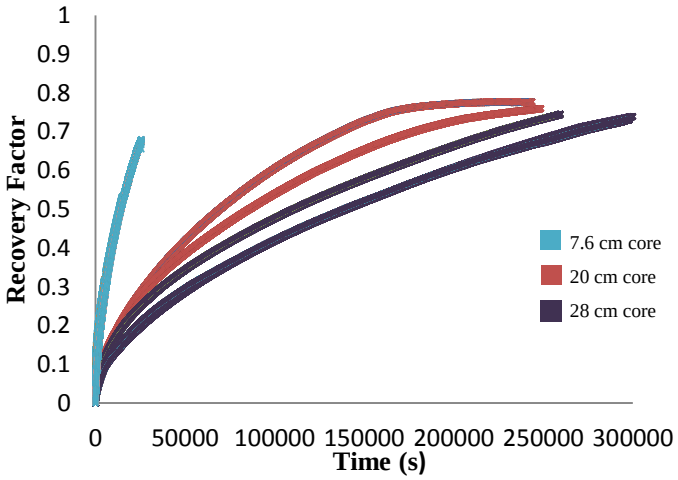

Fig. 9: SI rate (recovery factor vs time) into Portland cores of varying length.

Table 2: The petrophysical properties found.

	Length	ϕ (%)	K (10^{-11}m²)	S_{gr} (%)
Ketton	7.6 cm	21-23	113-235	28-35
	20 cm	22-23	240-295	28-34
	28 cm	22-24	250-345	28-35
Estaillades	7.6 cm	26-28	13-20	25-29
	20 cm	26	13-16	24
	28 cm	28	30-40	22-23
Portland	7.6 cm	16-19	1-2	21-25
	20 cm	19	0.4-0.9	22-24
	28 cm	13-25	2-6	26

Experiment 2

This experiment was run on each of the 7.6 cm cores with limited success. This was due to the inability to adequately mimic the drainage process to create an irreducible water saturation (S_{wi}) before the experiment took place. This was evident during the experiment when air bubbles could be seen being emitted from the core during the imbibition experiment. There were further issues with contamination from the containing Nitrogen fluid. The S_{wi} values found for the Ketton, Estaillades and Portland cores were 32%, 30% and 19% respectively, although the validity of these values is questionable. While the S_{wr} values are taken as 0.5,0.73, and 0.4 for the Ketton, Estiellades and Portland cores respectively. Although Bourbiaux and Kaladjian (1990) has shown this method of imbibition to be much slower than the method used in Experiment 1 so these results may not be final residual values.

Analysis

There SI rate is usually divided up into two parts.

- Early time imbibition: This describes the imbibition before the advancing water front reached the boundary (the top edge) (Travassoli et al., 2005a).
- Late time imbibition; This applies when the saturation front due to imbibition reaches the boundary of the core (the top edge) (Travassoli et al., 2005b).

For counter current flow, there is a large amount of experimental and theoretical evidence for a square root of time dependency (Morrow and Mason, 2001; Li and Horne 2004; Kashchiev and Firoozabadi, 2003; Tavassoli et al., 2005a and 2005b). However there was no evidence of this square root time dependency in the early time behaviour (first 10 seconds) of the co-current imbibition experiments undertaken. There is no correlation for any of the cores, with the straight line behaviour going from $t^{0.05}$ to t^{1}. There is an average t power value of 0.53, and a standard deviation of 0.29, with no real trend in terms of what length and core type are close to the $t^{0.5}$ relationship.

Analysing the imbibition data for the $t^{0.5}$ relationship later in time is more promising. **Fig. 10, Fig. 11** and **Fig. 12** show the portions of the graph which fit the $t^{0.5}$ relationship for Ketton, Estaillades and Portland cores respectfully. **Table 3, Table 4** and **Table 5** show the value of the power of time along with the constant A* proposed by Schmid and Geiger (2012) (**Equation 10**). The constant A* is related to the characteristics of the fluid rock system, and is acquired by examining the power trend shown by the respective plot.

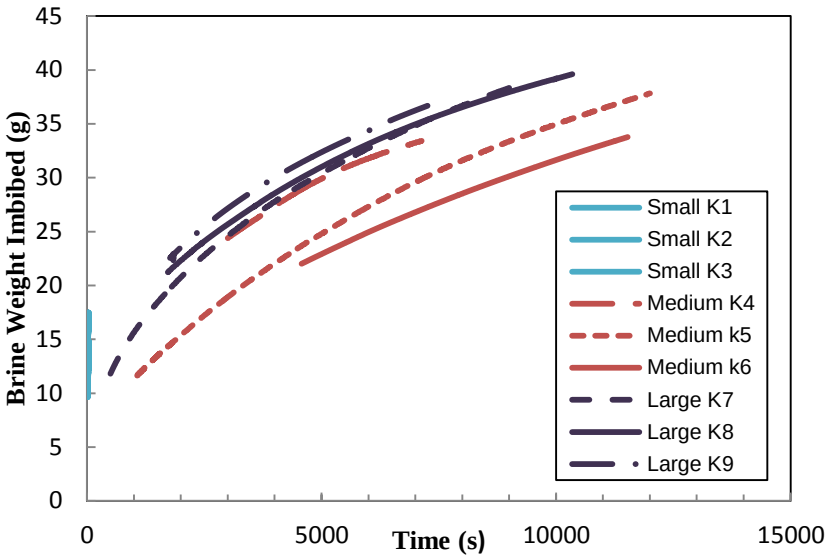

Fig. 10: Ketton SI curves where the power factor is closest to 0.5.

Table 3: Constant "A" along with the power factor taken from the curves in Fig. 10.

	"A*" (cm/√s)	Power Factor
Small K1	2.6	0.47
Small K2	2.5	0.51
Small K3	4.3	0.4
Medium K4	1.3	0.37
Medium K5	0.3	0.5
Medium K6	0.4	0.47
Large K7	0.9	0.41
Large K8	1.5	0.36
Large K9	1.7	0.34

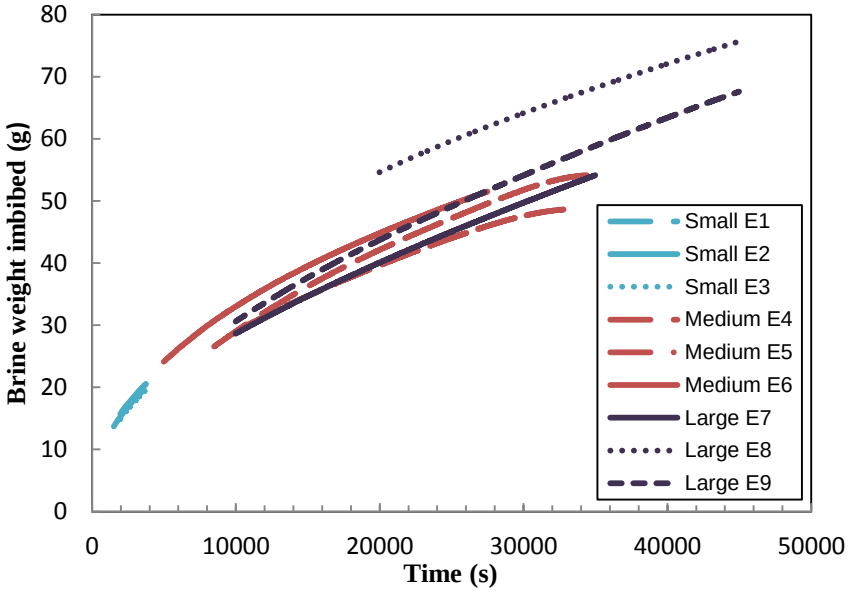

Fig. 11: Estaillades SI curves where the power factor is closest to 0.5.

Table 4: Constant "A" along with the power factor taken from the curves in Fig. 11

	"A*" (cm/√s)	Power Factor
Small E1	0.7	0.41
Small E2	0.66	0.41
Small E3	0.61	0.42
Medium E4	0.45	0.45
Medium E5	0.25	0.52
Medium E6	0.56	0.44
Large E7	0.25	0.51
Large E8	1	0.4
Large E9	0.23	0.53

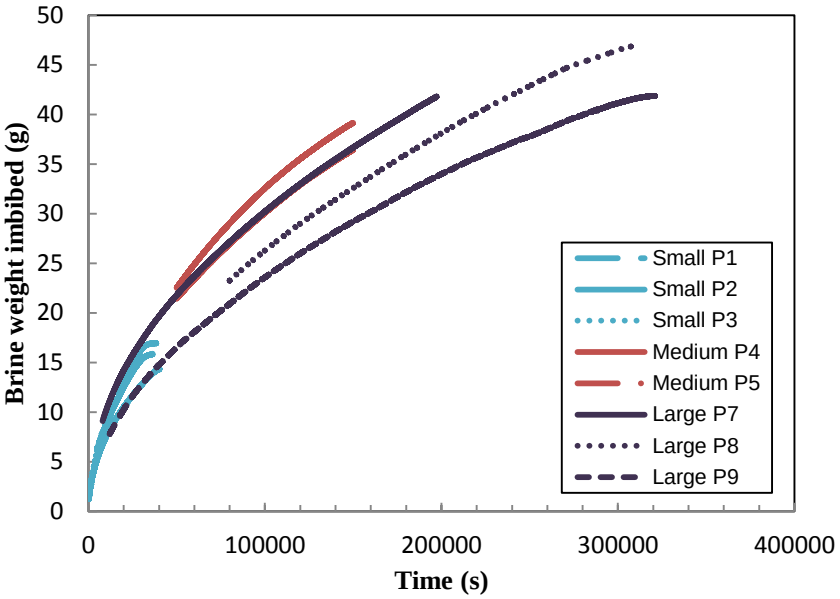

Fig. 12: Portland SI curves where the power factor is closest to 0.5.

Table 5: Constant "A*" along with the power factor taken from the curves in Fig. 12.

	"A" (cm/√s)	Power Factor
Small P1	0.09	0.49
Small P2	0.07	0.50
Small P3	0.06	0.54
Medium P4	0.11	0.49
Medium P5	0.09	0.50
Medium P6		
Large P7	0.13	0.47
Large P8	0.06	0.53
Large P9	0.07	0.51

Dimensionless time; Schmid and Geiger (2012): Using the scaling model defined Schmid and Geiger (**Equation 10**) the graph of recovery factor against dimensionless time (**Fig. 13**) is obtained. The correlation can be fitted by a single parameter mass transfer function proposed by Aronofky et al. (1958).

$$\frac{R}{R_\infty} = 1 - e^{ct_D} \quad \text{.....(12)}$$

Where R is oil recovery by imbibition R_∞ is ultimate oil recovery by imbibition and c is the oil decline constant. Ma et al. (1995) found this equation along with the dimensionless time in **Equation 5** and an oil decline constant of 0.05 fit the experimental data of Mattax and Kyte (1962), and Hamon and Vidal (1986). The same oil decline constant of 0.05 used by Ma et al. (1995) can be used to fit the data in **Fig. 13**.

A better fit can be obtained using the analytical oil recovery solution (**Equation 13**) presented by Tavossoli et al. (2005 a) with a γ=0.01.

$$\bar{S}(t_D) = (\gamma t_D)^{0.5} \quad \text{.....(13)}$$

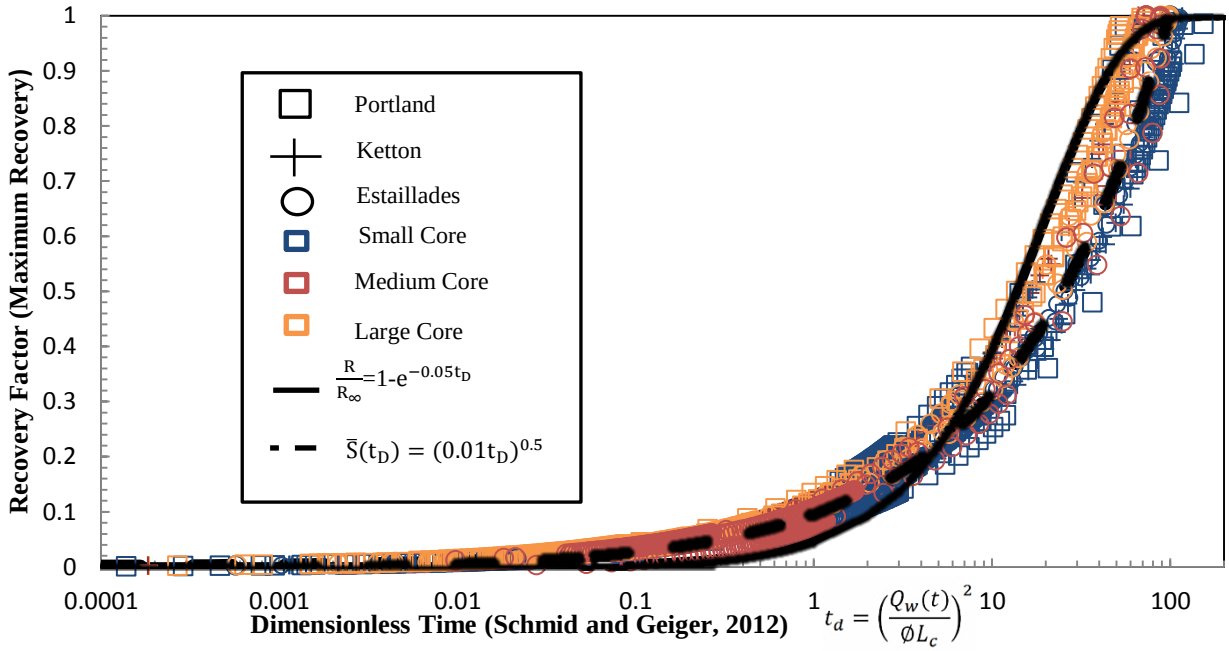

Fig. 13: A semi-log graph showing the correlation between recovery and Schmid and Geigers dimensionless time.

Dimensionless time; Ma et al. (1995): Analysing the results using the scaling dimensionless time proposed by Ma et al. (1995) (**Equation 15**), with the parameters in **Table 6** gives the graph in **Fig. 14** (Pooladi Darvish and Firoozabadi (2000) have shown numerically that the viscosity of air can be ignored in the calculations)

Table 6: The parameters used for the calculation of t_D

Interfacial tension of air/brine (σ)	72 mN/m [a]
Viscosity of air (μ_a)	0.018 mPa s [a]
Viscosity of brine (μ_b)	1.085 mPa s [f]
Boundary conditions	L_c=L_s

[a] Tavassoli, 2005b [f] CRC Handbook, 2007

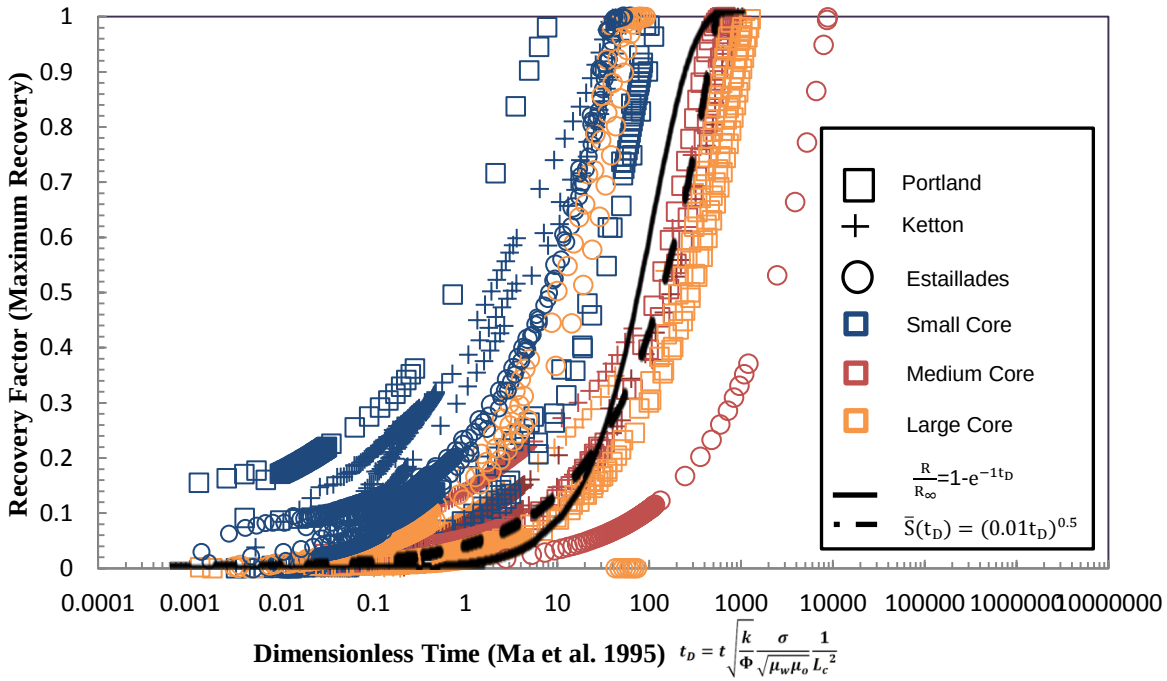

Fig. 14: Recovery as a function of Ma et al. dimensionless time

Dimensionless time and normalized recovery; Li and Horne (2004): Using **Equation 9** proposed by Li and Horne (2004) **Fig. 15** is produced for the 3 inch cores.

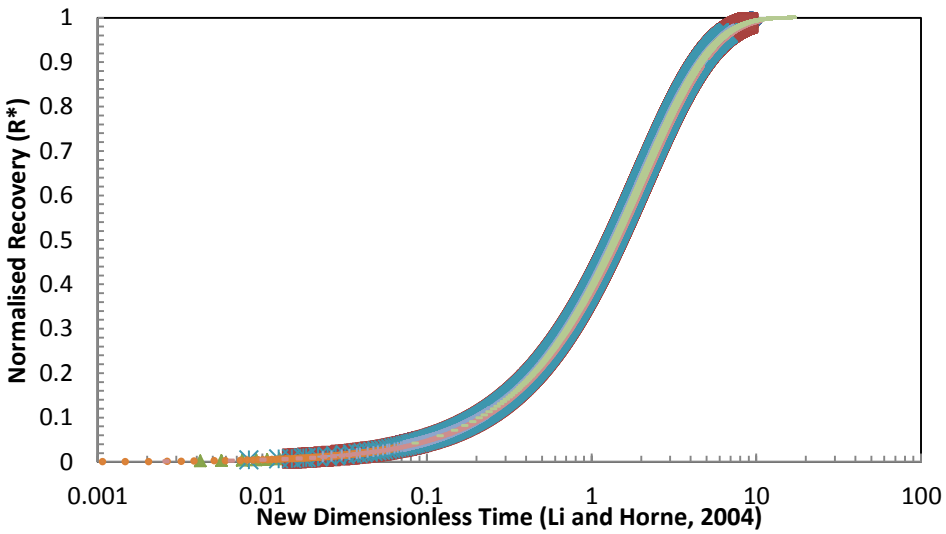

Fig. 15: New dimensionless time against normalized recovery for all 3 inch cores (Li and Horne, 2004)

Capillary Trapping in Carbonates

Ignoring the anomalies from the Portland and Ketton oil/brine systems performed in Experiment 2, which the inaccuracies have been discussed, **Fig. 16** shows many points of interest which are important for capillary trapping and therefore important for CO_2 storage. The plot shows that the amount of the non-wetting phase that is surrounded and trapped during spontaneous imbibition is less when the non-wetting phase is gas rather than oil. This leads to the conclusion that more CO_2 can be stored in liquid form than in gaseous form in a water wet system.

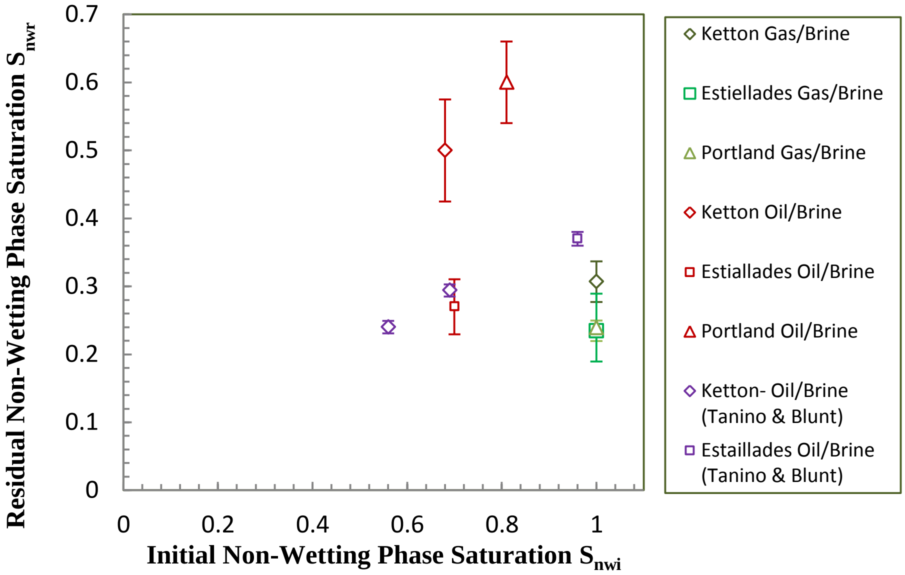

Fig. 16: S_{nwr} as a function of S_{nwi} for the 7.6 cm cores analyzed in Experiment 2, data courtesy of Tanino and Blunt (2012)

Discussion

The lack of an early time $t^{0.5}$ behaviour in the imbibition experiments may have been due to the initial buoyancy forces and interfacial forces acting between the core and the brine in the first few seconds of imbibition. The buoyancy forces were minimised by submerging the core by a slight margin but if any buoyancy forces still existed they would act to decrease the apparent core weight, while the interfacial forces between the core and the water will increase the cores apparent weight. These forces may have led to the lack of an early time correlation. Theoretically a correlation should have been observed because the advancing rate of the water front should be proportional to the capillary pressure gradient which is inversely proportional to the distance the water front has already travelled (Tavassoli et al., 2005a).

The dimensionless time proposed by Schmid and Geiger (2012) was developed for co-current flow and correlates the laboratory data very well. Furthermore, it is easy to implement and the permeability of the core is not needed. This is important because permeability measurements are subject to large amounts of uncertainty, cannot be obtained from logs, and take a large amount of preparation and laboratory time to collect. The dimensionless time proposed by Ma et. al (1997) does not correlate cores of varying length very well. This dimensionless time was developed for strongly water-wet cases and counter current flow, which may be why the correlation is not strong when using this dimensionless time. The correlation presented by Li and Horne is found to be unreliable due to the exponential on the y-axis containing the t_D parameter from the x-axis. The unsuitability of this dimensionless time is further discussed by Olafuyi et al. (2007).

The useful areas of this analysis are that field scale recovery rates can be predicted from the mass transfer function (**Equation 12**) with a constant of 0.05 or the analytical oil recovery solution (**Equation 13**) with a γ=0.01. These functions along with the t_D proposed by Schmid and Geiger (2012) could be used with field data for a fractured reservoir to predict future field recovery rates.

Further analysis using the Equation described by Handy (1960) and shown in **Equation 14** can be used to find the effective capillary pressure which can be used to measure rock wettability. To do this the effective water permeability k_w in each core needs to be found. Wettability can also be assessed from the reduction in SI rate relative to the predicted results for a strongly water wet case (Ma et al., 1995).

$$\boldsymbol{Q_w}^2 = \left(\frac{2P_c k_w \phi A^2 S_w}{\mu_w}\right) \boldsymbol{t}, \quad \ldots\ldots(14)$$

Where Φ is the fractional porosity, S_w is the fractional water content of the pore spaces, k_w is the effective water permeability, μ_w is the water viscosity, P_c is the capillary pressure, A is the cross sectional area, and t is the time

Fig. 13 shows a correlation using Tavassoli et al. (2005 a). From the γ of 0.01, the Corey exponent for the relative permeability plots could be found using **Equation 15**.

$$\gamma = \frac{2}{(2+b)(1+b)} k_{ro}{}^{max} J' \quad \text{.....(15)}$$

Where b is the Corey exponent, $k_{ro}{}^{max}$ is the maximum non wetting phase relative permeability, and J' is the dimensionless gradient of the capillary pressure.

From an imbibition experiment on a single core along with knowledge of the porosity and length of the core, one can use the scaling Equation along with the mass transfer function to find the production from a reservoir along with the S_{gr}, S_{or}, corey parameters, P_c curves, and rock wettability. All these parameters are extremely important factors when simulating a reservoir.

The results from analysing **Fig. 16** are very promising in the field of CO_2 storage due if CO_2 is being injected as a supercritical liquid as in secondary oil recovery. Trapping efficiency (residual saturation/initial saturation) decreases as porosity increases under water-wet conditions (e.g., Tanino & Blunt 2012). Therefore residual saturation should be largest in the Portland cores, then the Ketton cores then the Estaillades cores. The Ketton and Estaillades cores are consistent with this trend but the Portland residual saturation is low. This may be due to the length of time the Portland cores needed for imbibition to occur leading brine evaporation. High permeability has been correlated with less trapping (Tanino & Blunt 2012), so the Ketton cores should have a lower residual non-wetting phase saturation than shown in **Fig. 16.** This would need to be investigated further with analysis of the Ketton cores pore structure and the saturation profile during imbibition.

Conclusions and Future Work

1. The rate of imbibition is highly dependent on the permeability of the core, with an increase in permeability leading to a much steeper imbibition rate curve.
2. The amount of brine imbibed is proportional to the square root of time. This relationship means that a small increase in the length of the core leads to a large increase in the time needed for imbibition to fully occur.
3. Schmid and Geiger (2012) dimensionless time correlates the carbonate cores very well, and is easy to implement on laboratory data due to not requiring a permeability measurement.
4. This correlation can be fitted by the mass transfer function proposed by Aronofky et al. (1958) using the 0.05 constant proposed by Ma et al. (1995) and by using the analytical oil recovery solution presented by Tavossoli et al. (2005 a) with a γ=0.01.
5. Ma et al. (1995) dimensionless time fails to take into account the varying core length data.
6. The correlation seen when using Li and Horne (2004) is unreliable due to the mathematical manipulation of using the t_D component in the x axis as the main component in the y axis.
7. Capillary trapping seen to be larger when the non-wetting phase is oil compared to gas.

Further work using Micro Computerized Tomography (CT) could be used to analyse the movement of the brine saturation front. This would give more accurate results than analysing the weight increase due to imbibition. Further analysis could also be done using pore scale modelling as to try represent the experimental results theoretically. Further work needs to be done on the spontaneous imbibition into cores of varying wettability to analyse how this affects the correlation found from the scaling equation. Experiment 2 needs repeating with further time taken to fully saturate the core with brine. The work done on capillary trapping is interesting but not consistent with current industry opinion. The experiments may have to be repeated to examine this effect further.

Conversion factors

D x 9.869233e-13 = m^2

Nomenclature

SI= Spontaneous Imbibition
CCS= Carbon Capture and Storage
Q= Flow rate
μ= Viscosity
P= Pressure
K= Permeability
σ= Interfacial Tension
Pc=capillary pressure

R=recovery.
S=saturation.
t=time
V=volume
Φ=porosity
ρ=density
A=Area
F_s=Shape factor proposed by Kazemi et al.
L_c=characteristic length
G=The acceleration due to gravity

Subscripts

D=dimensionless.
I=initial.
O=oil.
R=residual.
T=total.
W=water.
∞ **=**ultimate (at infinite time).
D,MK=dimensionless time shown by Mattax and Kyte (1962)
b=bulk volume
f=front

Acknowledgements

Thank you to Tanino and Blunt (2012) for allowing me to use their Unpublished XRD measurments. Further thanks to Nayef Al-Ansi and Martin Blunt for their supervision and guidence throughout the project. This material is based on work supported by Qatar Petroleum, Shell and the Qatar Science and Technology Park under the Qatar Carbonates and Carbon Storage Research Centre.

References

Aronofsky, J. S., L. Masse, and S. G. Natanson, "A model for the mechanism of oil recovery from the porous matrix due to water invasion in fractured reservoirs," *Petrol. Trans. AIME* (1958) 213, 17–19.

Albion Stone Technical Data, "Jordans Basebed, Revision 6", *Albion Stone, Robert Denholm House, Bletchingly Road, Nutfield Surrey, RH1 4HW, England* (March 2010),

Blunt, M. J., B. Bijeljic, H. Dong, O. Gharbi, S. Iglauer, P. Mostaghimi, A. Paluszny, and C. Pentland.: "Porescale imaging and modelling*", Advances Water Res.* (April 2012), doi: 10.1016/j.advwatres.

Boubiaux, B. J., Kalaydjian, F. J. and the Ins. Francais du Petrole.: " Experimental study of cocurrent and countercurrent flows in natural porous media". *SPE Reservoir Engineering*. (August 1990) 5 (3), 361-368

Ceil, M., Reis, J. C., Miller, M. A. and Misra, D.: "An Examination of Counter Current Capillary Imbibition Recover form Single Matrix-Blocks and Recovery Predictions by Analytical Matrix/Fracture Transfer Functions". In: SPE 49005, Proceeding of the SPE Annual Technical Conference Exhibition, (1998), New Orleans, Louisiana, USA, 27-30. Richardson, Texas, Society of Petroleum Engineers.

CRC Handbook of Chemistry and Physics; 87th Edition (2006-2007). Editor; Lide, D.R.

Dautriat, J., N. Gland, A. Dimanov, and J. Raphanel, "Hydromechanical behavior of heterogeneous carbonate rock under proportional triaxial loadings" *J. Geophys. Res.*, (January 2011), 116(B01205), doi:10.1029/2009JB000830.

Garg, A., Zwahlen, E. and Patzek, T.W. "Experimental and numerical studies of one-dimensional imbibition in Berea sandstone" In: Proceedings of the Sixteenth Annual American Geophysical Union Hydrology Days, Fort Collins, CO, 15–18 (April 1996), pp. 171–183.

Hamon, G. and Vidal, J. "Scaling-up the capillary imbibiton process from laboratory experiments on homogenous and heterogenous samples" In: SPE European Petroleum Conference, London 20-22 October 1986, SPE 15852

Kashchiev, D., Firoozabadi, A.: "Analytical solutions for 1D counter-current imbibition in water-wet media". *SPE J.* (December 2003) 8, 401-408.

Kazemi, H.,Gilman, J.R., and Eisharkawy, A.M.: "Analytical and Numerical Solution of Oil Recovery From Fractured Reservoirs with Empierical Transfer Function," *SPERE* (May 1992) 219

Klinkenberg, L. J.: "The Permeability Of Porous Media To Liquids And Gases," *Drilling and Production Practice*, (1941), pg. 200-213

Le Guen, Y., F. Renard, R. Hellmann, E. Brosse, M. Collombet, D. Tisserand, and J.-P. Gratier, "Enhanced deformation of limestone and sandstone in the presence of high PCO2 fluids", *J. Geophys. Res.*, (May 2007), 112, B05421, doi:10.1029/2006JB004637

Lefebvre Du Prey, E.: "Gravity and Capillary Effects on Imbibition Porous Media". *Society of Petroleum Engineers Journal*. (June 1978) SPE no. 6192, 195-206.

Li, K. and Horne, R. N.: "An Analytical Scaling Method for Spontaneous Imbibition in Gas/Water/Rock Systems." *SPE Paper (*September 2004) 88996 In: presented at the 2002 SPE/DOE Improved Oil Recovery Symposium, Tulsa, 13–17 April

Ma Shouxiang., Morrow, N. R. and Zhang, X.: " Generalized scaling of spontaneous imbibition data for strongly water-wet systems." *Journal of Petroleum Science and Engineering.* (October 1997) 18 (3-4), 165-178

Mattax, C. C., Kyte, J. R.: "Imbibiton oil recovery from fractured, water- drive reservoir." *Society of Petroleum Engineers Journal*. (June 1962) 2 (2), 177-184.

Morrow, N. R., Mason, G.: "Recovery of oil by spontaneous imbibition." *Current Opinion in Colloid & Interface Science*. (August 2001) 6 (4), 321-337

Olafuyi, O.A. , Cinar, Y., Knackstedt, M.A., Pinczewski. W.V.: "Spontaneous Imbibition in Small Cores." *SPE* (November 2007) 109724

Pooladi-Darvish, M. and Firoozabadi, A.: "Cocurrent and Countercurrent Imbibition in a Water-Wet Matrix Block." *Society of Petroleum Engineers.* (March 2000). 5 (1), 3-11

Rapoport, L. A., "Scaling laws for use in design and operation of water-oil flow models", *Trans. AIME*, (October 1955) 204, 143–150.

Schmid K.S. , Geiger. S: "Universal scaling of spontaneous imbibition for water-wet systems", Water Resources Research, (2012) VOL. 48, W03507

Tanino, Y. and Blunt, M.: "Capillary trapping in sandstones and carbonates: dependence on pore structure" *Water Resources Research* (June 2012) doi:10.1029/2011WR011712, in press.

Tanino Y, El-Maghraby RM, Blunt MJ, "Capillary trapping of CO_2in brine: a review of recent laboratory measurements on Berea sandstone", under review, *International Journal of Greenhouse Gas Control*.

Tavassoli, Z., Zimmerman, R. W. and Blunt, M. J.: "Analytical analysis for oil recovery during counter-current imbibition in strongly water wet systems." *Transp Porous Med.* (April 2005a) 58, 173-189.

Tavassoli, Z., Zimmerman, R. W. and Blunt, M. J. "Analysis of counter- current imbibition with gravity in weakly water- wet systems." *Journal of Petroleum Science and Engineering*. (April 2005b) 48, 94-104.

Viksund, B.G., Morrow, N.R., Ma, S., Wang, W., and Graue, A. "Initial Water Saturation and Oil Recovery From Chalk and Sandstone by Spontaneus Imbibition." Paper Presented at the Intl. Symposium of the Soc. Of Core Analysts, The Hague, 14-16 September 1998.

Watson, J.,"British and Foreign Building Stones: A Descriptive Catalogue of the Specimens in the Sedgwick Museum", *Cambridge Univ. Press, Cambridge*, U. K., (1911) doi:10.1017/S0016756800111410.

Zhang, X., Morrow, N. R. and Ma, S.: "Experimental verification of a modified scaling group for spontaneous imbibition." *SPE Reservoir Engineering.* (November 1996) 11, 280-285.

Zimmerman, R. W., Bodvarson, G.S. and Kwicklis, E. M.: "Absorption of water into porous blocks of various shapes and sizes". *Water Resour. Res.* (June 1990) 26 (11), 2797-2806.

APPENDICES

Appendix A: Milestones

Table A - 1: Milestones in the understanding of Spontaneous Imbibition

TABLE OF CONTENT SPE Paper n°	Year	Title	Authors	Contribution
Phys Rev 1921;17:273 283.	1921	The dynamics of capillary flow	Washburn EW	First to provide an analysis of imbibition into a capillary tube.
SPE 415-G	1955	Scaling Laws for Use in Design and Operation of Water-Oil Flow Models	L.A. Rapoport	First to take into account gravity and capillary forces to create an accurate scaling group.
SPE932-G	1958	A Model for the Mechanism of Oil Recovery from the Porous Matrix Due to Water Invasion in Fractured Reservoirs	J. S. Aronofsky L. Masse	First to develop a method of extrapolating field recoveries in fractured reservoirs.
SPE 1361-G	1960	Determination of Effective Capillary Pressures for Porous Media from Imbibition Data	L.L. Handy	First to develop a scaling equation when looking at the piston like water advance in oil recovery From the slope of Q2 vs. t, one can compute an effective Pc.
SPE J 1962;June:17 7 184	1962	Imbibition oil recovery from fractured, water-drive reservoir.	Mattax CC, Kyte JR	First to define a scaling group to accurately scale laboratory data to actual fractured reservoirs, then test this scaling equation on experimental data.
SPE 18283-PA	1990	Experimental Study of Co current and Counter current Flows in Natural Porous Media	Bourbiaux, Bernard J., Kalaydjian, Francois J.	First to investigated the differences between co-current and counter current spontaneous imbibition. Noticed that countercurrent oil production is much slower than that of co current productions, with final oil recovery being greater in co current flow. Viscous coupling has opposite effects in co current and countercurrent flows, which is why relative permeabilities are lower in countercurrent flows
Journal of Petroleum Science and Engineering (1997), 18, 165-178.	1995	Generalized Scaling of Spontaneous Imbibition Data for Strongly Water-Wet Systems	Ma, S., Morrow, N.R., & Zhang, X.	First to analyze the viscosity ratio with respect to the dimensionless time proposed by Mattax and Kyte (1962). Found taking the geometric mean of the water and oil viscosities worked well to scale imbibition data.
SPE 30762-PA	1996	Experimental Verification of a Modified Scaling Group for Spontaneous Imbibition	Zhang, Xiaoyun, Morrow, Norman R., Ma, Shouxiang	First to analyze all the scaling equations developed experimentally varying boundary conditions. Furthermore, a characteristic length was developed that can correlate imbibition results for systems with different shapes and boundary conditions
SPE/DOE 35436	2000	Interrelationship of Wettability, Initial Water Saturation, Aging Time, and Oil Recovery by Spontaneous Imbibition and Water flooding	Zhou X, Morrow NR and Ma S	First paper to examine the relationship between wettability, initial water saturation, aging time and oil recovery with respect to Spontaneous Imbibition. Found correlated spontaneous imbibition data can be used to characterize wettability.
Petroleum Society of CIM Paper No. 95-138	2000	Cocurrent and Countercurrent Imbibition in a Water-Wet Matrix Block	Mehran Pooladi-Darvish, Abbas Firoozabadi	First to analyze the differences in co-current and counter current flow in actual reservoirs. Found that when a water-wet porous media is partially in contact with water, oil recovery is dominated by co current imbibition, not counter current.
Transp Porous Med. 58, 173-189.	2005a	Analysis of counter-current imbibition with gravity in weakly water-wet systems	Tavassoli, Z., Zimmerman, R. W. and Blunt, M. J.	Two analytical solutions are found, one for early time and one for late time recovery. These give a better match than Aronofsky et al., 1958 for early and late time flow.
SPE 109724	2007	Spontaneous Imbibition in Small Cores	Olafuyi O.A,Cinar Y, Knackstedt MA, Pinczewski WV	First to examine spontaneous imbibition into cores with bulk volumes of 0.1 to 12 cm^3 to validate information gained from micro CT images.
WATER RESOURCES RESEARCH, VOL. 48, W03507	2012	Universal scaling of spontaneous imbibition for water-wet systems	K. S. Schmid and S. Geiger	Using the Darcy Equation along with 70 years literature into SI created a “Master Equation” for scaling.

Appendix B: Critical Literature Review

SPE 415-G, 1955
Scaling Laws for Use in Design and Operation of Water-Oil Flow Models
Authors: L.A. Rapoport
Contribution to field of Spontaneous Imbibition
Created a scaling law which takes into account gravitational and capillary forces.
Objective of the paper:
To take into account as many forces and petrophysical properties as needed in a mathematical formulation for 3D 2-phase flow systems. Then test the Equation developed along with laboratory data on representative field behaviour.
Methodology used:
Establish a scaling law based on a three-dimensional, homogeneous, porous medium simulating the flow of two immiscible, incompressible fluids such as oil and water. Then test this scaling model against experimental data along with field data.
Conclusion reached:

1. Found the scaling laws to adequately describe the physical concepts of micro-behavior of fluids in porous media

Comments:
The scaling equations are complex and scattered throughout the paper. However, Does give useful background knowledge.

SPE932-G, 1958

A Model for the Mechanism of Oil Recovery from the Porous Matrix Due to Water Invasion in Fractured Reservoirs

Authors: J. S. Aronofsky and L. Masse

Contribution to field of Spontaneous Imbibition

The paper presents a method of extrapolating field recoveries in fractured oil reservoirs being produced by water invasion.

Objective of the paper:

The objective is to create a model of the physical process occurring when fractured oil reservoirs have an aquifer influx and imbibition is occurring, then test this model on real oil field data. Furthermore, the paper aims to understand and explain the increase of recovery with time observed in this type of oil field recovery process.

Methodology used:

An abstract model is created based on results from water flood and imbibition tests relating a function of time to the relative production from a matrix volume. The recoveries seen are then compared to a model involving the whole reservoir. This whole reservoir model is in turn compared to actual field data.

Conclusion reached:

1. The considerable variation in observed recoveries in fractured reservoirs with time is explained.
2. A method of extrapolating field recoveries is presented

$$\frac{R}{R_\infty} = 1 - e^{ct_D}$$

Where R is oil recovery by imbibition, R_∞ is ultimate oil recovery by imbibition and c is the oil decline constant
3. It has been found that the mechanism of oil production from water invasion in a fractured reservoir may be a very lengthy process.

Comments:

Very interesting, will test out the model on experimental data after scaling.

SPE 1361-G, 1960
Determination of Effective Capillary Pressures for Porous Media from Imbibition Data
Authors: L.L. Handy
Contribution to field of Spontaneous Imbibition
Investigated experimentally the effect on oil recovery from imbibition and presented an Equation to predict this process.
Objective of the paper:
To mimic a piston like water advance in an air saturated water wet rock, then analyse the results using a combination of Darcy's Equation, capillary pressure Equation and the Equation of continuity, with the required boundary conditions.
Methodology used:
The two main boundary conditions used to simplify the Equation proposed are that the water imbibes in a piston like manner and that the pressure gradient in the gas ahead of the water front can be neglected. In the experimental method consolidated sandstone which had been fired was used. The imbibition experiments involved placing a core on a saturated sand pack and examining how the amount of brine in the sand pack decreases over time.
Conclusion reached:

1. Following Equation found for predicting water imbibition in porous media

$$Q_w{}^2 = \left(\frac{2P_c k_w \phi A^2 S_w}{\mu_w}\right) t$$

Where ϕ is fractional porosity, S_w is the fractional water content of the pore spaces, k_w, is the effective water permeability in darcies, μ_w is the water viscosity in centipoises, P_c is the capillary pressure, A is the cross sectional area and t is the time in seconds

2. Using the Equation above the effective capillary pressure can be derived from an imbibition experiment which is a measure of the wettability properties of the rock surfaces.
3. Main assumption being that water displaces air in a piston-like manner.
4. From the slope of Q^2 vs. t, one can compute an effective P_c which can be used to measure rock wettability

Comments:
Good paper, especially when explaining how to apply the scaling equations and model to a real resevoir.

SPE 187-PA (June 1962):
Imbibition Oil Recovery from Fractured, Water-Drive Reservoirs
Authors: Mattax, C.C. and Kyte, J.R.,
Contribution to field of Spontaneous Imbibition
A scaling Equation to predict recovery behaviour for fractured- matrix, water- drive reservoirs is defined.
Objective of the paper:
The objective of the paper is that using the scaling relationship devised, the recovery behaviour for a large reservoir can be found from an imbibition test on a small reservoir core sample.
Methodology used:
Rapoports scaling laws were used, which were produced for scaling water floods for model tests of imbibition oil displacements. Then these scaling laws were tested on experimental data. Linear and 3-dimensional experiments were done on Al undum and Sandstone cores.
Conclusion reached:

1. Using the following Equation imbibition tests on small reservoir samples can be used to predict imbibition oil recovery behavior for large reservoir matrix blocks.

   $$t_{D,MK} = t\sqrt{\frac{k}{\Phi}}\frac{\sigma}{\mu_w}\frac{1}{L^2}$$

   $t_{D,MK}$=dimensionless time, t=imbibition rate, k=permeability, Φ=porosity, σ=interfacial tension, μ_w=water viscosity L=characteristic length

Comments:
The scaling law laid down by this paper is refined by papers later on.

Journal of Petroleum Technology, October 1987
Wettability Literature Survey- Part 4: The Effects of Wettability on Capillary Pressure
Authors: W.G. Anderson
Contribution to field of Spontaneous Imbibition
The paper gives a synopsis of some of the important advances in knowledge of spontaneous imbibition.
Objective of the paper:
The objective is to investigate the role of wettability on the capillary pressure curve, residual saturations, and imbibition behaviour. Furthermore, investigate the interaction of wettability, initial saturation and saturation history on imbibition.
Methodology used:
The paper looked at the following areas of core analysis; contact angles, capillary pressures (in different wettability systems), experimental wettability effects, effects of surface roughness, effects of wettability on irreducible saturations, and displacement capillary pressure.
Conclusion reached:

1. No simple relationship exists that relates the capillary pressures determined at two different wettibilities. An apparent contact angle calculated from either the displacement capillary pressure or the complete capillary pressure curve is only a rough estimate.
2. The drainage Pc in a uniformly wetted porous medium is less than 50 degrees (due to pore geometry effects and the rough surfaces of the porous medium). The spontaneous imbibition capillary pressure curve in a uniformly wetted curve is insensitive when the contact angle is less than 20 degrees

Comments:
Good for background information. A bit dated compared to Morrow and Mason (2001).

SPE 18283-PA, (August 1990)
Experimental Study of Co current and Counter current Flows in Natural Porous Media
Authors: Bourbiaux, Bernard J., Kalaydjian, Francois J.
Contribution to field of Spontaneous Imbibition
Experimental analysis of both co current and counter current spontaneous water/oil imbibition
Objective of the paper:
To analyse co current and counter current spontaneous water/oil imbibition with various boundary conditions experimentally then test a numerical model against the results. The experimental work was done using various boundary conditions to test various stages of co current and counter current imbibition. The capillary pressure and relative permeabilities will also be tested in the cores as to be analysed along with the other SI parameters.
Methodology used:
Perform experiments on the same vertical sample of fine water-wet sandstone under various boundary conditions to generate co current and counter current flow. Then simulate the results with a 1 D model using Darcy generalized Equations. The fluids used are a paraffinic refined oil and brine; with saturation measurements performed using the X-ray absorption method. One or two ends of the sample were put in contact with the brine to study the two mechanisms of co current and counter current flow separately or simultaneously.
Conclusion reached:

1. The rate of countercurrent oil production is much slower than that of co current productions.
2. A desaturation front with a smooth slope is observed in co current flow, in counter current flow the desaturation front is diffuse and extended.
3. Final oil recovery is greater in co current flow, which may be due to local heterogeneities.
4. Countercurrent half recovery time is underestimates by about 25% if co current relative permeabilities are used in the numerical model
5. Viscous coupling has opposite effects in co current and countercurrent flows, which is why relative permeabilities are lower in countercurrent flows

Comments:
Very useful in reference to the two experiments completed. The paper gives a good background into the physical processes occurring in the varying imbibition methods.

Proceedings of the Sixteenth Annual American Geophysical Union Hydrology Days, Fort Collins, 15-18 pp. 171-183 (April 1996)

Experimental and Numerical Studies of One-Dimensional Imbibition in Berea Sandstone

Authors: Garg, A., Zwahlen, E. and Patzek, T.Garg,

Contribution to field of Spontaneous Imbibition

By using Computerized Tomography could better understand the physical processes going on during imbibition.

Objective of the paper:

Experimentally measure the cumulative imbibition in sandstone. Then from the slope of saturation vs. square root of time measure the cumulative imbibition, permeability, and capillary pressure.

Methodology used:

Use Computerized Tomography (CT) visualisation to image the water saturation during imbibition to better understand the physical processes going on during imbibition. A mathematical model is also developed to simulate imbibition.

Conclusion reached:

1. CT images show a homogenous, very sharp water front at the early stages of imbibition, changing gradually into a less sharp front at later times.
2. Good matching between the non-linear numerical model and the experiment
3. Square root t dependency found at early times.

Comments:

Square root dependency will be analysed further in the experimental reports analysis.

Petroleum Society of CIM Paper No. 95-138, (October 1995)
Generalized Scaling of Spontaneous Imbibition Data for Strongly Water-Wet Systems
Authors: S. Ma, M.R. Morrow and X. Zhang
Contribution to field of Spontaneous Imbibition
Scaling group that can correlate data on oil recovery from strongly water wet media by SI.
Objective of the paper:
To define a new dimensionless time for strongly water wet rocks with varying porous media, dimensions, boundary conditions and oil and water viscosities. Then compare this new scaling model to that presented by Mattax and Kyte (1962) using data from Zhang et al.
Methodology used:
By correlating the differences in sample size, shape and boundary conditions by a generalised characteristic length the data can related on a plot of % oil recovery by imbibition vs. dimensionless time. The difference in viscosity ratio also need correlated by taking the geometric mean of the water and oil viscosities.
Conclusion reached:

1. The correlation implies that $\sqrt{(k/\emptyset)}$ provides a satisfactory correlation for the effects of pore structure and transport properties for two-phase counter-current flow.
2. Wettability can be assessed from the reduction in imbibition rate relative to the predicted results for the strongly water wet case.

Comments
Very useful paper, will use scaling equation in analytical analysis.

SPE 30762-PA, (November 1996)
Experimental Verification of a Modified Scaling Group for Spontaneous Imbibition
Authors: Zhang, Xiaoyun, Morrow, Norman R., Ma, Shouxiang
Contribution to field of Spontaneous Imbibition
The validity of different scaling Equations was checked using experimental SI data with Berea sandstone.
Objective of the paper:
To check the assumption that a characteristic length along with a geometric mean of water and oil viscosities is appropriate in creating a generalized correlation between oil recovery and dimensionless time. This was checked for systems with different sample shapes, boundary conditions, and oil/water viscosity ratios.
Methodology used:
13 experiments were undertaken using brine and white oil. The cores were suspended from a balance and immersed in brine with the change in weight being monitored. A Teflon rod was used to remove expelled oil from the core surface before measuring each data point.
Conclusion reached:

1. A characteristic length can be defined that correlates imbibition results for systems with different shapes and boundary conditions.
2. A generalized correlation could be obtained between oil recovery and dimensionless time.
3. Ultimate oil recovery by SI is approximately constant for systems with difference core lengths, boundary conditions, and viscosity ratios.

Comments
Good discussion of the effect of boundary conditions.

SPE/DOE 35436 (June 2000)
Interrelationship of Wettability, Initial Water Saturation, Aging Time, and Oil Recovery by Spontaneous Imbibition and Water flooding
Authors: Xianmin Zhou, Norman R. Morrow, and Shouxiang Ma
Contribution to field of Spontaneous Imbibition
Experiments were performed to examine the relationship between wettability, Swi, aging time and oil recovery with respect to Spontaneous Imbibition.
Objective of the paper:
To examine how the wettability of Berea sandstone cores along with prude bay crude oil and synthetic formation brine changes with varying changes of initial water saturation and length of aging time. Then pairs of spontaneous imbibition and waterflood curves were created for several induced wetting states and any trends were analysed.
Methodology used:
Dry Berea core samples were vacuumed and saturated with brine, with porosity being determined from the change in weight. The brine was displaced by the crude oil to get to the S_{wi}'s required. The core samples were then immersed with crude oil and aged. The spontaneous imbibition and waterflood measurements were made after displacing the oil in the core during aging with stock crude oil. The spontaneous imbibition measurements were done by suspending the core in degassed brine by monofilament line attached to an electronic balance, with the weight change recorded vs. time. The amount of oil expelled was determined gravimetrically. The waterflood tests were done at slow rates with oil production vs time determined from volumetric measurements.
Conclusion reached:

1. Correlated spontaneous imbibition data can be used to characterize wettability.
2. Increasing the aging time results in a decrease in the water wetness of the cores.
3. When wetness is decreased from very strongly water wet, the oil recovery due to spontaneous imbibition passes through a maximum.
4. For this rock type, a decrease in water wetness leads to a high oil recovery due to waterflooding.

Comments
Interesting, would like to look into the difference in wettability on spontaneous imbibition in the future.

Petroleum Society of CIM Paper No. 95-138, (March 2000)
Cocurrent and Countercurrent Imbibition in a Water-Wet Matrix Block
Authors: Mehran Pooladi-Darvish, Abbas Firoozabadi
Contribution to field of Spontaneous Imbibition
Mathematically and physically compare the differences between co-current and counter current imbibition.
Objective of the paper:
Create a theoretical study comparing the two imbibition processes, studying the similarities and differences to point out the consequences for physical applications.
Methodology used:
By investigating the Equations and boundary conditions for co current and counter current imbibition a numerical model can be developed to compare the behaviour and recovery efficiencies. This numerical model can then be validated against analytical solutions for the two imbibition processes. The scaling criterion presented by Rapoport is tested against the solutions to check its validity.
Conclusion reached:

1. When a water-wet porous media is partially in contact with water, oil recovery is dominated by co current imbibition, not counter current.
2. Co current imbibition can be much more efficient than countercurrent imbibition.
3. The time for a specific recovery by co current imbibition is a fraction of that by countercurrent imbibition.
4. The scaling criterion of Rapoport is valid for both co and countercurrent imbibition. However, oil recovery calculations based on scaling studies of countercurrent imbibition, when used for a co current process, lead to pessimistic recovery predictions.
5. The diffusion Equation may be inappropriate for the description of oil recovery by co current imbibition; the oil pressure gradient must be included.

Comments
Well explained theoretical explanation which supports this report for use in real reservoir analysis.

PETROPHYSICS.V OL. 42. NO. 4: P. 313-322; 9 FIG.S (July-August 2001)
Oil Recovery by Spontaneous Imbibition from Weakly Water-Wet Rocks
Authors: Xina Xie and Norman R. Morrow
Contribution to field of Spontaneous Imbibition
Oil recovery and wetting property prediction through analysis of spontaneous imbibition in fractured reservoirs
Objective of the paper:
To test semi-empirical correlations set up for the imbibition of brine into porous media initially saturated with oil for weakly water-wet conditions and different geometries.
Methodology used:
After initial water saturations are calculated (ranging from 14 – 31%) the wettability of samples was changed through aging in crude oil at an increased temperature. This changed the wettability to a weakly water wet. This was done for varying geometries of cores (cylindrical, annular, and rectangular) and boundary conditions (using epoxy resin to seal off part of the cores).
Conclusion reached:

1. S_{wi} is extremely important on the rate of oil recovery.
2. Imbibition time will decrease systematically with a decrease in the S_{wi}.
3. An epoxy resin presence during the aging of sandstone with crude oil will have a reduced water wetness to just aging with crude oil alone
4. A characteristic length used to scale size, shape and boundary conditions for strongly water wet cores shows scaling for weakly water wet cores.

Comments
Good analysis of the effect of Swi on oil recovery. Will analyze this further in comparing Experiment 1 to Experiment 2.

Current Opinion in Colloid & Interface Science 6 Ž2001. 321337 (August 2001)
Recovery of oil by spontaneous imbibition
Authors: Norman R. Morrow, Geoffrey Mason,
Contribution to field of Spontaneous Imbibition
Review of developments in the scaling of laboratory imbibition data.
Objective of the paper:
Results for variation in interfacial tension, wetting and non-wetting phase viscosity, sample size, shape and boundary conditions, and initial wetting phase saturation have been correlated for a variety of strongly water-wet rocks as plots of normalized oil recovery vs. dimensionless time. Correlations have been tested for weakly water-wet conditions induced by adsorption from crude oil. In situ fluid saturation measurements have been used to distinguish between modes of imbibition that range from frontal to global displacement. Research on surfactant-enhanced imbibition has advanced from laboratory to field tests.
Methodology used:
The following components of spontaneous imbibition are discussed, Imbibition into completely wetted capillaries (Cylindrical capillary, Tubes with corners), Imbibition in porous media, Scaling of spontaneous imbibition, Very strongly water-wet media (Characteristic length, Viscosity ratio, Rock properties, Mobility ratio, Initial water saturation, Co-current imbibition), Wettability and imbibition (Wettability control, Uniformly wet porous media, Mixed wettability, Mixed wettability in tubes with corners, Contact angles after adsorption from crude oil, Preparation of mixed-wet cores) Large-scale laboratory models and imbibition Mechanisms, Imbibition of surfactant solutions.
Conclusion reached:

1. Emphasis of research on low permeability fractured reservoirs
2. Mixed wet imbibition behavior is now well recognized and is likely to be the focus of research for a long time
3. Advances in pore scale mechanisms will come from further spontaneous potential experiments in single capillaries and laboratory micromodels.
4. Effects of gravity segregation need a better understanding.

Comments
An extremely useful paper for introducing the basics of spontaneous imbibition.

SPE 87333-PA, (December 2003)
Analytical Solutions for 1D Counter current Imbibition in Water-Wet Media
Authors: Dimo Kashchiev, Abbas Firoozabadi,
Contribution to field of Spontaneous Imbibition
Supply's analytical solutions for 1D counter current flow of water and oil.
Objective of the paper:
Define expressions for the time dependence of the water saturation profile and the oil recovered during spontaneous counter current imbibition in cylindrical cores. Then compare the analytical solutions found with existing numerical solutions and experimental data for cores with strong water wettability.
Methodology used:
Diffusivity coefficient is found for the flow of water and oil, then this is analysed with respect to linear imbibition, cylindrical imbibition and spherical imbibition to find further Equations. These models are then analysed with respect to oil recovery and finally with respect to experimental data.
Conclusion reached:

1. The advancement of the water front obeys the Einstein-type relation and the normalized water saturation profile can be given by a general Equation for linear cylindrical and spherical cores.
2. General expressions of the fraction of oil recovered during the initial stages of countercurrent imbibition can be produced.
3. For linear imbibition, initially the fraction of oil recovered is proportional to $t^{1/2}$

Comments
Useful conclusions reached.

SPE 88996-PA, (September 2004)
An Analytical Scaling Method for Spontaneous Imbibition in Gas/Water/Rock Systems
Authors: Kewen Li and Roland N. Horne
Contribution to field of Spontaneous Imbibition
The paper further develops scaling coefficients which take into account capillary and gravity forces.
Objective of the paper:
A method was developed to scale the experimental data of spontaneous water imbibition (co current) for gas/water/rock systems.
Methodology used:
In this method, a dimensionless time was defined with the effects of relative permeability, wettability, and gravity included. The definition was not empirical but based on a theoretical derivation. scaled. The scaling model proposed in this study for gas/water/rock systems was verified experimentally for different rocks (Berea, chalk, and graywacke from The Geysers).
Conclusion reached:

1. The following scaling coefficients are found

$$t_d = \left(\frac{b}{a}\right)^2 \frac{k_w}{\phi} \frac{P_c}{\mu_w} \frac{S_{wf} - S_{wi}}{{L_a}^2} t$$

Q_w=the volumetric rate of water imbibition N_{wt} =the accumulative volume of water imbibed into rocks R=the recovery in terms of pore volume and is equal to N_{wt}/V_p (V_p=the pore volume).
The constant a is associated with capillary forces

$$a = \frac{Ak_w(S_{wf} - S_{wi})}{\mu_w L} P_c$$

A and L = the cross sectional area and the length of the core $\mu_w = \text{the viscosity of water}$ $S_{wi} = \text{the initial water saturation}$ S_{wf}= the water saturation behind the imbibition front k_w= the effective permeability of the water phase at a water saturation S_{wf}, P_c= the capillary pressure at S_{wf}.
The constant b is associated with gravity forces

$$b = \frac{Ak_w}{\mu_w} \Delta p g \sin\beta$$

Δp= the density difference difference between water and gas, g= the gravity constant, β= the longitudinal angle between the axis of the core sample and the horizontal direction.

Comments
Interesting paper, although do not trust the mathematical manipulation to create the correlating graph. Will analyze further in report

SPE 96812-MS (9-12 October 2005)
Spontaneous imbibition with matched liquid viscosities
Authors: H. Fischer and N.R. Morrow,
Contribution to field of Spontaneous Imbibition
A study analysing the effect of spontaneous imbibition on strongly water wet cores for varying viscosity ratios.
Objective of the paper:
Report the effect of spontaneous imbibition for boundary conditions of all core faces open, two end closed (radial imbibition), and one end open (linear imbibition). Then correlate the results using the Mattax and Kyte scaling group using a characteristic length.
Methodology used:
The densities of the oleic and aqueous phases were measured by Paar Density Meter 48, and viscosities by Cannon viscometers, and interfacial tension by a Kruss Drop Volume Tensiometer DVT-10. The oil production as a function of time was measured in standard glass imbibition cells at ambient temperature. The boundary conditions were put into place by using an epoxy resin seal.
Conclusion reached:

1. The Mattax and Kyte scaling group was satisfactory for viscosities for all boundary conditions
2. In radially dominated imbibition final oil recoveries were independent of viscosity.
3. In linear imbibition the final oil recoveries were consistently lower decreasing up to 2.5 %PV with increase in volume.

Comments
Interesting experimental technique.

Transp Porous Med. 58, 173-189. (2005 a)
Analytical analysis for oil recovery during counter-current imbibition in strongly water wet systems
Authors: Tavassoli, Z., Zimmerman, R. W. and Blunt, M. J.
Contribution to field of Spontaneous Imbibition
Analytical solution for early and late time developed for counter current SI
Objective of the paper:
To create early and late time solutions for counter current imbibition with fewer approximations about the functional form of the saturation profile, capillary pressures and relative permeabilities. The boundary conditions will be treated differently than that of Barenblatt et al. (1990).
Methodology used:
By following the approach of Zimmerman and Bodvarson (1989, 1991) and Zimmerman et al. (1990), the countercurrent imbibition was studied in one dimension for oil/water or NAPL/water systems. The boundary conditions will include making the water mobility zero at the inlet for strongly water-wet systems. The analytical solutions for early and late time are then compared to experimental data.
Conclusion reached:

1. Infinite saturation gradient reached which results in a different functional form of from the exponential recovery previously found.
2. Two analytical solutions are found, one for early time and one for late time recovery. These are compared with experimental data found by Zhang et al. (1996), Hamon and Vidal (1986) and Mattax and Kyte (1962, and a better match than Aronofsky et al., 1958 for early and late time flow.

Comments
Very good theoretical discussion with an analytical solution which will be tested on the experimental data.

Journal of Petroleum Science and Engineering 48 (2005b) 94– 104
Analysis of counter-current imbibition with gravity in weakly water-wet systems
Authors: Tavassoli, Z., Zimmerman, R. W. and Blunt, M. J.
Contribution to field of Spontaneous Imbibition
Found a transfer function for dual- porosity simulation of fractured reservoirs.
Objective of the paper:
Analyse one-dimensional counter-current imbibition in which a non-wetting phase (oil or NAPL) is displaced by a wetting phase (water) under gravity in a system where the displaced fluid mobility remains finite. Then find a transfer function to model this behaviour in fractured reservoirs.
Methodology used:
The integral method has been used to develop an approximate analytical expression for the recovery of non-wetting phase. This approximate solution for oil recovery was then used to derive a transfer function for dual-porosity simulation of fractured reservoirs.
Conclusion reached:

1. The model predicts a square-root and an exponential functional form for the early and late time solutions, respectively. Which were found to provide a good fit to several sets of data from the literature.
2. Transfer function found should provide a more accurate method for modeling counter-current imbibition in fractured reservoirs, as well as providing a sounder mathematical basis for the choice of transfer function.

Comments
Very good theoretical discussion with an analytical solution which will be tested on the experimental data.

SPE 109724 (2007)
Spontaneous Imbibition in Small Cores
Authors: O.A. Olafuyi, Y. Cinar, M.A. Knackstedt, W.V. Pinczewski,
Contribution to field of Spontaneous Imbibition
Co-current spontaneous imbibition into cores with bulk volumes of 0.1 to 12 cm^3.
Objective of the paper:
Sandstone and carbonate cores analysed as to validate the predictive value of network models based on micro-CT images of rock fragments with bulk volumes as small as 0.3 cm^3. These were tested against a range of scaling predictive tools.
Methodology used:
Porosity and permeability of cores was measured using a helium porosimeter and micropermeameter, with the Amott wettability being tested too to confirm the cores are strongly water wet. The bottom face of the core was brought down in contact with the brine and the weight change was measured with respect to time, the core was suspended from a hook underneath a suspended balance. Experiments were conducted at zero initial water saturation.
Conclusion reached:

1. Reliable experiments can be done on cores of homogeneous porous rock have a bulk volume of 0.3 cm^3.
2. Ma et al and Viksund et al models produced a good match for the gas recovery data
3. Li and Horne model failed to correlate the normalised recovery data

Comments
Interesting analysis of the work done by Li and Horne (2004).

SCA2010-12 (October 2010)
Effect of Salinity on Oil Recovery by Spontaneous Imbibition
Authors: Siluni Wickramathilaka, Norman R. Morrow and James Howard
Contribution to field of Spontaneous Imbibition
Analysed the effect of brine salinity during spontaneous imbibition on overall oil recovery.
Objective of the paper:
To analyse sandstone, limestone and reservoir sandstone with results spanning difference in porosity, permeability, pore structure, mineralogy, initial water saturation, and initial and invading water composition. Oil recovery versus time along with changes in the pH and conductivity of the brine were monitored along with the produced crude oil which was checked for the presence of water-in-oil emulsions.
Methodology used:
Cores were vacuum saturated in seawater and pressurized at 1000 psi. The cores were then vacuum saturated and pressurized in the crude oil and aged at 75ºC (Ta) for ten days. The weight of the cores was recorded for the porosity and mass balance calculations. Cores were then oil flooded with RS crude oil. The prepared cores were placed in glass imbibition cells and immersed in the desired brine. The oil recovery versus time was recorded until the imbibition had stabilized or the imbibition rate was extremely slow.
Conclusion reached:

1. Very strongly water wet or mixed wet limestone showed an increase in oil recovery when invading brine salinity decreased
2. Sandstone showed improved oil recovery by imbibition for variations in salinity and composition of brine
3. While a strong correlation has not been established for final oil recoveries versus mineral contents, there was a satisfactory correlation of final oil recovery with total clay content.

Comments
The aging process of the cores was interesting with relation to spontaneous imbibition.

WATER RESOURCES RESEARCH, VOL. 48, W03507, doi:10.1029/2011WR011566, 2012

Universal scaling of spontaneous imbibition for water-wet systems

Authors: K. S. Schmid and S. Geiger

Contribution to field of Spontaneous Imbibition

Scaling group that derived from a direct analytical solution and can serve as a “master Equation” for SI

Objective of the paper:

To create an analytic solution from the 2 phase Darcy Equation by relating the water phase imbibed to the normalised pore volume. Then apply the solution to 42 water oil and water air experiments where water is the wetting phase to investigate the validity compared to other scaling models.

Methodology used:

Vast array of scaling Equations along with proportionality constant taken and analysed with an array of different experimental data to check the validity of each assumption and where each Equation fails and is successful. A model and solution is then devised to correct the limitations of the other Equations. The scaling group was derived from an exact solution to Darcys Equation without the introduction of fitting parameters. This was done by relating the cumulative water phase imbibed to a normalised pore volume.

Conclusion reached:

1. Evidence that the Darcy model is suitable for describing SI
2. Scaling Equation found

$$t_d \propto \left(\frac{2A}{\emptyset L_c}\right)^2 t$$

$$Q_w(t) = 2At^{0.5}$$

A= A constant for each rock which includes all the information about the capillary-hydraulic properties and the initial fluid content (it is still dependent on L_c).

3. Dynamic effects in capillary pressure is not necessary for counter-current SI
4. Scaling group fails for early time for the data group analyzed

Comments

Very good paper which will be further analyzed against the experimental data found.

Appendix C: Porosity and Residual Gas Calculations

7.6 cm Cores – Porosity calculations

Ketton Cores

Table C - 1 Table documenting the pore volume and porosity for the Ketton 7.6

First Reading					After Cleaning			After Cleaning		
Reading 1 (V)	**Reading 2 (V)**	**Φ (%)**	**Average Φ (%)**	**Pore volume ml**	**Φ (%)**	**Average Φ (%)**	**Pore volume ml**	**Φ (%)**	**Average Φ (%)**	**Pore volume ml**
K1										
57.77	19.15	23.45			22.80			22.06		
56.99	18.91	23.34			20.18			18.68		
60.96	20.23	23.31	23.36	19.95	19.11	20.70	17.68	19.21	19.98	17.07
61.81	20.5	23.37			18.75					
60.23	19.98	23.36			19.95					
61.07	20.26	23.34	23.36	19.95	21.53	20.07	17.14			
K2										
66.05	21.99	23.18			22.47					
65.31	22.52	19.36			19.58					
65.66	23.06	17.40	19.98	17.12	19.17	20.41	17.49			
65.24	22.36	20.01								
65.39	22.56	19.30								
65.13	21.9	22.09	20.47	17.54						
K3										
65.85	21.99	22.91			22.57			22.86		
65.08	22.62	18.57			18.30			22.17		
65.11	21.97	21.77	21.08	18.08	22.64	21.17	18.16	22.79	22.23	19.06
65.24	21.93	22.19						21.08		
65.45	22.01	22.14								
65.35	22.38	20.16	21.50	18.43						

Estaillades Cores

Table C - 2 Table documenting the pore volume and porosity for the Estaillades

First Reading					After Cleaning			After Cleaning		
Reading 1 (V)	**Reading 2 (V)**	**Φ (%)**	**Average Φ (%)**	**Pore volume ml**	**Φ (%)**	**Average Φ (%)**	**Pore volume (ml)**	**Φ(%)**	**Average Φ (%)**	**Pore volume (ml)**
E1										
65.31	20.75	28.41			28.63			28.13		
64.38	20.48	28.27			20.01			21.89		
65.06	20.71	28.19	28.29	24.20	22.25	23.63	20.22	21.67	25.01	21.40
64.48	20.54	28.11								
64.96	20.72	27.95								
63.88	20.36	28.04	28.03	23.99						
E2										
64.93	20.73	28.12629			28.34			28.15		
66.09	21.84	24.20359			21.37			26.22		
65.25	20.88	27.86012	26.73	22.96	23.07	24.26	20.84	22.81	25.73	22.10
64.89	21.14	25.81194								
64.6	20.84	26.93135								
64.87	20.84	27.40921	26.72	22.95						
E3										
65.26	20.72	28.54068			28.38			28.38		
64.26	20.61	27.36844			20.24			21.47		
64.54	20.99	25.76963	27.23	23.3119	21.27	23.29	19.95	17.19	19.33	16.55
64.53	20.44	28.81858			25.26					
65.22	20.91	27.40901			26.84					
65.24	20.94	27.2787	27.84	23.8335	25.83	25.98	22.24			

Portland Cores

Table C - 3 Table documenting the pore volume and porosity for the Portland 7.6

First Reading					After Cleaning			After Cleaning		
Reading 1 (V)	**Reading 2 (V)**	**Φ (%)**	**Average Φ (%)**	**Pore volume (ml)**	**Φ(%)**	**Average Φ (%)**	**Pore v (ml)**	**Φ(%)**	**Average Φ (%)**	**Pore v (ml)**
P1										
65.49	22.83	17.92			16.35					
67.05	23.84	15.83			15.40					
65.33	23.35	15.29	16.35	13.96	12.51	14.75	12.60			
64.78	23.16	15.26								
64.85	22.7	17.48								
64.88	23.16	15.42	16.06	13.71						
P2										
64.93	22.53	19.00			19.17					
63.95	22.47	17.67			12.47					
64.33	22.56	17.87	18.18	15.64	12.43	14.69	12.64			
64.08	22.39	18.26								
64.68	22.68	17.89								
65.47	22.74	18.89	18.35	15.78						
P3										
64.94	22.41	19.68			20.12			19.61		
64.02	22.41	18.17			15.64			9.50		
64.88	22.27	20.25	19.36	16.68	18.51	18.09	15.58	10.98		
64.59	22.36	19.34						13.15	13.36	11.51
65.12	22.42	19.92								
64.35	22.27	19.37	19.55	16.83						

7.6 cm Cores – Residual gas saturation calculations

Residual Gas Saturation 1= 1 - (Weight after Vacuum – Dry Weight) / (Pore Volume x Average of before and after Densities)
Residual Gas Saturation 2= 1 - (Weight after Vacuum with Heat Shrink – Dry Weight with Heat Shrink) / (Pore Volume x Average of before and after Densities)

Table C - 4: Residual gas saturations for the 7.6 cm cores.

	Pore Volume (ml)	Weight before w/o sleeve (g)	Weight before w sleeve (g)	Brine Density before experiment (g/cm3)	Weight after w sleeve (g)	Weight after w/o sleeve (g)	Brine Density after experiment (g/cm3)	Sgr 1	Sgr 2
K1	19.94873	176.293	184.8613	1.0462	198.3297	189.6317	1.0463	0.354698	0.36091
K2	17.53781	177.706	187.133	1.0464	200.521	1.0465	1.0465	0.270506	10.62594
K3	18.43428	177.41	186.925	1.0464	200.103	190.473	1.0464	0.316835	0.322797
E1	23.98666	164.452	173.929	Average	191.7567	182.220	1.0411	0.286108	0.288498
E2	22.94977	165.53	174.995	1.0282	191.933	182.377		0.282196	0.286052
E3	23.31187	163.66	173.046	1.0412	194.5976	185.023	1.041	0.112008	0.119763
P1	13.96053	188.3865	197.871	1.0127	208.956	181.997		0.215933	1.451967
P2	15.6391	186.681	196.198	1.04	208.504	198.960	1.0415	0.243936	0.245595
P3	16.8333	185.86	195.421	1.0277	208.563	198.952	1.0439	0.246269	0.249137

Mass Balance Equation:
Pore Volume = (Weight after Vacuum - Dry weight) / (Density after Vacuum)
Total Volume = (PI*Diameter²/4) x Length
Porosity = Total Volume – Pore Volume

20 cm Cores

Table C - 5 Table documenting the pore volume, Sgr and porosity for the K4

K4

Before		After		After Vacuum
Weight (w sleeve) (g)	Weight (w/o sleeve) (g)	Weight (w sleeve) (g)	Weight (w/o sleeve) (g)	Weight (w/o sleeve) (g)
502.058	476.396	541.1	515.438	530.524
Density (g/cu.cm)	1.0401			1.041
	Pore Volume (cu.cm)	51.99615754	Length	20.4465
	Pore Volume (cu.cm)	5.19962E-05	Area	11.38396784
	Total Volume (m3)	0.000232762	Sg1	0.278085592
	Porosity (%)	0.223387369	Sg2	0.278085592

Table C - 6 Table documenting the pore volume, Sgr and porosity for the K5

K5

Before		After		After Vacuum
Weight (w sleeve) (g)	Weight (w/o sleeve) (g)	Weight (w sleeve) (g)	Weight (w/o sleeve) (g)	Weight (w/o sleeve) (g)
503.696	478.331	540.859	515.373	534.48
Density (g/cu.cm)	1.041			1.0406
	Pore Volume (cu.cm)	53.95829329	Length	20.4585
	Pore Volume (cu.cm)	5.39583E-05	Area	11.39095
	Total Volume (m3)	0.000233042	Sg1	0.338390349
	Porosity (%)	0.231539169	Sg2	0.340544502

Table C - 7 Table documenting the pore volume, Sgr and porosity for the K6

K6

Before		After		After Vacuum
Weight (w sleeve) (g)	Weight (w/o sleeve) (g)	Weight (w sleeve) (g)	Weight (w/o sleeve) (g)	Weight (w/o sleeve) (g)
	482.371		520.217	535.323
Density (g/cu.cm)	1.0407			1.0429
	Pore Volume (cu.cm)	50.77380382	Length	20.475
	Pore Volume (cu.cm)	5.07738E-05	Area	11.4214
	Total Volume (m3)	0.000233853	Sg1	
	Porosity (%)	0.217118309	Sg2	0.283766336

Table C - 8 Table documenting the pore volume, Sgr and porosity for the E4

E4

Before		After		After Vacuum
Weight (w sleave) (g)	Weight (w/o sleave) (g)	Weight (w sleave) (g)	Weight (w/o sleave) (g)	Weight (w/o sleave) (g)
466.577	441.119	515.479	490.021	
Density (g/cu.cm)	1.026		1.0303	1.0616
	Pore Volume (cu.cm)	63.27518451	Length	20.375
	Pore Volume (cu.cm)	6.32752E-05	Area	11.25873
	Total Volume (m3)	0.000229397	Sg1	0.2467384
	Porosity (%)	0.275833112	Sg2	0.2467384

Table C - 9 Table documenting the pore volume, Sgr and porosity for the E5

E5

Before		After		After Vacuum
Weight (w sleave) (g)	Weight (w/o sleave) (g)	Weight (w sleave) (g)	Weight (w/o sleave) (g)	Weight (w/o sleave) (g)
514.09	440.671		490.365	506.686
Density (g/cu.cm)	1.043	1.0436		1.0433
	Pore Volume (cu.cm)	63.27518451	Length	20.375
	Pore Volume (cu.cm)	6.32752E-05	Area	11.29345
	Total Volume (m3)	0.000230104	Sg1	0.2452987
	Porosity (%)	0.274985104	Sg2	0.2485934

Table C - 10 Table documenting the pore volume, Sgr and porosity for the E6

E6

Before		After		After Vacuum
Weight (w sleave) (g)	Weight (w/o sleave) (g)	Weight (w sleave) (g)	Weight (w/o sleave) (g)	Weight (w/o sleave) (g)
463.911	440.422	513.618	489.912	545.112
Density (g/cu.cm)	1.0409		1.0428	1.0616
	Pore Volume (cu.cm)	63.27518451	Length	20.3815
	Pore Volume (cu.cm)	6.32752E-05	Area	11.26864
	Total Volume (m3)	0.000229672	Sg1	
	Porosity (%)	0.275502645	Sg2	0.2472317

Table C - 11 Table documenting the pore volume, Sgr and porosity for the P4

P4

Before		After		After Vacuum
Weight (w sleeve) (g)	Weight (w/o sleeve) (g)	Weight (w sleeve) (g)	Weight (w/o sleeve) (g)	Weight (w/o sleeve) (g)
	496.241	557.899	533.362	545.112
Density (g/cu.cm)	1.0474		1.0524	1.0616
	Pore Volume (cu.cm)	46.65934695	Length	20.4515
	Pore Volume (cu.cm)	4.66593E-05	Area	11.51892
	Total Volume (m3)	0.000235579	Sg1	
	Porosity (%)	0.198062259	Sg2	0.2404289

P5

Table C - 12 Table documenting the pore volume, Sgr and porosity for the P5

Before		After		After Vacuum
Weight (w sleeve) (g)	Weight (w/o sleeve) (g)	Weight (w sleeve) (g)	Weight (w/o sleeve) (g)	Weight (w/o sleeve) (g)
520.786	496.694	558.23	534.168	544.993
Density (g/cu.cm)	1.0421	1.0457		1.0459
	Pore Volume (cu.cm)	46.17936705	Length	20.455
	Pore Volume (cu.cm)	4.61794E-05	Area	11.34015
	Total Volume (m3)	0.000231963	Sg1	0.2232606
	Porosity (%)	0.199080945	Sg2	0.2226382

28 cm cores

Table C - 13 Table documenting the pore volume, Sgr and porosity for the K7

K7

Before		After		After Vacuum
Weight (w sleeve) (g)	Weight (w/o sleeve) (g)	Weight (w sleeve) (g)	Weight (w/o sleeve) (g)	Weight (w/o sleeve) (g)
689.745	655.518	743.526	709.299	730.938
Density (g/cu.cm)	1.041		1.0418	1.0435
	Pore Volume (cu.cm)	72.27599425	Length	28.014
	Pore Volume (m3)	7.2276E-05	Area	11.33817
	Total Volume (m3)	0.000317627	Sg1	0.285475335
	Porosity (%)	0.227549553	Sg2	0.285475335

Table C - 14 Table documenting the pore volume, Sgr and porosity for the K8

K8

Before		After		After Vacuum
Weight (w sleeve) (g)	Weight (w/o sleeve) (g)	Weight (w sleeve) (g)	Weight (w/o sleeve) (g)	Weight (w/o sleeve) (g)
	655.668		690.42	705.879
Density (g/cu.cm)	1.041		1.0409	1.0427
	Pore Volume (cu.cm)	48.15479045	Length	28.1565
	Pore Volume (m3)	4.81548E-05	Area	11.3521
	Total Volume (m3)	0.000319635	Sg1	0
	Porosity (%)	0.150655371	Sg2	0.306717182

Table C - 15 Table documenting the pore volume, Sgr and porosity for the K9

K9

Before		After		After Vacuum
Weight (w sleeve) (g)	Weight (w/o sleeve) (g)	Weight (w sleeve) (g)	Weight (w/o sleeve) (g)	Weight (w/o sleeve) (g)
723.819	688.126	774.093	738.4	765.824
Density (g/cu.cm)	1.0411		1.0416	1.0426
	Pore Volume (cu.cm)	74.52330712	Length	29.3
	Pore Volume (m3)	7.45233E-05	Area	11.32524
	Total Volume (m3)	0.00033183	Sg1	0.35217963
	Porosity (%)	0.224583106	Sg2	0.35217963

Table C - 16 Table documenting the pore volume, Sgr and porosity for the E7

E7

Before SI		After SI		After Vacuum
Weight (w sleeve) (g)	Weight (w/o sleeve) (g)	Weight (w sleeve) (g)	Weight (w/o sleeve) (g)	Weight (w/o sleeve) (g)
662.832	629.606	735.611	701.907	724.061
Density (g/cu.cm)	1.0426		1.045	1.0446
	Pore Volume (cu.cm)	90.42217117	Length	28.166
	Pore Volume (cu.m)	9.04222E-05	Area	
	Total Volume (m3)	0.000319684	Sg1	0.228006875
	Porosity (%)	0.282848509	Sg2	0.233077194

Table C - 17 Table documenting the pore volume, Sgr and porosity for the E8

E8

Before SI		After SI		After Vacuum
Weight (w sleeve) (g)	Weight (w/o sleeve) (g)	Weight (w sleeve) (g)	Weight (w/o sleeve) (g)	Weight (w/o sleeve) (g)
662.832	629.606	735.611	701.907	724.061
Density (g/cu.cm)	1.0428		1.0451	1.0453
	Pore Volume (cu.cm)	90.36161867	Length	29.278
	Pore Volume (cu.m)	9.03616E-05	Area	11.2865
	Total Volume (m3)	0.000330446	Sg1	0.227637714
	Porosity (%)	0.273453389	Sg2	0.233555692

Table C - 18 Table documenting the pore volume, Sgr and porosity for the E9

E9

Before		After		After Vacuum
Weight (w sleeve) (g)	Weight (w/o sleeve) (g)	Weight (w sleeve) (g)	Weight (w/o sleeve) (g)	Weight (w/o sleeve) (g)
662.72	628.842	737.015	702.991	725.179
Density (g/cu.cm)	1.0427	1.044		1.0445
	Pore Volume (cu.cm)	92.2326472	Length	29.2825
	Pore Volume (cu.cm)	9.22326E-05	Area	11.26269
	Total Volume (m3)	0.0003298	Sg1	0.227469669
	Porosity (%)	0.2796626	Sg2	0.228987798

Table C - 19 Table documenting the pore volume, Sgr and porosity for the P7

P7

Before		After		After Vacuum
Weight (w sleeve) (g)	Weight (w/o sleeve) (g)	Weight (w sleeve) (g)	Weight (w/o sleeve) (g)	Weight (w/o sleeve) (g)
718.347	684.297	761.661	727.611	748.835
Density (g/cu.cm)	1.0469		1.0509	1.0508
	Pore Volume (cu.cm)	61.4179673	Length	28.032
	Pore Volume (cu.cm)	6.1418E-05	Area	11.43586
	Total Volume (m3)	0.00032057	Sg1	0.3276448
	Porosity (%)	0.19158986	Sg2	0.3276448

Table C - 20 Table documenting the pore volume, Sgr and porosity for the P8

P8

Before		After		After Vacuum
Weight (w sleeve) (g)	Weight (w/o sleeve) (g)	Weight (w sleeve) (g)	Weight (w/o sleeve) (g)	Weight (w/o sleeve) (g)
714.444	680.683	761.481	727.72	744.25
Density (g/cu.cm)	1.0471	1.0478		1.0545
	Pore Volume (cu.cm)	62.3454198	Length	28.1605
	Pore Volume (cu.cm)	6.2345E-05	Area	11.3521
	Total Volume (m3)	0.00031968	Sg1	
	Porosity (%)	0.19502397	Sg2	0.35881192

Table C - 21 Table documenting the pore volume, Sgr and porosity for the P9

P9

Before		After		After Vacuum
Weight (w sleeve) (g)	Weight (w/o sleeve) (g)	Weight (w sleeve) (g)	Weight (w/o sleeve) (g)	Weight (w/o sleeve) (g)
	706.917	782.736	748.725	772.255
Density (g/cu.cm)	1.0429		1.0488	1.048
	Pore Volume (cu.cm)	60.2816501	Length	28.0035
	Pore Volume (cu.cm)	6.0282E-05	Area	11.3143
	Total Volume (m3)	0.00031684	Sg1	0.25506019
	Porosity (%)	0.19025896	Sg2	0.25506019

Appendix D: Permeability Results

7.6 cm cores

For the 7.6 cm cores the flow rate through the core was verified through analyzing the weight of brine expelled out of the system against time, with the gradient of this line giving the mass flow rate. The permeability could then be found by one of two methods. One method is finding the permeability for each flow rate then taking the average. The other is by analyzing the slope of Q/A against dp/L. The graphical method of finding the permeability was preferred for this analysis.

K1

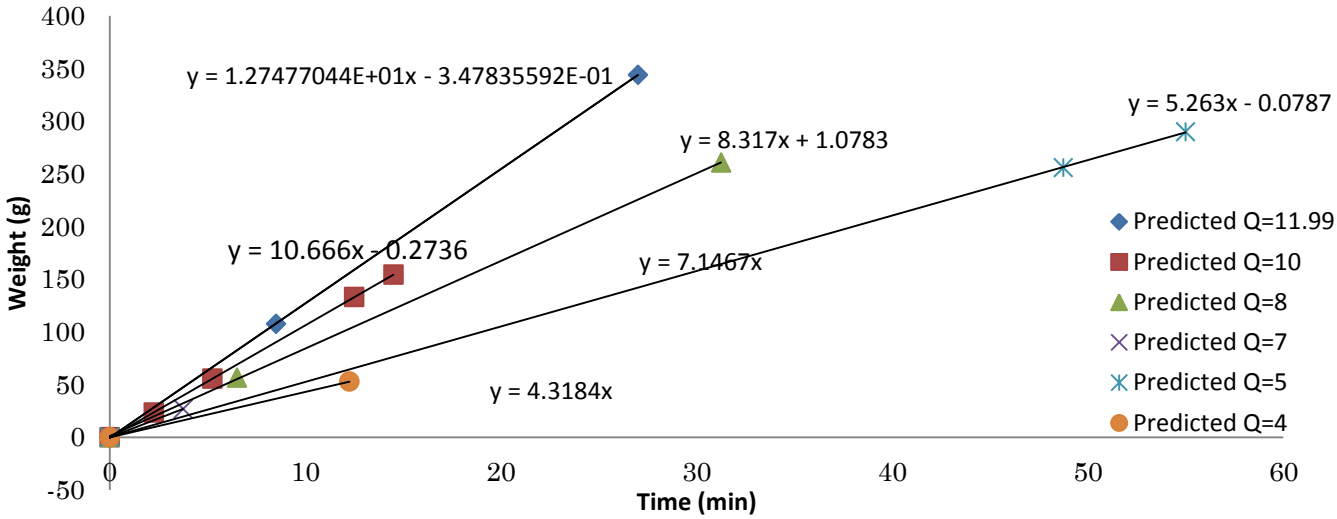

Fig. D - 1 Graph used to find the mass flow rate of brine into the K1 core for the permeability measurements.

Table D - 1: Table showing the parameters used for the permeability measurements for the K1 core.

Q (m3/s)	Inlet P (psi)	Outlet P (psi)	Dp (psi)	dp (Mpa)	Length (m)	Viscosity (Pas)	Area (m2)	Permeability (m3)	Permeability (mD)
2.0339E-07	12.4	1.65	10.8	0.074118641	0.076355	0.0010903	0.001124981	2.03068E-13	2002.70386
1.7018E-07	9.7	1.52	8.18	0.056399115	0.076355	0.0010903	0.001124981	2.23289E-13	2202.122582
1.327E-07	8	1.6	6.4	0.044126447	0.076355	0.0010903	0.001124981	2.22538E-13	2194.724149
1.1403E-07	6.8	1.6	5.2	0.035852738	0.076355	0.0010903	0.001124981	2.35353E-13	2321.108399
8.3972E-08	4.1	1.32	2.78	0.019167425	0.076355	0.0010903	0.001124981	3.24195E-13	3197.28823
							Average Permeability (mD)		2383.589444

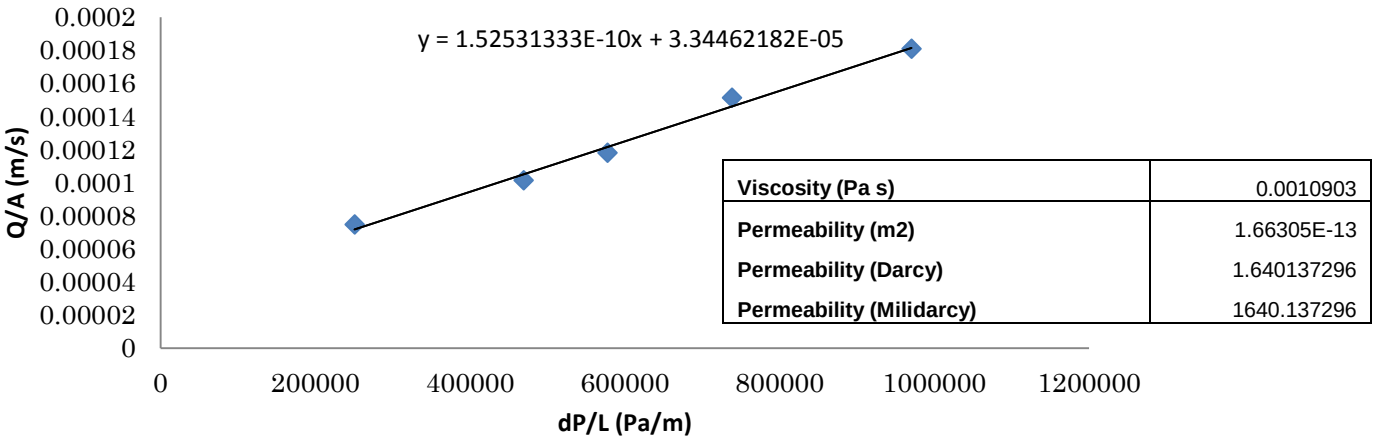

Viscosity (Pa s)	0.0010903
Permeability (m2)	1.66305E-13
Permeability (Darcy)	1.640137296
Permeability (Milidarcy)	1640.137296

Fig. D - 2 Graph of Q/A against dP/L, used to find the permeability of the K1 core

K2

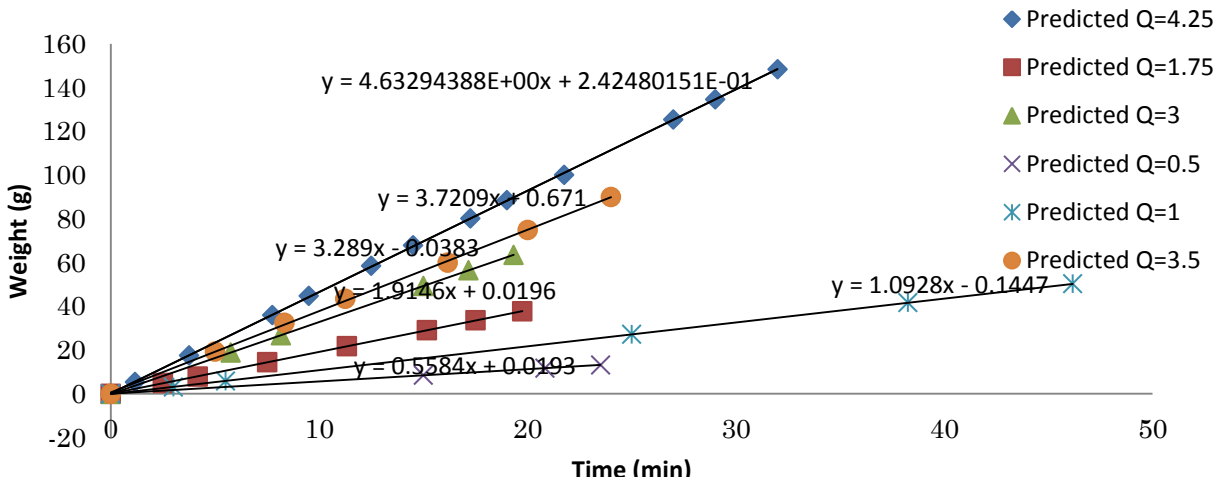

Fig. D - 3 Graph used to find the mass flow rate of brine into the K2 core for the permeability measurements.

Table D - 2: Table showing the parameters used for the permeability measurements for the K2 core.

Q (m3/s)	Inlet P (psi)	Outlet P (psi)	Dp (psi)	dp (Mpa)	Length (m)	Viscosity (Pas)	Area (m2)	Permeability (m3)	Permeability (mD)
7.37636E-08	18.2	3.4	14.8	0.102042408	0.076345	0.0010903	0.0011232	5.34933E-14	527.5636283
3.04834E-08	9.03	2.6	6.43	0.044333289	0.076345	0.0010903	0.0011232	5.08829E-14	501.8184261
5.23659E-08	9.8	2.83	6.97	0.048056458	0.076345	0.0010903	0.0011232	8.06372E-14	795.262708
1.73991E-08	3.21	2.55	0.66	0.00455054	0.076345	0.0010903	0.0011232	2.82944E-13	2790.46303
5.92425E-08	7.93	3.08	4.85	0.033439573	0.076345	0.0010903	0.0011232	1.31102E-13	1292.962062
								Average Permeability (mD)	1153.776

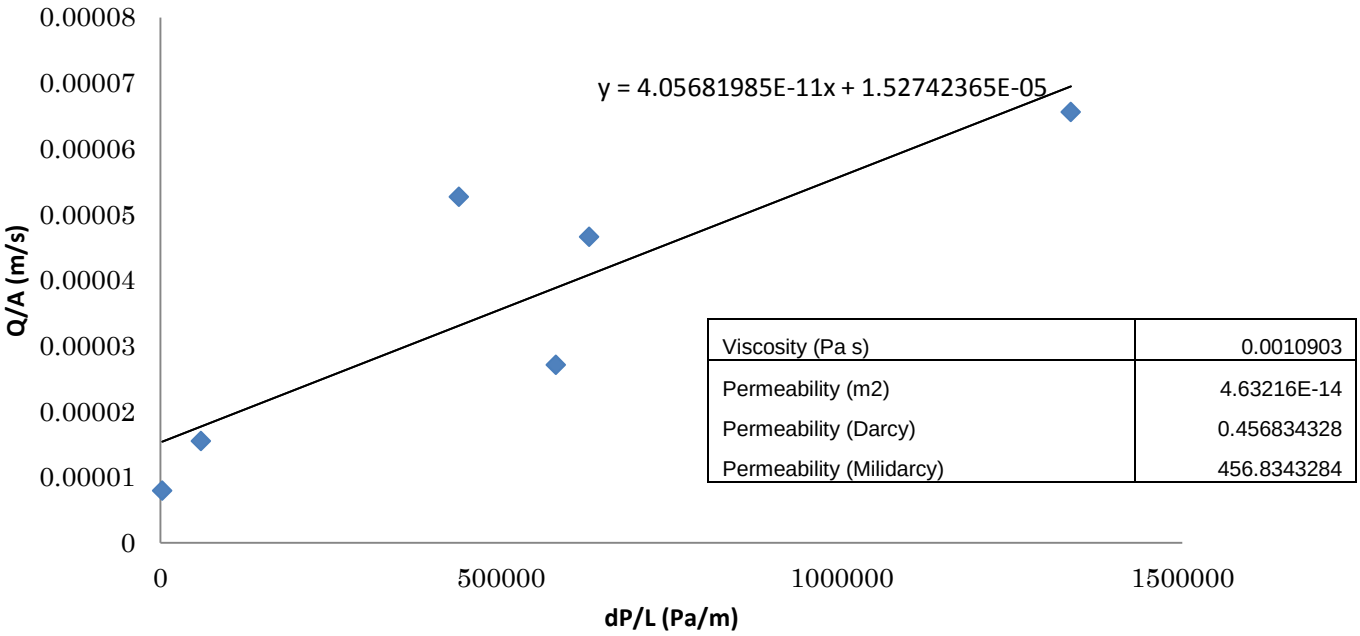

Fig. D - 4 Graph of Q/A against dP/L, used to find the permeability of the K2 core

K3

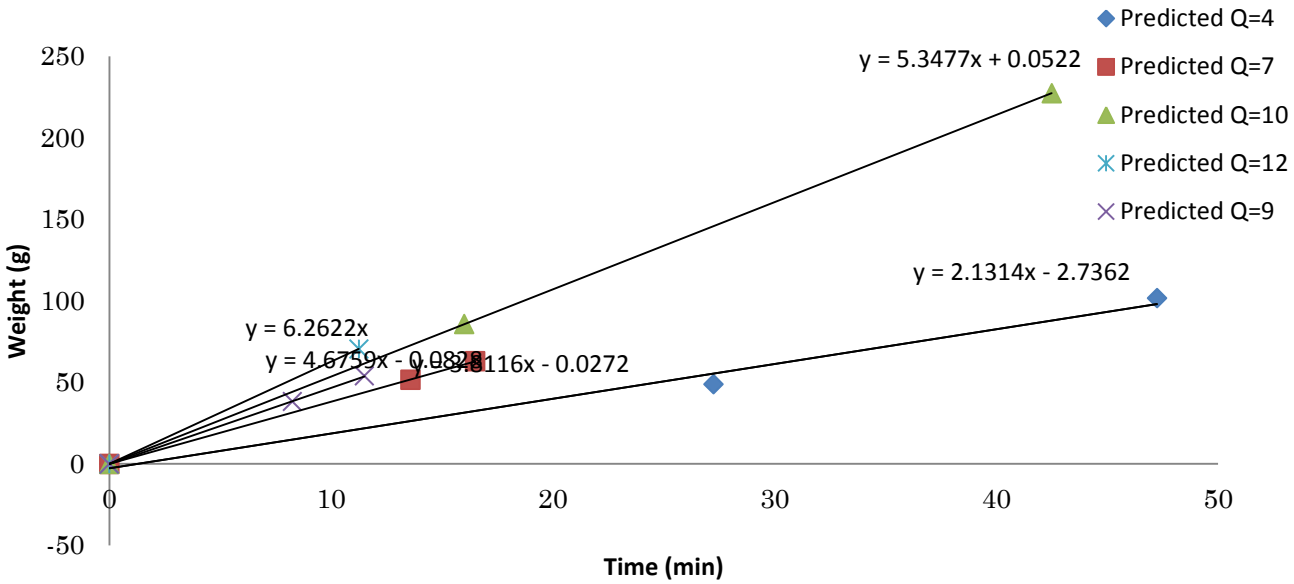

Fig. D - 5 Graph used to find the mass flow rate of brine into the K3 core for the permeability measurements.

Table D - 3: Table showing the parameters used for the permeability measurements for the K3 core.

Q (m3/s)	Inlet P (psi)	Outlet P (psi)	Dp (psi)	dp (Mpa)	Length (m)	Viscosity (Pas)	Area (m2)	Permeability (m3)	Permeability (mD)
9.9818E-08	10.6	2.4	8.2	56537.0098	0.076355	0.0010903	0.00112498	1.307E-13	1288.5188
8.5241E-08	8.5	2.1	6.4	44126.4467	0.076355	0.0010903	0.00112498	1.43E-13	1409.8234
7.4533E-08	9	2.25	6.75	46539.6117	0.076355	0.0010903	0.00112498	1.185E-13	1168.797
6.0756E-08	7.4	2	5.4	37231.6894	0.076355	0.0010903	0.0011249	1.208E-13	1190.9437
							Average Permeability (mD)		1264.5207

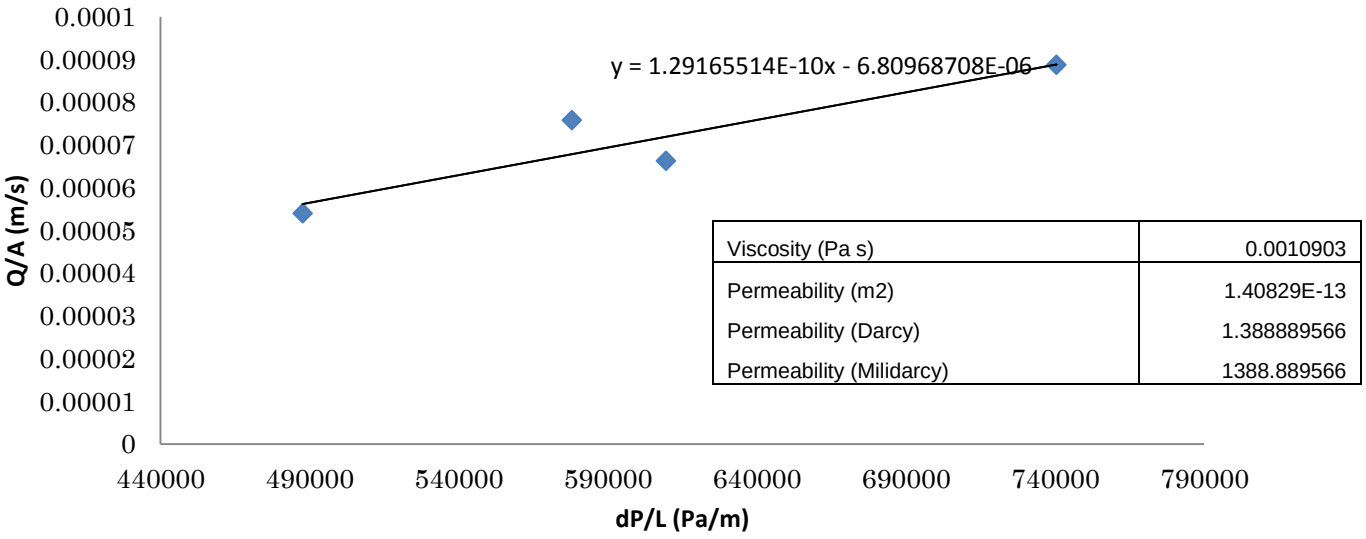

Viscosity (Pa s)	0.0010903
Permeability (m2)	1.40829E-13
Permeability (Darcy)	1.388889566
Permeability (Milidarcy)	1388.889566

Fig. D - 6 Graph of Q/A against dP/L, used to find the permeability of the K3 core

E1

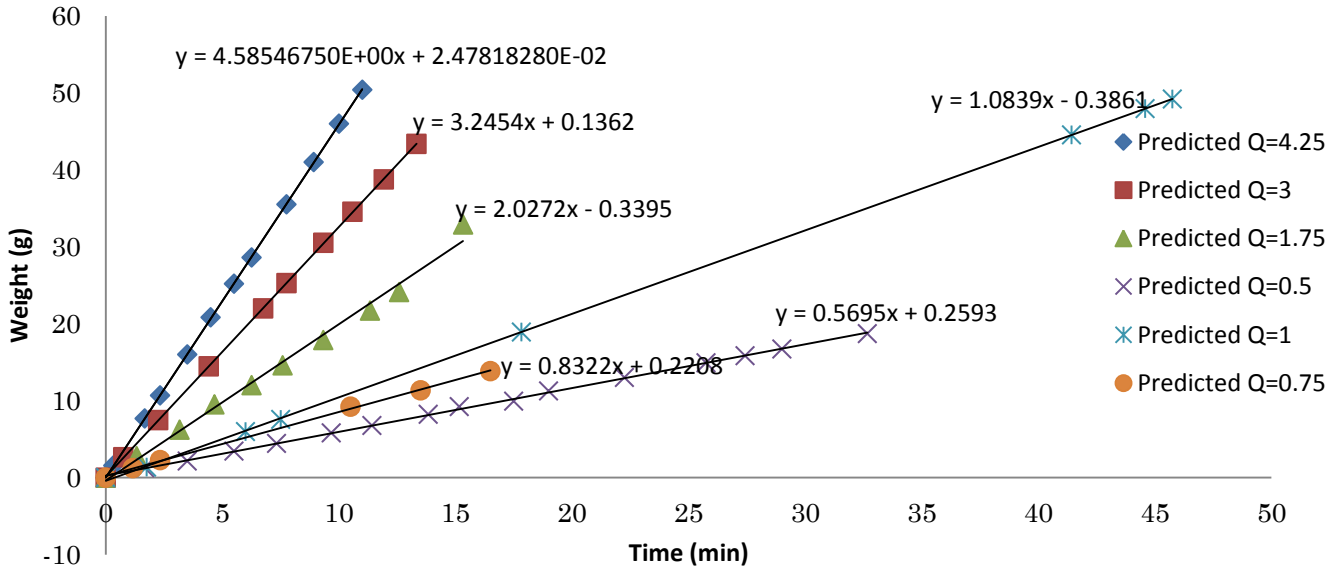

Fig. D - 7 Graph used to find the mass flow rate of brine into the E1 core for the permeability measurements.

Table D - 4: Table showing the parameters used for the permeability measurements for the E1 core.

Q (m3/s)	Inlet P (psi)	Outlet P (psi)	Dp (psi)	dp (Mpa)	Length (m)	Viscosity (Pas)	Area (m2)	Permeability (m3)	Permeability (mD)
7.332E-08	67.37	2.4	64.9	0.44795238	0.07305	0.001090	0.00112498	1.211E-14	119.5514134
5.197E-08	55.24	2.3	52.9	0.36500845	0.07305	0.001090	0.00112498	1.091E-14	103.8408554
3.244E-08	35.78	2.14	33.6	0.23193963	0.07305	0.001090	0.00112498	1.002E-14	102.0762184
1.752E-08	25.63	2	23.6	0.16292311	0.07305	0.001090	0.00112498	7.833E-15	77.69793143
1.333E-08	19.59	2	17.5	0.12127878	0.07305	0.001090	0.00112498	8.189E-15	80.13935339
9.116E-09	20.84	2	18.8	0.12989722	0.07305	0.001090	0.00112498	5.184E-15	51.20316326
								Average Permeability (mD)	89.084822

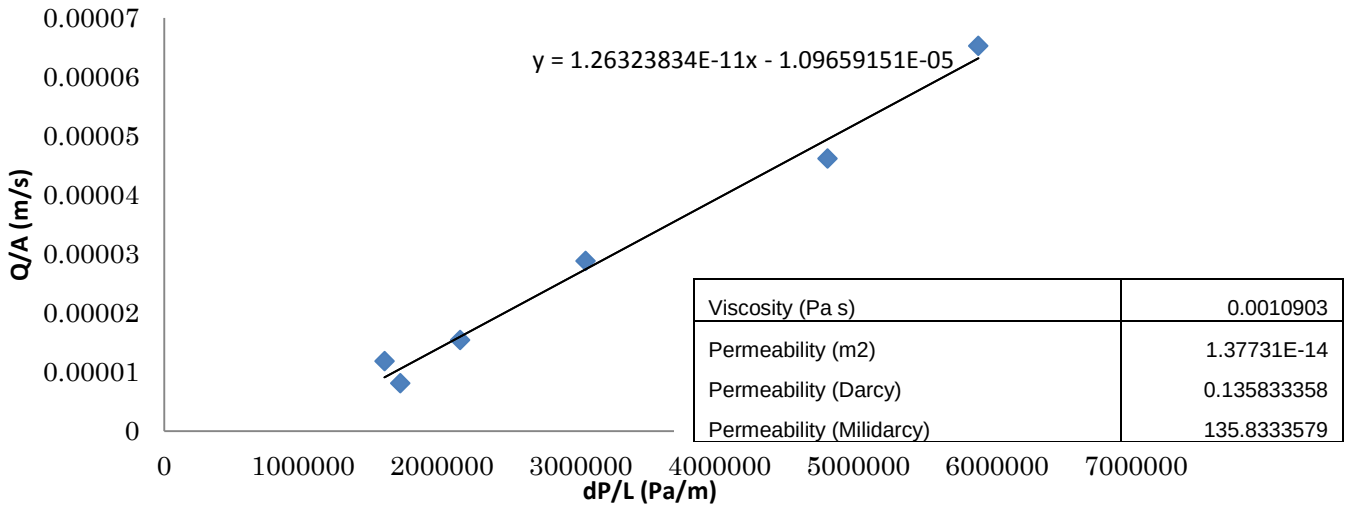

Fig. D - 8 Graph of Q/A against dP/L, used to find the permeability of the E1 core

E2

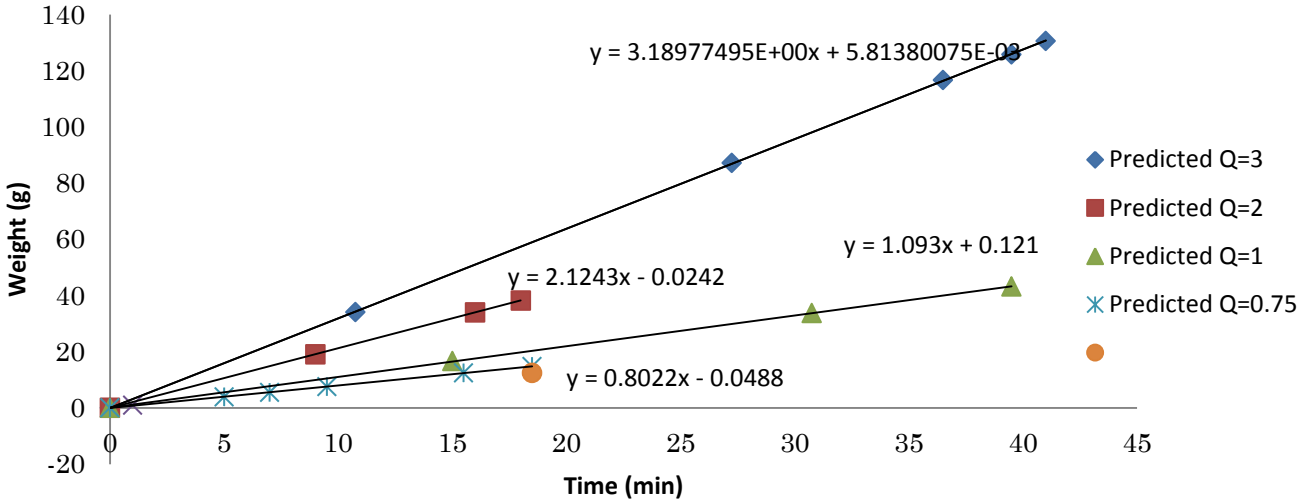

Fig. D - 9 Graph used to find the mass flow rate of brine into the E2 core for the permeability measurements.

Table D - 5: Table showing the parameters used for the permeability measurements for the E2 core.

Q (m3/s)	InletP (psi)	Outlet P (psi)	Dp (psi)	dp (Mpa)	Length (m)	Viscosity (Pas)	Area (m2)	Permeability (m3)	Permeability (mD)
5.16496E-08	40.23	2.25	37.98	0.26186288	0.076355	0.0010903	0.00112498	1.45959E-14	143.948236
3.43972E-08	32.67	1.95	30.72	0.21180694	0.076355	0.0010903	0.00112498	1.20177E-14	118.521162
1.76981E-08	22.06	1.85	20.21	0.13934304	0.076355	0.0010903	0.00112498	9.39896E-15	92.6947445
1.29894E-08	19.63	1.85	17.78	0.12258878	0.076355	0.0010903	0.00112498	7.8411E-15	77.3307397
								Average Permeability (mD)	108.1237

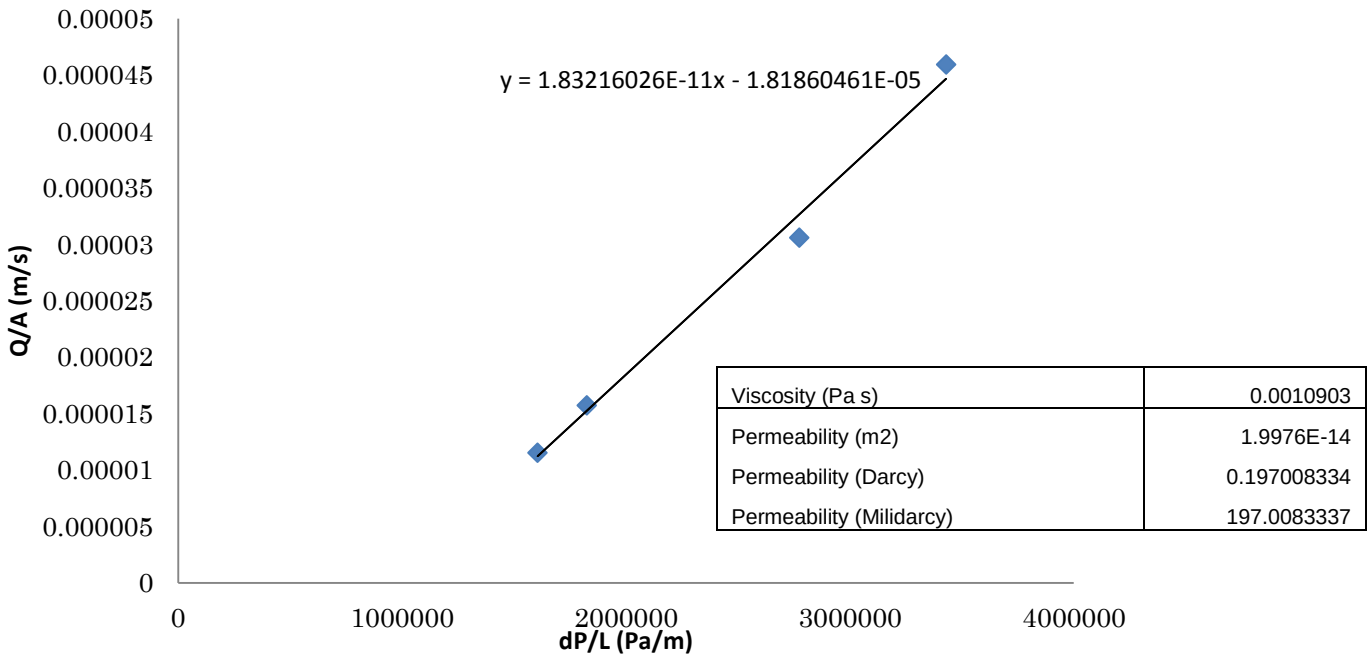

Viscosity (Pa s)	0.0010903
Permeability (m2)	1.9976E-14
Permeability (Darcy)	0.197008334
Permeability (Milidarcy)	197.0083337

Fig. D - 10 Graph of Q/A against dP/L, used to find the permeability of the E2 core

E3

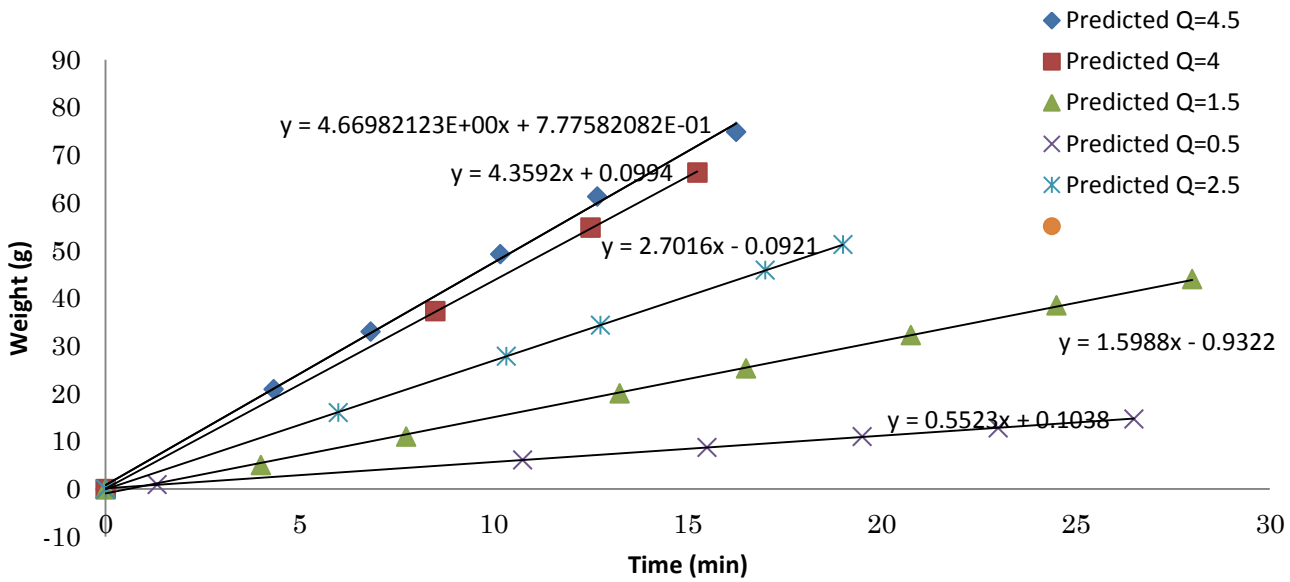

Fig. D - 11 Graph used to find the mass flow rate of brine into the E3 core for the permeability measurements.

Table D - 6: Table showing the parameters used for the permeability measurements for the E3 core.

Q (m3/s)	Inlet P(psi)	Outlet P (psi)	Dp (psi)	dp (Mpa)	Length (m)	Viscosity (Pas)	Area (m2)	Permeability (m3)	Permeability (mD)
7.47363E-08	26.2	3.65	22.55	0.15547678	0.076285	0.0010903	0.00112498	3.55717E-14	350.815983
4.32367E-08	16.62	3.05	13.57	0.09356186	0.076285	0.0010903	0.00112498	3.41973E-14	337.261574
2.55874E-08	11.07	3	8.07	0.05564069	0.076285	0.0010903	0.00112498	3.40307E-14	335.61879
8.83906E-09	5.91	2.83	3.08	0.02123585	0.076285	0.0010903	0.00112498	3.08017E-14	303.773573
								Average Permeability (mD)	331.86

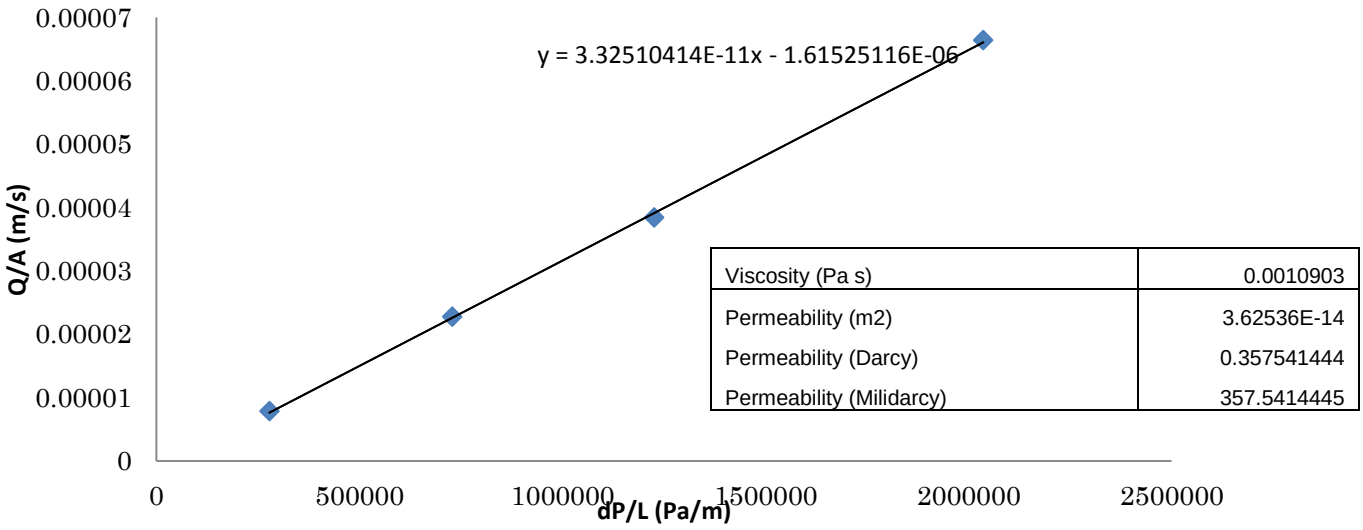

Viscosity (Pa s)	0.0010903
Permeability (m2)	3.62536E-14
Permeability (Darcy)	0.357541444
Permeability (Milidarcy)	357.5414445

Fig. D - 12 Graph of Q/A against dP/L, used to find the permeability of the E3 core

P1

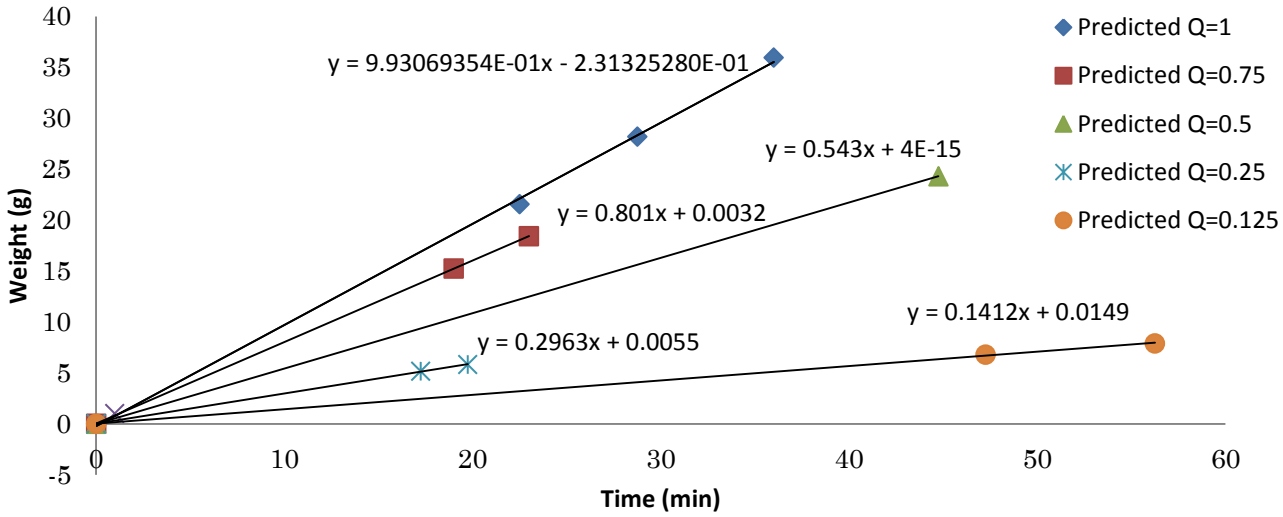

Fig. D - 13 Graph used to find the mass flow rate of brine into the P1 core for the permeability measurements.

Table D - 7: Table showing the parameters used for the permeability measurements for the P1 core.

Q (m3/s)	Inlet P(psi)	Outlet P (psi)	Dp (psi)	dp (Mpa)	Length (m)	Viscosity (Pas)	Area (m2)	Permeability (m3)	Permeability (mD)
1.608E-08	260.1	1.5	258.6	1.78298424	0.076305	0.0010903	0.00112498	6.67386E-16	6.58191581
1.297E-08	225	1.58	223.42	1.54042667	0.076305	0.0010903	0.00112498	6.2307E-16	6.14485631
8.79238E-09	163.2	1.55	161.65	1.11453752	0.076305	0.0010903	0.00112498	5.83781E-16	5.75738649
4.79776E-09	146	1.48	144.52	0.99643032	0.076305	0.0010903	0.00112498	3.56311E-16	3.51402593
2.28634E-09	120.7	1.5	119.2	0.82185507	0.076305	0.0010903	0.00112498	2.05866E-16	2.03029762
							Average Permeability (mD)		4.805

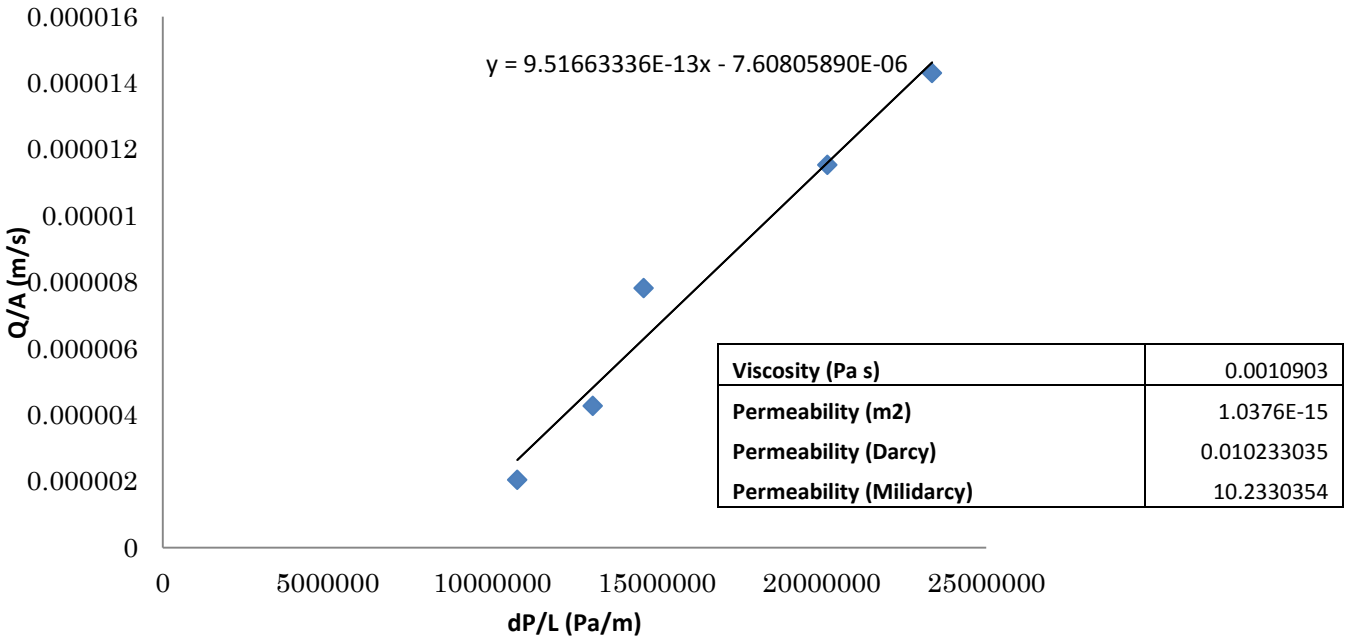

Fig. D - 14 Graph of Q/A against dP/L, used to find the permeability of the P1 core

P2

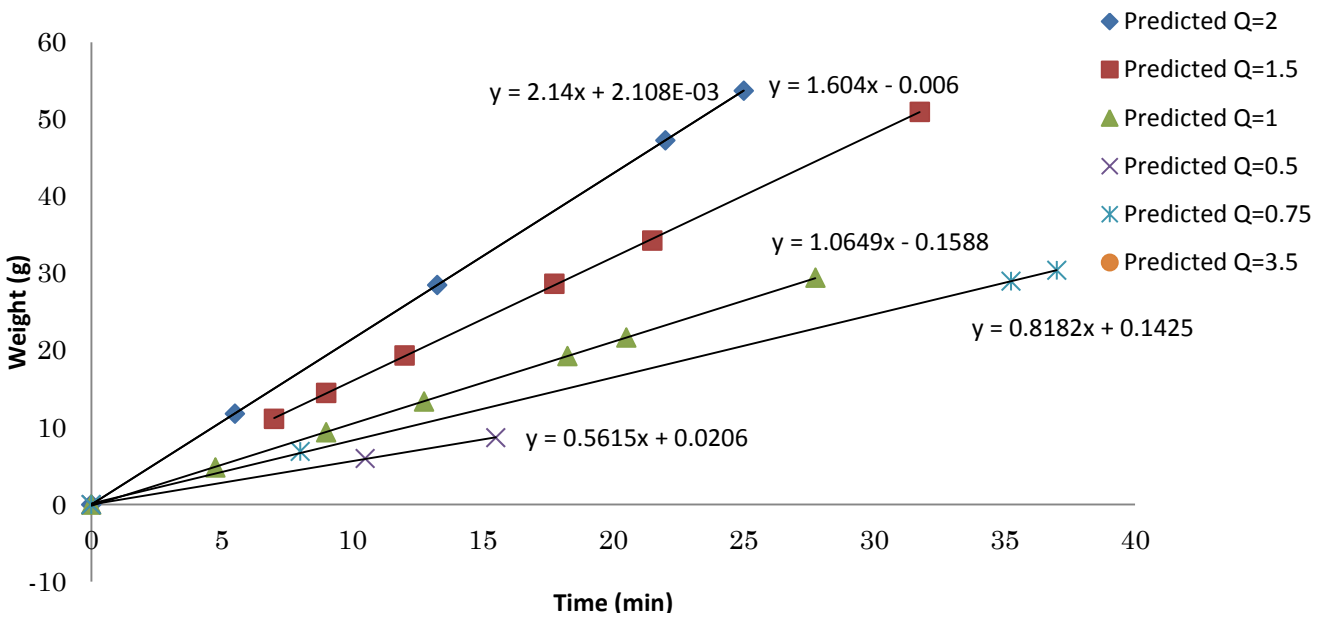

Fig. D - 15 Graph used to find the mass flow rate of brine into the P2 core for the permeability measurements.

Table D - 8: Table showing the parameters used for the permeability measurements for the P2 core.

Q (m3/s)	Inlet P(psi)	Outlet P (psi)	Dp (psi)	dp (Mpa)	Length (m)	Viscosity (Pas)	Area (m2)	Permeability (m3)	Permeability (mD)
3.42473E-08	350.3	0.32	349.98	2.41302716	0.076395	0.0010903	0.00112498	1.08368E-15	10.6875198
2.55723E-08	282.4	0.72	281.68	1.94211523	0.076395	0.0010903	0.00112498	1.00539E-15	9.91535418
1.69249E-08	239	0.47	238.53	1.64460646	0.076395	0.0010903	0.00112498	7.85783E-16	7.74957315
8.95192E-09	165.1	0.32	164.78	1.13611811	0.076395	0.0010903	0.00112498	6.01631E-16	5.9334207
1.30444E-08	177.2	0.47	176.73	1.21851046	0.076395	0.0010903	0.00112498	8.17399E-16	8.06137414

Average Permeability (mD)	8.469

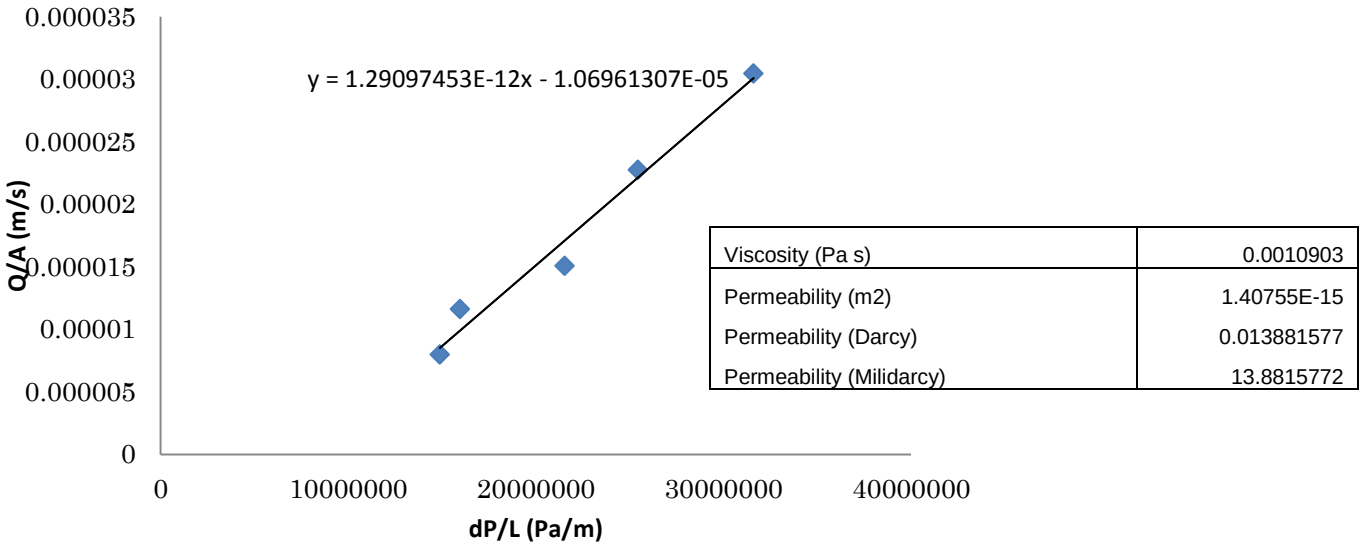

Viscosity (Pa s)	0.0010903
Permeability (m2)	1.40755E-15
Permeability (Darcy)	0.013881577
Permeability (Milidarcy)	13.8815772

Fig. D - 16 Graph of Q/A against dP/L, used to find the permeability of the P2 core

P3

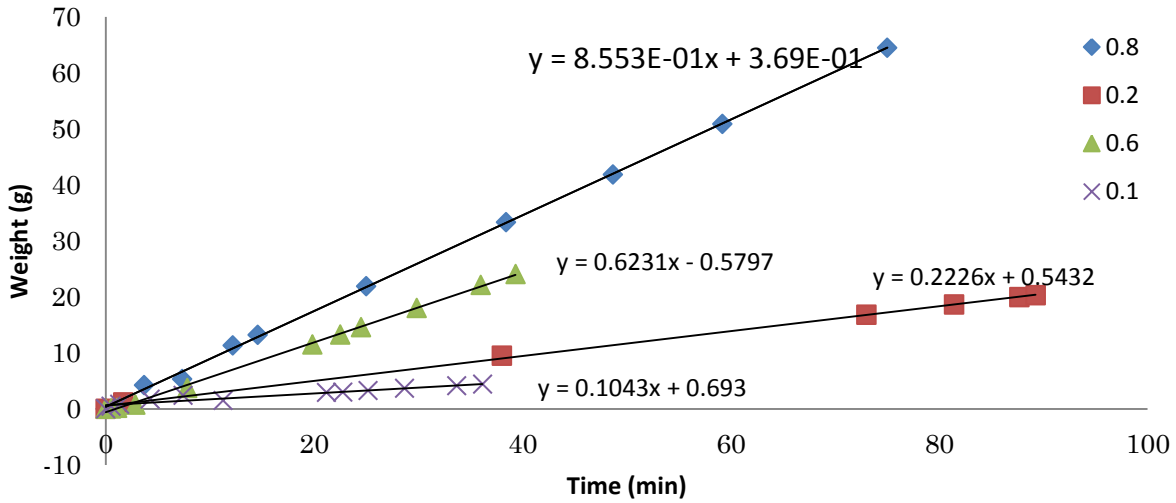

Fig. D - 17 Graph used to find the mass flow rate of brine into the P3 core for the permeability measurements.

Table D - 9: Table showing the parameters used for the permeability measurements for the P3 core.

Q (m3/s)	Inlet P(psi)	Outlet P (psi)	Dp (psi)	dp (Mpa)	Length (m)	Viscosity (Pas)	Area (m2)	Permeability (m3)	Permeability (mD)
1.36381E-08	125.91	1.94	123.97	0.85474306	0.076345	0.0010903	0.00112498	1.18059E-15	11.6432822
9.93305E-09	108.67	2	106.67	0.73546376	0.076345	0.0010903	0.00112498	9.99316E-16	9.85547982
3.54854E-09	70	1.98	68.02	0.46898139	0.076345	0.0010903	0.00112498	5.59855E-16	5.52142083
1.66268E-09	42.33	1.98	40.35	0.27820346	0.076345	0.0010903	0.00112498	4.42209E-16	4.36117071
1.36381E-08	125.91	1.94	123.97	0.85474306	0.076345	0.0010903	0.00112498	1.18059E-15	11.6432822
							Average Permeability (mD)		7.845

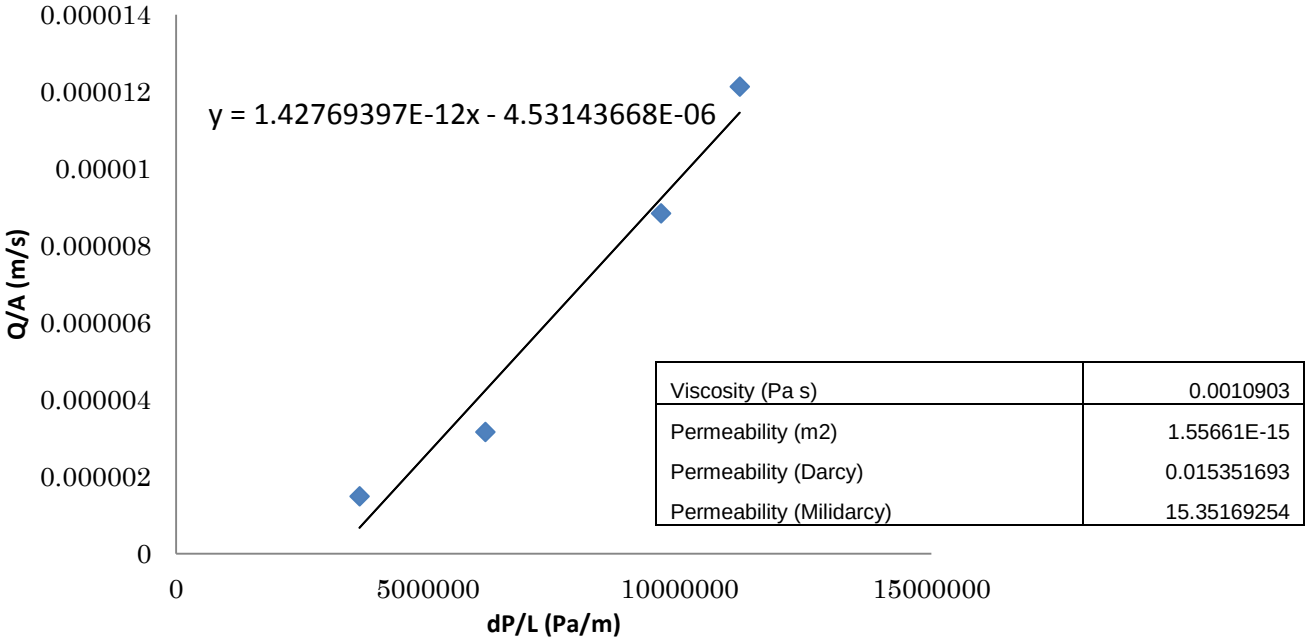

Viscosity (Pa s)	0.0010903
Permeability (m2)	1.55661E-15
Permeability (Darcy)	0.015351693
Permeability (Milidarcy)	15.35169254

Fig. D - 18 Graph of Q/A against dP/L, used to find the permeability of the P2 core

20 cm and 28 cm Cores

K4 **Table D - 10: Table showing the parameters used for the permeability measurements for the K4 core.**

Q_w cm3/sec	D_{core} mm	A CM2	L cm	ΔP psi	P1 psia	P1 atm	$P1^2$ atm2	P2 psig	P2 atm	$P2^2$ atm2	$P2^2$-$P1^2$	Pmean	1/Pmean	ΔP (atm)	K_{N2} (mD)	Average K_{N2} (mD)
8.04	38.1	11.38	20.4	1.15	1.63	1.11	1.23	0.5	1.03	1.1	0.17	1.055	0.947867	0.08	2546	2296.7
8.47	38.1	11.38	20.4	1.21	1.72	1.12	1.25	0.5	1.03	1.1	0.18	1.115	0.896861	0.08	2539	
7.56	38.1	11.38	20.4	1.09	1.53	1.1	1.22	0.4	1.03	1.1	0.16	0.985	1.015228	0.07	2538	
7.03	38.1	11.38	20.4	1.04	1.42	1.1	1.2	0.4	1.03	1.1	0.15	0.9	1.111111	0.07	2488	
6.66	38.1	11.38	20.4	1	1.35	1.09	1.19	0.4	1.02	1.0	0.14	0.85	1.176471	0.07	2458	
6.44	38.1	11.38	20.4	1.1	1.3	1.09	1.18	0.2	1.01	1.0	0.16	0.75	1.333333	0.07	2176	
5.39	38.1	11.38	20.4	0.93	1.09	1.07	1.15	0.2	1.01	1.0	0.13	0.625	1.6	0.06	2171	
5.068	38.1	11.38	20.4	0.93	1.02	1.07	1.14	0.1	1.01	1.0	0.13	0.555	1.801802	0.06	2051	
4.75	38.1	11.38	20.4	0.89	0.96	1.07	1.13	0.1	1	1.0	0.13	0.515	1.941748	0.06	2013	
4.14	38.1	11.38	20.4	0.79	0.84	1.06	1.12	0.1	1	1.0	0.11	0.445	2.247191	0.05	1988	

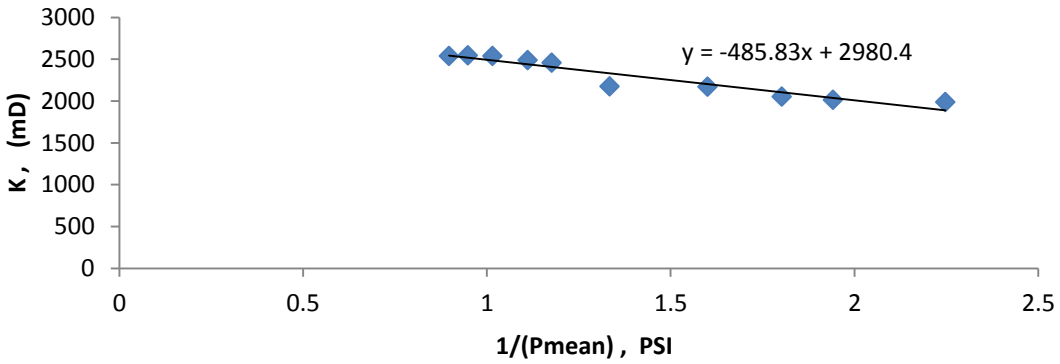

Fig. D - 19 Graph of K against 1/(Pmean), used to find the Klinkenberg permeability of the K4 core

Table D - 11: Table showing the parameters used for the permeability measurements for the K5 core.

K5

Qw cm3/sec	Dcore mm	A CM2	L cm	ΔP psi	P1 psia	P1 atm	P12 atm2	P2 psig	P2 atm	P22 atm2	P22-P12	Pmean	1/Pmean	ΔP (atm)	KN2 (mD)	Average KN2 (mD)
3.55	38.1	11.39	20.5	0.68	0.74	1.05	1.1	0.1	1	1.0	0.1	0.4		0.05		1900.3
4.70	38.1	11.39	20.5	0.88	0.98	1.07	1.14	0.1	1.01	1.0	0.12	0.54	1.851852	0.06	2009	
5.39	38.1	11.39	20.5	0.98	1.13	1.08	1.16	0.2	1.01	1.0	0.14	0.64	1.5625	0.07	2056	
6.26	38.1	11.39	20.5	1.13	1.33	1.09	1.19	0.2	1.01	1.0	0.16	0.765	1.30719	0.08	2056	
5.90	38.1	11.39	20.5	1.07	1.25	1.09	1.18	0.2	1.01	1.0	0.15	0.715	1.398601	0.07	2053	
6.55	38.1	11.39	20.5	1.19	1.39	1.09	1.2	0.2	1.01	1.0	0.17	0.795	1.257862	0.08	2038	
7.03	38.1	11.39	20.5	1.2	1.5	1.1	1.21	0.3	1.02	1.0	0.17	0.9	1.111111	0.08	2155	
7.272	38.1	11.39	20.5	1.23	1.56	1.11	1.22	0.3	1.02	1.0	0.18	0.945	1.058201	0.08	2169	
7.60	38.1	11.39	20.5	1.23	1.63	1.11	1.23	0.4	1.03	1.1	0.18	1.015	0.985222	0.08	2258	
8.26	38.1	11.39	20.5	1.36	1.76	1.12	1.25	0.4	1.03	1.1	0.2	1.08	0.925926	0.09	2209	

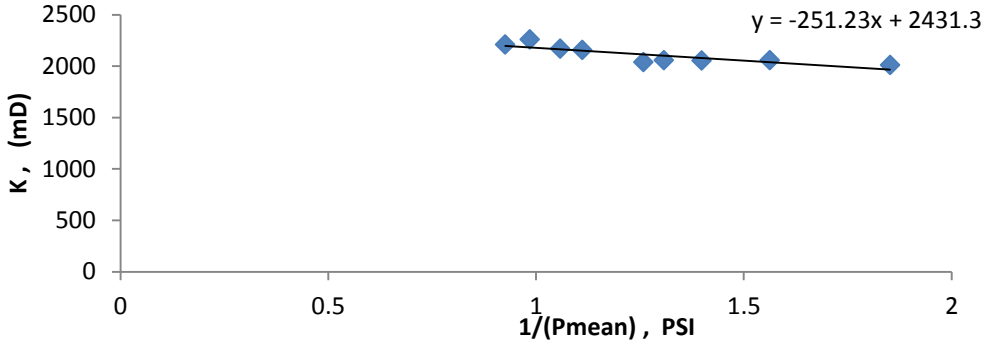

Fig. D - 20 Graph of K against 1/(Pmean), used to find the Klinkenberg permeability of the K5 core

K6 **Table D - 12: Table showing the parameters used for the permeability measurements for the K6 core.**

Qw cm3/sec	Dcore mm	A CM2	L cm	ΔP psi	P1 psia	P1 atm	P12 atm2	P2 psig	P2 atm	P22 atm2	P22-P12	Pmean	1/Pmean	ΔP (atm)	KN2 (mD)	Average KN2 (mD)
8.47	38.0	11.34	20.5	1.44	1.89	1.13	1.27	0.5	1.03	1.1	0.21	1.17	0.854701	0.10	2138	2022.7
7.92	38.0	11.34	20.5	1.39	1.77	1.12	1.26	0.4	1.03	1.1	0.2	1.075	0.930233	0.09	2084	
7.40	38.0	11.34	20.5	1.32	1.66	1.11	1.24	0.3	1.02	1.0	0.19	1	1	0.09	2060	
6.55	38.0	11.34	20.5	1.28	1.47	1.1	1.21	0.2	1.01	1.0	0.18	0.83	1.204819	0.09	1900	
5.94	38.0	11.34	20.5	1.17	1.32	1.09	1.19	0.2	1.01	1.0	0.17	0.735	1.360544	0.08	1896	
5.39	38.0	11.34	20.5	1.11	1.2	1.08	1.17	0.1	1.01	1.0	0.16	0.645	1.550388	0.08	1824	
4.81	38.0	11.34	20.5	1	1.08	1.07	1.15	0.1	1.01	1.0	0.14	0.58	1.724138	0.07	1815	
8.417	38.0	11.34	20.5	1.41	1.9	1.13	1.28	0.5	1.03	1.1	0.21	1.195	0.83682	0.10	2167	
8.01	38.0	11.34	20.5	1.35	1.8	1.12	1.26	0.5	1.03	1.1	0.2	1.125	0.888889	0.09	2163	
7.38	38.0	11.34	20.5	1.24	1.66	1.11	1.24	0.4	1.03	1.1	0.18	1.04	0.961538	0.08	2181	
8.13	38.0	11.34	20.5	1.34	1.83	1.12	1.26	0.5	1.03	1.1	0.2	1.16	0.862069	0.09	2206	

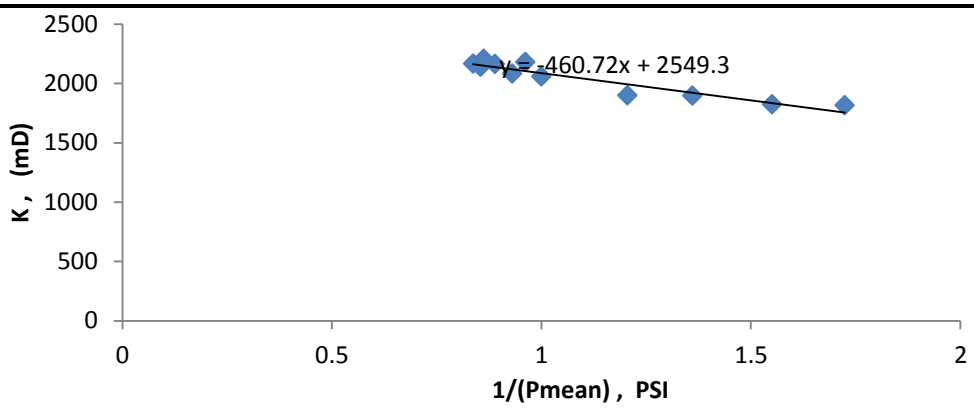

Fig. D - 21 Graph of K against 1/(Pmean), used to find the Klinkenberg permeability of the K6 core

K7 **Table D - 13: Table showing the parameters used for the permeability measurements for the K7 core.**

Qw cm3/sec	Dcore mm	A CM2	L cm	ΔP psi	P1 psia	P1 atm	P12 atm2	P2 psig	P2 atm	P22 atm2	P22-P12	Pmean	1/Pmean	ΔP (atm)	KN2 (mD)	Average KN2 (mD)
7.05	38.0	11.34	28.0	1.2	1.63	1.11	1.23	0.4	1.03	1.1	0.17	1.03	0.970874	0.08	2949	2255.2
7.95	38.0	11.34	28.0	1.38	1.84	1.13	1.27	0.5	1.03	1.1	0.2	1.15	0.869565	0.09	2870	
8.29	38.0	11.34	28.0	1.47	1.95	1.13	1.28	0.5	1.03	1.1	0.22	1.215	0.823045	0.10	2799	
6.32	38.0	11.34	28.0	1.08	1.48	1.1	1.21	0.4	1.03	1.1	0.16	0.94	1.06383	0.07	2953	
6.70	38.0	11.34	28.0	1.16	1.57	1.11	1.23	0.4	1.03	1.1	0.17	0.99	1.010101	0.08	2907	
5.75	38.0	11.34	28.0	1.05	1.34	1.09	1.19	0.3	1.02	1.0	0.15	0.815	1.226994	0.07	2787	
4.82	38.0	11.34	28.0	0.92	1.12	1.08	1.16	0.2	1.01	1.0	0.13	0.66	1.515152	0.06	2691	
3.75	38.0	11.34	28.0	0.75	0.88	1.06	1.12	0.1	1.01	1.0	0.11	0.505	1.980198	0.05	2597	

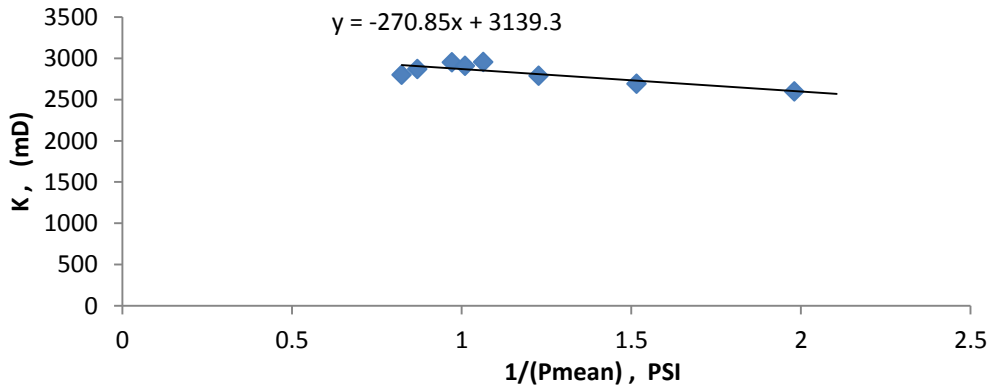

Fig. D - 22 Graph of K against 1/(Pmean), used to find the Klinkenberg permeability of the K7 core

K8 **Table D - 14: Table showing the parameters used for the permeability measurements for the K8 core.**

Qw cm3/sec	Dcore mm	A CM2	L cm	ΔP psi	P1 psia	P1 atm	P12 atm2	P2 psig	P2 atm	P22 atm2	P22-P12	Pmean	1/Pmean	ΔP (atm)	KN2 (mD)	Average KN2 (mD)
8.17	38.0	11.35	28.2	1.12	1.65	1.11	1.24	0.5	1.04	1.1	0.16	1.09	0.917431	0.08	3663	3293.8
7.70	38.0	11.35	28.2	1.07	1.55	1.11	1.22	0.5	1.03	1.1	0.16	1.015	0.985222	0.07	3629	
7.22	38.0	11.35	28.2	1	1.44	1.1	1.21	0.4	1.03	1.1	0.14	0.94	1.06383	0.07	3658	
6.78	38.0	11.35	28.2	0.94	1.34	1.09	1.19	0.4	1.03	1.1	0.14	0.87	1.149425	0.06	3669	
6.27	38.0	11.35	28.2	0.85	1.85	1.13	1.27	1	1.07	1.1	0.13	1.425	0.701754	0.06	3624	
5.62	38.0	11.35	28.2	0.79	1.09	1.07	1.15	0.3	1.02	1.0	0.11	0.695	1.438849	0.05	3663	
4.958	38.0	11.35	28.2	0.69	0.94	1.06	1.13	0.3	1.02	1.0	0.1	0.595	1.680672	0.05	3724	
4.93	38.0	11.35	28.2	0.68	1.38	1.09	1.2	0.7	1.05	1.1	0.1	1.04	0.961538	0.05	3651	
4.55	38.0	11.35	28.2	0.63	1.25	1.09	1.18	0.6	1.04	1.1	0.09	0.935	1.069519	0.04	3657	
4.22	38.0	11.35	28.2	0.59	1.15	1.08	1.16	0.6	1.04	1.1	0.09	0.855	1.169591	0.04	3645	

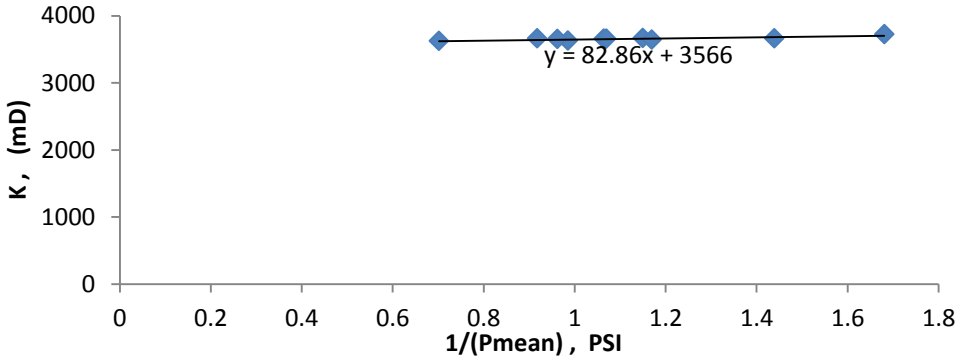

Fig. D - 23 Graph of K against 1/(Pmean), used to find the Klinkenberg permeability of the K8 core

K9 **Table D - 15: Table showing the parameters used for the permeability measurements for the K9 core.**

Qw cm3/sec	Dcore mm	A CM2	L cm	ΔP psi	P1 psia	P1 atm	P12 atm2	P2 psig	P2 atm	P22 atm2	P22-P12	Pmean	1/Pmean	ΔP (atm)	KN2 (mD)	Average KN2 (mD)
4.41	38.0	11.33	29.3	0.96	1.1	1.07	1.16	0.1	1.01	1.0	0.14	0.62	1.612903	0.07	2480	2570
3.73	38.0	11.33	29.3	0.83	0.93	1.06	1.13	0.1	1.01	1.0	0.12	0.515	1.941748	0.06	2439	
8.11	38.0	11.33	29.3	1.57	2	1.14	1.29	0.4	1.03	1.1	0.23	1.215	0.823045	0.11	2682	
8.46	38.0	11.33	29.3	1.6	2.09	1.14	1.3	0.5	1.03	1.1	0.24	1.29	0.775194	0.11	2735	
7.46	38.0	11.33	29.3	1.42	1.84	1.13	1.27	0.4	1.03	1.1	0.21	1.13	0.884956	0.10	2742	
6.63	38.0	11.33	29.3	1.27	1.65	1.11	1.24	0.4	1.03	1.1	0.18	1.015	0.985222	0.09	2748	
5.56	38.0	11.33	29.3	1.1	1.38	1.09	1.2	0.3	1.02	1.0	0.16	0.83	1.204819	0.07	2689	
2.967	38.0	11.33	29.3	0.67	0.74	1.05	1.1	0.1	1	1.0	0.09	0.405	2.469136	0.05	2424	
1.98	38.0	11.33	29.3	0.45	0.5	1.03	1.07	0.1	1	1.0	0.06	0.275	3.636364	0.03	2434	
1.21	38.0	11.33	29.3	0.29	0.31	1.02	1.04	0	1	1.0	0.04	0.165	6.060606	0.02	2327	
3.43	38.0	11.33	29.3	0.75	0.85	1.06	1.12	0.1	1.01	1.0	0.11	0.475	2.105263	0.05	2489	

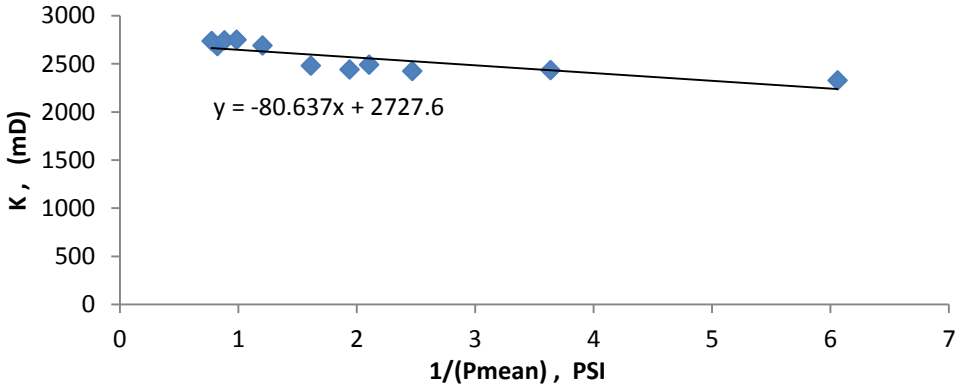

Fig. D - 24 Graph of K against 1/(Pmean), used to find the Klinkenberg permeability of the K9 core

E4 **Table D - 16: Table showing the parameters used for the permeability measurements for the E4 core.**

Qw cm3/sec	Dcore mm	A CM2	L cm	ΔP psi	P1 psia	P1 atm	P12 atm2	P2 psig	P2 atm	P22 atm2	P22-P12	Pmean	1/Pmean	ΔP (atm)	KN2 (mD)	Average KN2 (mD)
7.40	37.9	11.26	20.4	13.11	14.4	1.98	3.92	1.3	1.09	1.2	2.74	7.855	0.127307	0.89	144.7	143.87
7.97	37.9	11.26	20.4	13.97	15.3	2.04	4.17	1.4	1.09	1.2	2.98	8.335	0.119976	0.95	143.2	
8.23	37.9	11.26	20.4	14.15	15.7	2.07	4.28	1.6	1.11	1.2	3.06	8.625	0.115942	0.96	144.2	
8.01	37.9	11.26	20.4	13.49	15.9	2.09	4.35	2.5	1.17	1.4	2.99	9.195	0.108755	0.92	143.7	
6.62	37.9	11.26	20.4	11.78	13.8	1.94	3.77	2.1	1.14	1.3	2.47	7.94	0.125945	0.80	143.6	

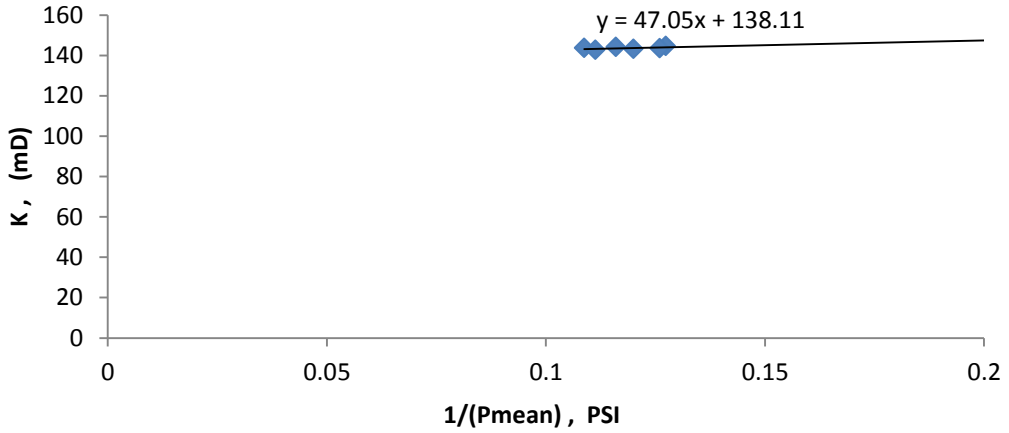

Fig. D - 25 Graph of K against 1/(Pmean), used to find the Klinkenberg permeability of the E4 core

E5 **Table D - 17: Table showing the parameters used for the permeability measurements for the E5 core.**

Qw cm3/sec	Dcore mm	A CM2	L cm	ΔP psi	P1 psia	P1 atm	P12 atm2	P2 psig	P2 atm	P22 atm2	P22-P12	Pmean	1/Pmean	ΔP (atm)	KN2 (mD)	Average KN2 (mD)
8.28	37.9	11.27	20.4	11.48	19.3	2.31	5.35	7.8	1.53	2.3	3	13.54	0.073855	0.78	147.5	120.52
7.91	37.9	11.27	20.4	12.99	15.3	2.04	4.17	2.3	1.16	1.3	2.83	8.795	0.113701	0.88	149.7	
7.12	37.9	11.27	20.4	11.92	13.7	1.93	3.74	1.8	1.12	1.3	2.48	7.76	0.128866	0.81	153.7	
7.67	37.9	11.27	20.4	12.58	14.6	1.99	3.97	2	1.14	1.3	2.68	8.29	0.120627	0.86	153.3	
6.61	37.9	11.27	20.4	11.96	12	1.82	3.3	0.1	1	1.0	2.3	6.03	0.165837	0.81	154.2	
6.17	37.9	11.27	20.4	10.56	12.8	1.87	3.49	2.2	1.15	1.3	2.17	7.48	0.13369	0.72	152.2	
4.58	37.9	11.27	20.4	7.97	11.7	1.79	3.22	3.7	1.25	1.6	1.65	7.685	0.130124	0.54	148.4	
3.38	37.9	11.27	20.4	6.5	9.1	1.62	2.62	2.6	1.18	1.4	1.24	5.85	0.17094	0.44	146.2	
3.17	37.9	11.27	20.4	5.75	10.2	1.69	2.86	4.4	1.3	1.7	1.17	7.275	0.137457	0.39	145	

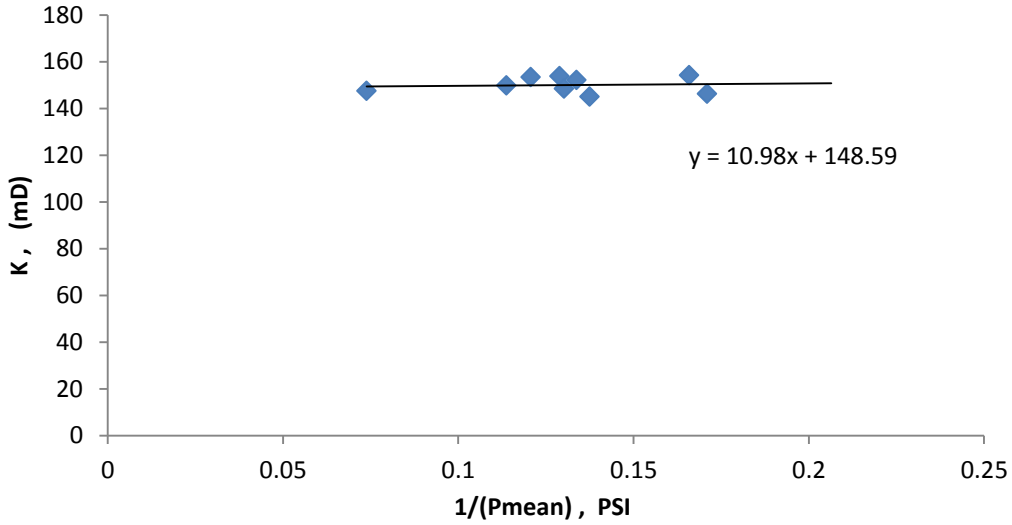

Fig. D - 26 Graph of K against 1/(Pmean), used to find the Klinkenberg permeability of the E5 core

E6 **Table D - 18: Table showing the parameters used for the permeability measurements for the E6 core.**

Qw cm3/sec	Dcore mm	A CM2	L cm	ΔP psi	P1 psia	P1 atm	P12 atm2	P2 psig	P2 atm	P22 atm2	P22-P12	Pmean	1/Pmean	ΔP (atm)	KN2 (mD)	Average KN2 (mD)
5.71	37.9	11.29	20.4	10.82	12.1	1.83	3.33	1.3	1.09	1.2	2.15	6.71	0.149031	0.74	142.1	157.28
6.93	37.9	11.29	20.4	12.32	14.1	1.96	3.85	1.8	1.12	1.3	2.59	7.96	0.125628	0.84	143.1	
7.40	37.9	11.29	20.4	12.04	16	2.09	4.38	4	1.27	1.6	2.76	10.02	0.0998	0.82	143.3	
8.35	37.9	11.29	20.4	13	17.6	2.2	4.83	4.6	1.31	1.7	3.11	11.1	0.09009	0.88	143.6	
7.59	37.9	11.29	20.4	13.94	14	1.95	3.81	0.1	1	1.0	2.8	7.02	0.14245	0.95	144.4	
5.75	37.9	11.29	20.4	10.86	12.2	1.83	3.34	1.3	1.09	1.2	2.16	6.73	0.148588	0.74	142.4	
6.81	37.9	11.29	20.4	11.79	14.6	1.99	3.97	2.8	1.19	1.4	2.56	8.695	0.115009	0.80	142.2	
2.885	37.9	11.29	20.4	6.42	7.26	1.49	2.23	0.8	1.06	1.1	1.12	4.05	0.246914	0.44	138.2	
4.53	37.9	11.29	20.4	8.55	11.5	1.78	3.17	2.9	1.2	1.4	1.73	7.175	0.139373	0.58	139.7	
3.50	37.9	11.29	20.4	7.26	9.26	1.63	2.66	2	1.14	1.3	1.37	5.63	0.17762	0.49	136.6	

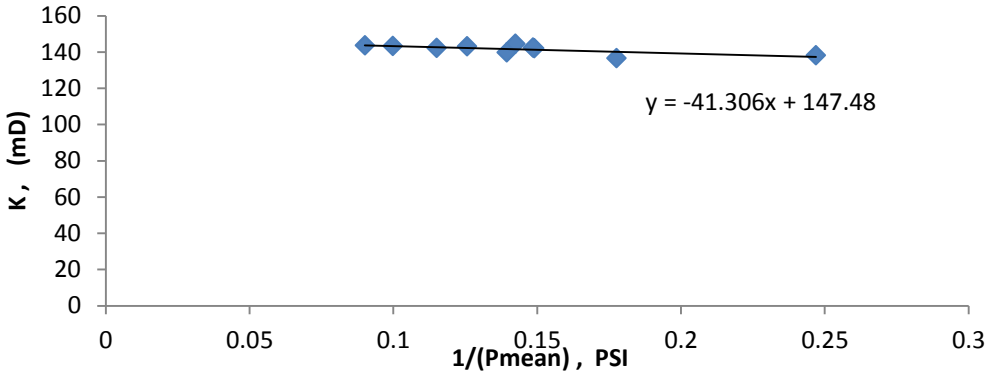

Fig. D - 27 Graph of K against 1/(Pmean), used to find the Klinkenberg permeability of the E6 core

E7 **Table D - 19: Table showing the parameters used for the permeability measurements for the E7 core.**

Qw cm3/sec	Dcore mm	A CM2	L cm	ΔP psi	P1 psia	P1 atm	P12 atm2	P2 psig	P2 atm	P22 atm2	P22-P12	Pmean	1/Pmean	ΔP (atm)	KN2 (mD)	Average KN2 (mD)
5.68	37.9	11.27	29.2	6.43	6.87	1.47	2.15	0.4	1.03	1.1	1.09	3.655	0.273598	0.44	398.4	398.86
4.92	37.9	11.27	29.2	5.15	7.54	1.51	2.29	2.4	1.16	1.4	0.94	4.965	0.20141	0.35	401.8	
8.24	37.9	11.27	29.2	7.53	11.9	1.81	3.27	4.3	1.3	1.7	1.59	8.105	0.123381	0.51	397.2	
8.05	37.9	11.27	29.2	8.47	9.32	1.63	2.67	0.9	1.06	1.1	1.55	5.085	0.196657	0.58	397.3	
6.72	37.9	11.27	29.2	6.49	10.1	1.69	2.86	3.7	1.25	1.6	1.3	6.895	0.145033	0.44	396.6	
6.25	37.9	11.27	29.2	6.23	9.51	1.65	2.71	3.3	1.22	1.5	1.22	6.395	0.156372	0.42	393.5	
5.11	37.9	11.27	29.2	5.63	7.08	1.48	2.2	1.5	1.1	1.2	0.99	4.265	0.234467	0.38	396	
4.523	37.9	11.27	29.2	4.49	8.39	1.57	2.47	3.9	1.27	1.6	0.87	6.145	0.162734	0.31	399.9	
3.57	37.9	11.27	29.2	3.69	6.79	1.46	2.14	3.1	1.21	1.5	0.67	4.945	0.202224	0.25	407.5	
4.00	37.9	11.27	29.2	4.81	5.01	1.34	1.8	0.2	1.01	1.0	0.77	2.605	0.383877	0.33	397.5	
2.92	37.9	11.27	29.2	3.61	3.76	1.26	1.58	0.2	1.01	1.0	0.56	1.955	0.511509	0.25	401.9	

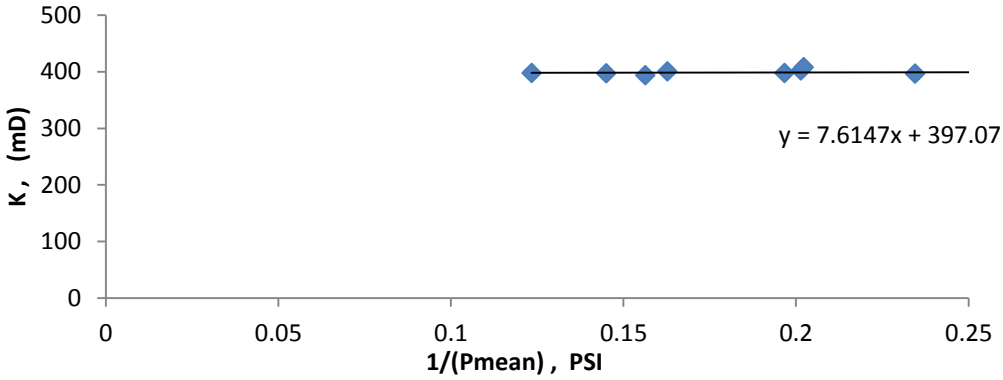

Fig. D - 28 Graph of K against 1/(Pmean), used to find the Klinkenberg permeability of the E7 core

E8 **Table D - 20: Table showing the parameters used for the permeability measurements for the E8 core.**

Qw cm3/sec	Dcore mm	A CM2	L cm	ΔP psi	P1 psia	P1 atm	P12 atm2	P2 psig	P2 atm	P22 atm2	P22-P12	Pmean	1/Pmean	ΔP (atm)	KN2 (mD)	Average KN2 (mD)
5.31	37.9	11.29	29.3	4.98	7.98	1.54	2.38	3	1.2	1.5	0.93	5.49	0.182149	0.34	437.8	439.64
7.99	37.9	11.29	29.3	6.72	11.5	1.78	3.18	4.8	1.33	1.8	1.42	8.16	0.122549	0.46	431	
8.13	37.9	11.29	29.3	7.74	9.24	1.63	2.65	1.5	1.1	1.2	1.44	5.37	0.18622	0.53	433.8	
7.09	37.9	11.29	29.3	6.92	8.16	1.56	2.42	1.2	1.08	1.2	1.24	4.7	0.212766	0.47	437.8	
6.11	37.9	11.29	29.3	5.69	8.59	1.58	2.51	2.9	1.2	1.4	1.08	5.745	0.174064	0.39	435.6	
6.80	37.9	11.29	29.3	6.9	7.35	1.5	2.25	0.5	1.03	1.1	1.19	3.9	0.25641	0.47	438.9	
5.30	37.9	11.29	29.3	5.54	5.88	1.4	1.96	0.3	1.02	1.0	0.91	3.11	0.321543	0.38	445	
2.548	37.9	11.29	29.3	2.9	3	1.2	1.45	0.1	1.01	1.0	0.44	1.55	0.645161	0.20	448.3	
4.85	37.9	11.29	29.3	4.86	6.31	1.43	2.04	1.5	1.1	1.2	0.84	3.88	0.257732	0.33	445.5	
3.85	37.9	11.29	29.3	3.3	8.8	1.6	2.56	5.5	1.37	1.9	0.67	7.15	0.13986	0.22	442.8	

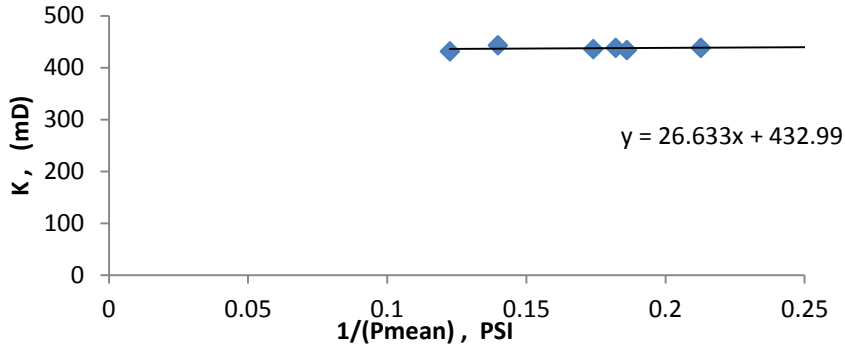

Fig. D - 29 Graph of K against 1/(Pmean), used to find the Klinkenberg permeability of the E8 core

E9 **Table D - 21: Table showing the parameters used for the permeability measurements for the E9 core.**

Qw cm3/sec	Dcore mm	A CM2	L cm	ΔP psi	P1 psia	P1 atm	P12 atm2	P2 psig	P2 atm	P22 atm2	P22-P12	Pmean	1/Pmean	ΔP (atm)	KN2 (mD)	Average KN2 (mD)
7.47	37.9	11.26	29.3	8.56	11.6	1.79	3.19	3	1.2	1.5	1.74	7.28	0.137363	0.58	329.8	332.54
8.05	37.9	11.26	29.3	9.28	11.8	1.8	3.25	2.5	1.17	1.4	1.88	7.14	0.140056	0.63	330	
6.99	37.9	11.26	29.3	7.83	11.5	1.78	3.19	3.7	1.25	1.6	1.62	7.615	0.13132	0.53	332.1	
6.78	37.9	11.26	29.3	7.68	11.2	1.76	3.1	3.5	1.24	1.5	1.57	7.34	0.13624	0.52	332.9	
2.97	37.9	11.26	29.3	4.34	4.39	1.3	1.69	0.1	1	1.0	0.68	2.22	0.45045	0.30	335.5	
4.40	37.9	11.26	29.3	5.46	8.26	1.56	2.44	2.8	1.19	1.4	1.02	5.53	0.180832	0.37	331.2	
4.15	37.9	11.26	29.3	5.79	5.89	1.4	1.96	0.1	1.01	1.0	0.95	2.995	0.33389	0.39	336.3	

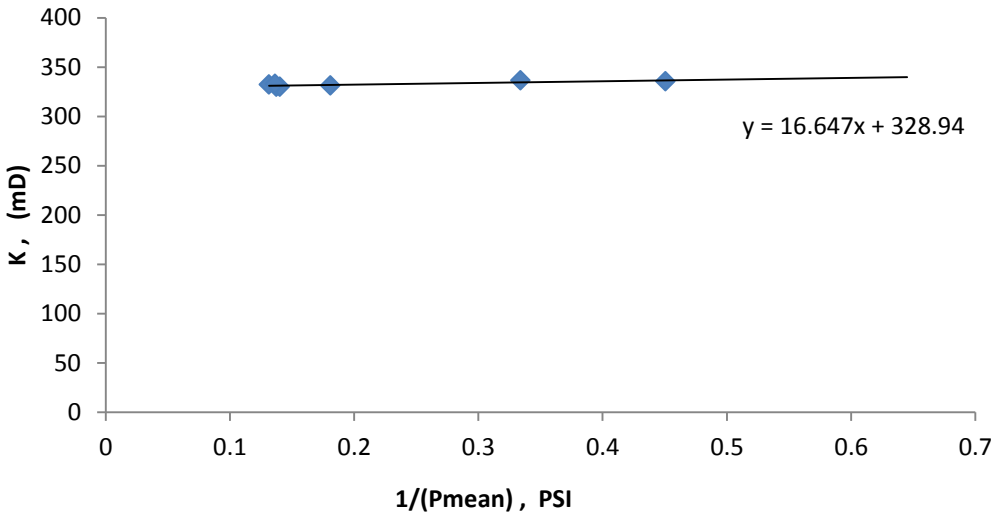

Fig. D - 30 Graph of K against 1/(Pmean), used to find the Klinkenberg permeability of the E9 core

P4 **Table D - 22: Table showing the parameters used for the permeability measurements for the P4 core.**

Qw cm3/sec	Dcore mm	A CM2	L cm	ΔP psi	P1 psia	P1 atm	P12 atm2	P2 psig	P2 atm	P22 atm2	P22-P12	Pmean	1/Pmean	ΔP (atm)	KN2 (mD)	Average KN2 (mD)
6.84	38.3	11.52	20.5	78.09	80.4	6.47	41.9	2.3	1.16	1.3	40.5	41.34	0.024193	5.32	8.859	9.0299
7.35	38.3	11.52	20.5	81.18	83.7	6.7	44.8	2.5	1.17	1.4	43.5	43.09	0.023207	5.53	8.885	
8.18	38.3	11.52	20.5	86.1	89	7.06	49.8	2.9	1.2	1.4	48.4	45.97	0.021753	5.86	8.876	
8.10	38.3	11.52	20.5	84.04	88.9	7.05	49.8	4.9	1.33	1.8	48	46.92	0.021313	5.72	8.867	
4.30	38.3	11.52	20.5	58.59	60.8	5.14	26.4	2.2	1.15	1.3	25.1	31.54	0.031711	3.99	9.01	
5.46	38.3	11.52	20.5	67.25	70.3	5.78	33.4	3	1.2	1.5	32	36.63	0.027304	4.58	8.966	
3.29	38.3	11.52	20.5	50.51	51.2	4.48	20.1	0.7	1.04	1.1	19	25.91	0.038603	3.44	9.094	
0.983	38.3	11.52	20.5	22.55	22.7	2.54	6.47	0.1	1.01	1.0	5.45	11.41	0.087681	1.54	9.476	
1.77	38.3	11.52	20.5	33.91	34.3	3.33	11.1	0.3	1.02	1.0	10.1	17.3	0.05782	2.31	9.236	

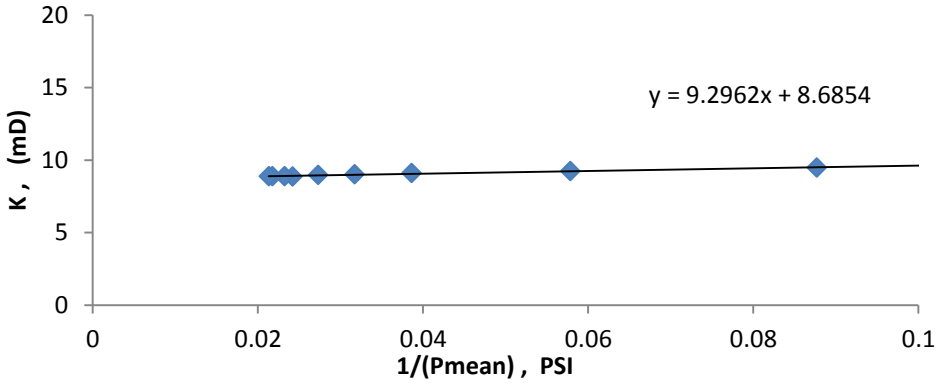

Fig. D - 31 Graph of K against 1/(Pmean), used to find the Klinkenberg permeability of the P4 core

P5 **Table D - 23: Table showing the parameters used for the permeability measurements for the P5 core.**

Qw cm3/sec	Dcore mm	A CM2	L cm	ΔP psi	P1 psia	P1 atm	P12 atm2	P2 psig	P2 atm	P22 atm2	P22-P12	Pmean	1/Pmean	ΔP (atm)	KN2 (mD)	Average KN2 (mD)
8.03	38.0	11.34	20.5	103.3	105	8.17	66.8	2.1	1.14	1.3	65.5	53.7	0.018622	7.03	6.545	6.6234
7.27	38.0	11.34	20.5	97.66	99.5	7.77	60.4	1.8	1.12	1.3	59.1	50.63	0.019751	6.65	6.564	
7.56	38.0	11.34	20.5	99.79	102	7.92	62.8	1.9	1.13	1.3	61.5	51.83	0.019296	6.79	6.56	
5.27	38.0	11.34	20.5	81.24	82.4	6.61	43.7	1.2	1.08	1.2	42.5	41.77	0.023941	5.53	6.619	
6.88	38.0	11.34	20.5	92.49	97	7.6	57.8	4.5	1.31	1.7	56.1	50.74	0.01971	6.30	6.545	
6.01	38.0	11.34	20.5	85.8	89.6	7.1	50.4	3.8	1.26	1.6	48.8	46.69	0.021418	5.84	6.572	
4.98	38.0	11.34	20.5	77.14	80.1	6.46	41.7	3	1.2	1.5	40.2	41.57	0.024056	5.25	6.606	
1.42	38.0	11.34	20.5	35.57	36.3	3.47	12.1	0.7	1.05	1.1	10.9	18.53	0.053981	2.42	6.924	
4.00	38.0	11.34	20.5	69.43	69.7	5.75	33	0.3	1.02	1.0	32	35.02	0.028559	4.73	6.674	

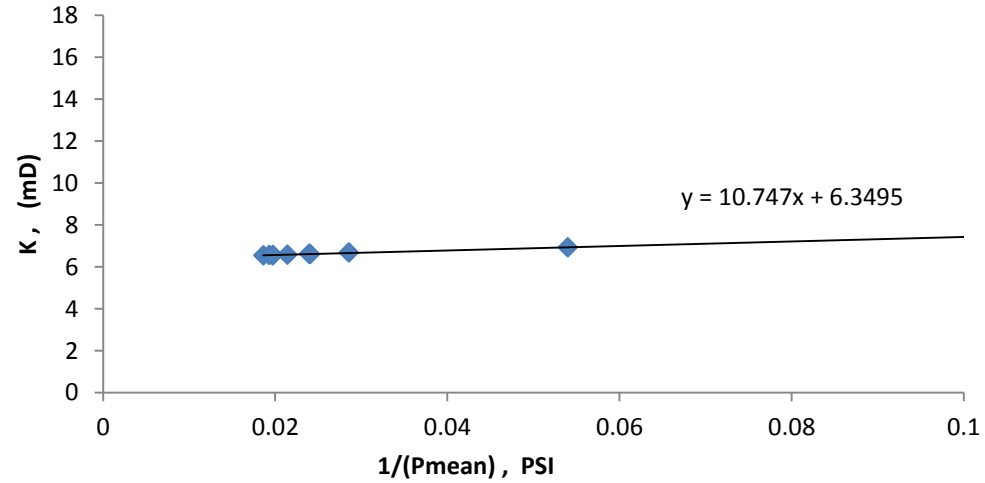

Fig. D - 32 Graph of K against 1/(Pmean), used to find the Klinkenberg permeability of the P5 core

P6 **Table D - 24: Table showing the parameters used for the permeability measurements for the P6 core.**

Qw cm3/sec	Dcore mm	A CM2	L cm	ΔP psi	P1 psia	P1 atm	P12 atm2	P2 psig	P2 atm	P22 atm2	P22-P12	Pmean	1/Pmean	ΔP (atm)	KN2 (mD)	Average KN2 (mD)
3.69	38.0	11.34	20.4	78.73	79	6.38	40.7	0.3	1.02	1.0	39.6	39.62	0.025243	5.36	4.968	4.9709
5.13	38.0	11.34	20.5	95.46	95.9	7.53	56.6	0.4	1.03	1.1	55.6	48.13	0.020777	6.50	4.929	
6.17	38.0	11.34	20.5	106.14	107	8.26	68.2	0.5	1.03	1.1	67.1	53.52	0.018685	7.23	4.908	
7.25	38.0	11.34	20.5	116.28	117	8.95	80.1	0.5	1.03	1.1	79	58.62	0.017059	7.92	4.9	
7.99	38.0	11.34	20.5	122.81	123	9.4	88.3	0.5	1.04	1.1	87.2	61.93	0.016149	8.36	4.893	
7.51	38.0	11.34	20.5	115.73	120	9.14	83.6	3.9	1.27	1.6	82	61.77	0.01619	7.88	4.891	
4.65	38.0	11.34	20.5	88.63	90.8	7.18	51.6	2.2	1.15	1.3	50.3	46.52	0.021498	6.03	4.944	
2.68	38.0	11.34	20.5	64.65	65.1	5.43	29.5	0.4	1.03	1.1	28.4	32.77	0.03052	4.40	5.035	
1.81	38.0	11.34	20.5	50.25	50.5	4.44	19.7	0.3	1.02	1.0	18.7	25.38	0.039409	3.42	5.191	
2.97	38.0	11.34	20.5	68.58	69	5.7	32.5	0.5	1.03	1.1	31.4	34.75	0.028777	4.67	5.051	

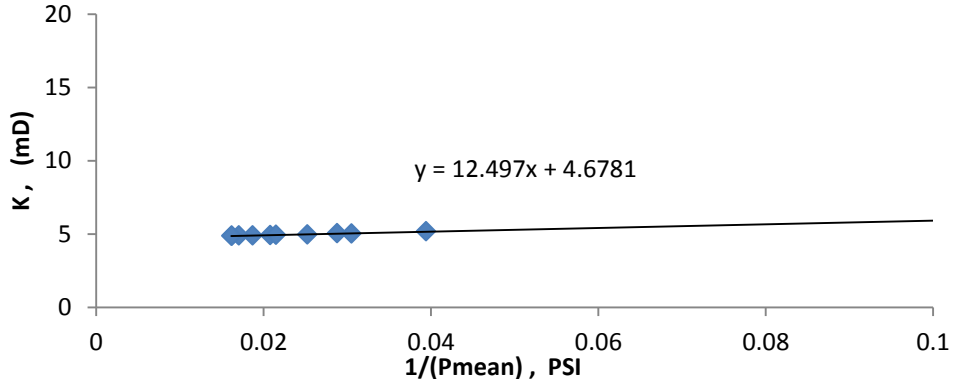

Fig. D - 33 Graph of K against 1/(Pmean), used to find the Klinkenberg permeability of the P6 core

P7 **Table D - 25: Table showing the parameters used for the permeability measurements for the P7 core.**

Qw cm3/sec	Dcore mm	A CM2	L cm	ΔP psi	P1 psia	P1 atm	P12 atm2	P2 psig	P2 atm	P22 atm2	P22-P12	Pmean	1/Pmean	ΔP (atm)	KN2 (mD)	Average KN2 (mD)
1.83	38.2	11.44	28.0	10.4	10.5	1.71	2.94	0.1	1.01	1.0	1.92	5.28	0.189394	0.71	68.79	62.343
7.55	38.2	11.44	28.0	29.36	29.8	3.03	9.17	0.4	1.03	1.1	8.11	15.11	0.066181	2.00	67.53	
7.05	38.2	11.44	28.0	28.33	28.7	2.96	8.73	0.4	1.03	1.1	7.68	14.56	0.068705	1.93	66.62	
7.47	38.2	11.44	28.0	29.44	29.9	3.03	9.21	0.5	1.03	1.1	8.15	15.17	0.06592	2.00	66.48	
1.23	38.2	11.44	28.0	7.52	7.57	1.52	2.3	0.1	1	1.0	1.29	3.81	0.262467	0.51	68.93	
0.86	38.2	11.44	28.0	5.53	5.58	1.38	1.9	0.1	1	1.0	0.9	2.815	0.35524	0.38	69.15	
0.602	38.2	11.44	28.0	4.02	4.07	1.28	1.63	0.1	1	1.0	0.62	2.06	0.485437	0.27	69.95	
2.79	38.2	11.44	28.0	14.2	14.9	2.01	4.04	0.7	1.04	1.1	2.95	7.75	0.129032	0.97	68.59	
2.76	38.2	11.44	28.0	14.04	14.7	2	4	0.7	1.04	1.1	2.91	7.67	0.130378	0.96	68.83	
0.41	38.2	11.44	28.0	2.83	2.85	1.19	1.43	0	1	1.0	0.42	1.435	0.696864	0.19	70.91	

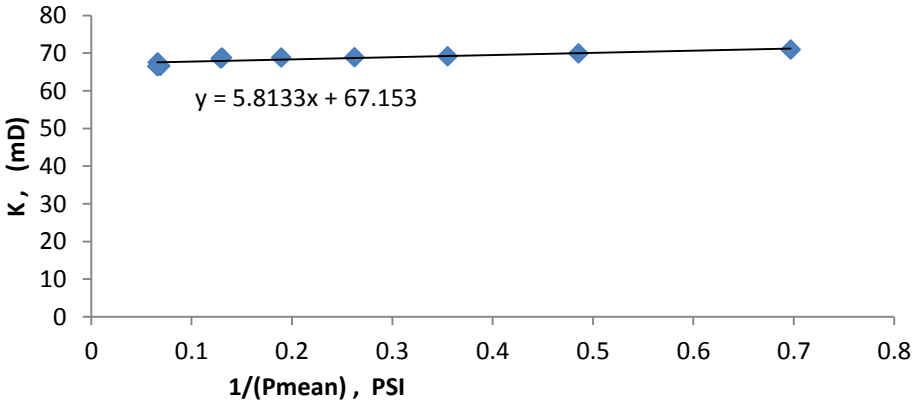

Fig. D - 34 Graph of K against 1/(Pmean), used to find the Klinkenberg permeability of the P7 core

P8 **Table D - 26: Table showing the parameters used for the permeability measurements for the P8 core.**

Qw cm3/sec	Dcore mm	A CM2	L cm	ΔP psi	P1 psia	P1 atm	P12 atm2	P2 psig	P2 atm	P22 atm2	P22-P12	Pmean	1/Pmean	ΔP (atm)	KN2 (mD)	Average KN2 (mD)
1.42	38.0	11.31	28.0	23.06	23.1	2.57	6.62	0.1	1	1.0	5.61	11.58	0.086356	1.57	18.51	18.412
1.62	38.0	11.31	28.0	25.09	25.5	2.74	7.49	0.4	1.03	1.1	6.43	12.98	0.077071	1.71	18.45	
2.06	38.0	11.31	28.0	29.41	30	3.04	9.23	0.5	1.04	1.1	8.16	15.25	0.065595	2.00	18.47	
2.43	38.0	11.31	28.0	32.72	33.5	3.28	10.8	0.8	1.05	1.1	9.66	17.15	0.058309	2.23	18.46	
3.42	38.0	11.31	28.0	40.52	41.8	3.84	14.8	1.2	1.08	1.2	13.6	21.49	0.046533	2.76	18.46	
4.26	38.0	11.31	28.0	46.3	47.9	4.26	18.2	1.6	1.11	1.2	16.9	24.78	0.040355	3.15	18.41	
5.50	38.0	11.31	28.0	53.98	56.1	4.82	23.2	2.1	1.14	1.3	21.9	29.11	0.034352	3.67	18.39	
7.383	38.0	11.31	28.0	63.94	67.1	5.57	31	3.1	1.21	1.5	29.5	35.1	0.02849	4.35	18.33	
7.83	38.0	11.31	28.0	66.09	69.4	5.73	32.8	3.3	1.23	1.5	31.3	36.39	0.027484	4.50	18.32	
8.34	38.0	11.31	28.0	68.45	72.2	5.91	34.9	3.7	1.25	1.6	33.4	37.93	0.026368	4.66	18.3	
3.75	38.0	11.31	28.0	42.99	44.2	4.01	16.1	1.2	1.08	1.2	14.9	22.7	0.044063	2.93	18.44	

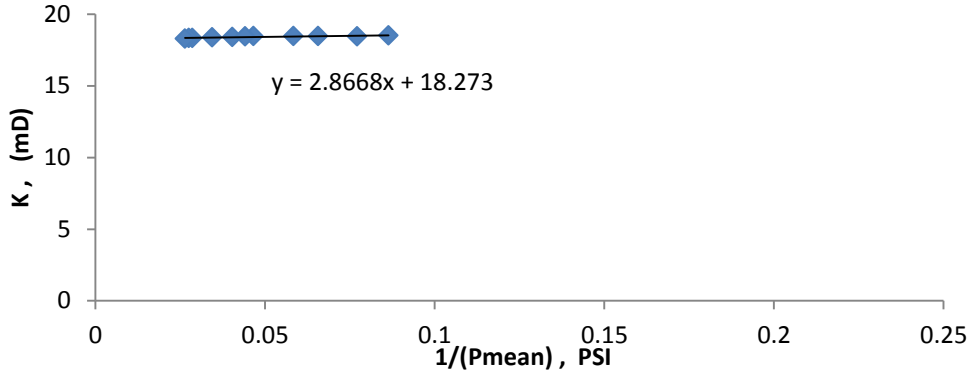

Fig. D - 35 Graph of K against 1/(Pmean), used to find the Klinkenberg permeability of the P8 core

P9 **Table D - 27: Table showing the parameters used for the permeability measurements for the P9 core.**

Qw cm3/sec	Dcore mm	A CM2	L cm	ΔP psi	P1 psia	P1 atm	P12 atm2	P2 psig	P2 atm	P22 atm2	P22-P12	Pmean	1/Pmean	ΔP (atm)	KN2 (mD)	Average KN2 (mD)
7.03	38.0	11.35	28.2	43.05	43.5	3.96	15.7	0.4	1.03	1.1	14.6	21.97	0.045527	2.93	35.3	35.506
7.98	38.0	11.35	28.2	46.71	47.2	4.21	17.7	0.5	1.03	1.1	16.7	23.84	0.041955	3.18	35.13	
8.17	38.0	11.35	28.2	47.39	47.9	4.26	18.1	0.5	1.03	1.1	17.1	24.2	0.041331	3.23	35.14	
8.09	38.0	11.35	28.2	45.97	47.9	4.26	18.2	1.9	1.13	1.3	16.9	24.92	0.040136	3.13	35.21	
8.36	38.0	11.35	28.2	46.88	48.9	4.33	18.7	2	1.14	1.3	17.4	25.44	0.039308	3.19	35.22	
6.22	38.0	11.35	28.2	37.38	41	3.79	14.4	3.7	1.25	1.6	12.8	22.34	0.044763	2.54	35.6	
5.98	38.0	11.35	28.2	34.94	40.9	3.79	14.3	6	1.41	2.0	12.4	23.47	0.042608	2.38	35.55	
5.515	38.0	11.35	28.2	36.69	37	3.52	12.4	0.4	1.02	1.0	11.4	18.7	0.05349	2.50	35.67	
3.26	38.0	11.35	28.2	24.08	26.7	2.82	7.95	2.6	1.18	1.4	6.55	14.68	0.06812	1.64	36.46	
3.96	38.0	11.35	28.2	28.12	30.6	3.08	9.49	2.5	1.17	1.4	8.13	16.51	0.060569	1.91	35.77	

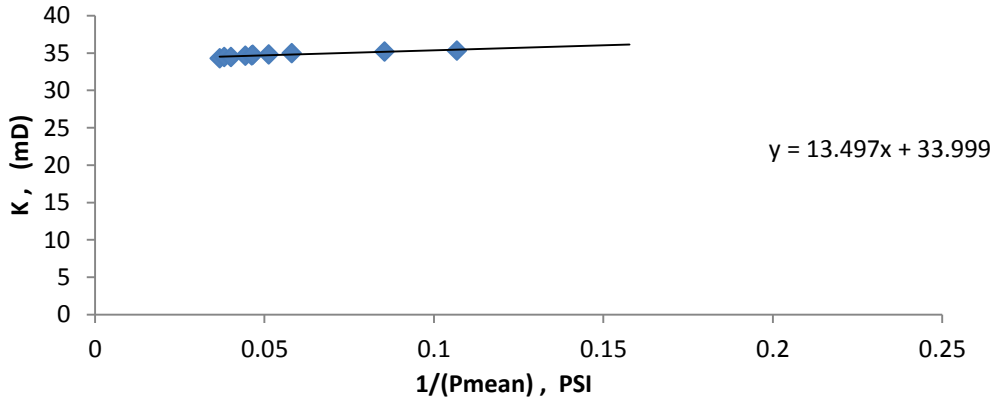

Fig. D - 36 Graph of K against 1/(Pmean), used to find the Klinkenberg permeability of the P9 core